CAVITATION EROSION EXPERIMENTS IN BLOCKED FLOW WITH TWO ICE-CLASS PROPELLER MODELS

J. MICHAEL DOUCET

CAVITATION EROSION EXPERIMENTS IN BLOCKED FLOW WITH TWO ICE-CLASS PROPELLER MODELS

by

© J. Michael Doucet, B. Eng.

A Thesis Submitted to the School of Graduate Studies

in Partial Fulfillment of the Requirements for the Degree of

Master of Engineering

Faculty of Engineering and Applied Science

Memorial University of Newfoundland

July 1996

St. John's, Newfoundland, Canada

ISBN 0-612-17588-X

Canada

Abstract

Ships that operate in ice-infested waters often experience momentary increased propeller cavitation because ice pieces can block the flow into the propeller. Model tests have shown that the presence of blockages in the flow field can lead to regions of violent cloud cavitation. For ducted propellers, this additional cavitation is more significant than it is for open propellers: ice pieces may become lodged against and within the duct and subject the propeller to longer periods of increased cavitation due to the blocked flow. Associated with this cavitation is the possibility of cavitation erosion.

The extent and severity of cavitation erosion that a marine propeller may experience cannot presently be determined theoretically. To gain an understanding of how this phenomenon affects a full scale propeller, it is necessary to perform model tests.

This thesis presents the results of an erosion study that was completed in the cavitation tunnel at the Institute for Marine Dynamics (IMD), a facility of the National Research Council (NRC) of Canada. Paint tests provided the medium through which the erosion was studied. A limited number of tests were attempted with pressure sensitive films to estimate the intensity of the cavitation. Two model propellers, both having a diameter of 200 mm, were used. The first model, an open, fixed pitch propeller, was of the type that is fitted to the Canadian Coast Guard (CCG) *R-Class* (1200-Series) ice-breakers. The second model, a variable pitch ducted propeller, was of the type that is fitted to the Canadian Marine Drilling (CANMAR) Ltd. vessel *MV Robert LeMeur*.

During testing, a simulated ice blockage was installed upstream of the model such that the nominal blade/blockage clearance was approximately 1 mm. Experiments were completed over a range of advance coefficients for various test conditions, including tests at reduced pressure and at atmospheric pressure. The effects of changes in the proximity of the blockage were also examined. A test was performed in open flow for each propeller to provide a baseline for the erosion results. For each experiment, the resulting types of cavitation and the erosion patterns were recorded. *VHS* video equipment and 35 mm still photography were used to document both the experiments and the results. In subsequent analysis, the areas of erosion were estimated using an image analysis program and comparisons between each test were made.

Generally, given the same test conditions, the ducted propeller experienced more erosion than the open propeller. Cavitation persisted longer on the ducted propeller due to the influence of the nozzle.

For both propellers, the amount of face erosion increased with increasing advance coefficient. Back erosion was minimally affected by changes in the advance coefficient.

Concerning proximity effects, erosion increased, for both propellers, as the blade/block clearance was increased, until it reached a peak. This peak occurred at a gap of 5 mm. Further increases in clearance resulted in reduced erosion.

Pressure sensitive film tests were unsuccessful as the films were torn from the blades by the violent cavitation. For future tests under such adverse conditions, a more robust fastening system is required.

Acknowledgements

First and foremost, gratitude and thanks are bestowed upon Dr. Neil Bose (Professor, Memorial University of Newfoundland) for his guidance and support during the work undertaken for this thesis. For this, I am truly indebted.

Thanks are also extended to Mr. Dan Walker (Marineering Limited) for his support during this project. Countless discussions and his assistance with experimental problems certainly aided in the successful completion of this work.

Financial support for these experiments came from the Natural Sciences and Engineering Research Council of Canada (NSERC), under a Strategic Grant entitled *Operation of Marine Propellers in Ice Blocked Flow*. Thanks are extended to the Faculty of Engineering and Applied Science (Memorial University of Newfoundland) for their support during this study. C-CORE is also acknowledged for their financial assistance.

Thanks are due to the Institute for Marine Dynamics, NRC, for funding the construction of the propeller models and for the use of the cavitation tunnel. Dr. Stephen Jones (IMD) is also acknowledged for his support of the project. For their assistance with IMD equipment during the experimental phase of this work, gratitude is expressed to Mr. Spence Butt and Mr. Trent Slade.

For his assistance with cavitation tunnel experiments, Mr. Brad Rixmann is also gratefully acknowledged.

For providing information pertaining to the propel . that were tested, recognition is duly given to LIPS BV (Mr. Tues van Beek), Canadian Marine Drilling Limited (Mr. Alex Brydon), Stone Marine Canada Ltee. (Mr. Gerry McLaughlin) and the Canadian Coast Guard, Newfoundland Region (Mr. Bill Conway). Thanks are also due to Mr. Conway for his assistance in providing access to dry-docked vessels for propeller examinations.

Special thanks and gratitude are extended to Betty and Tony Whalen for their moral support and encouragement during my program. Many friends, within and outside the university, are also thanked for their moral support and encouragement.

Finally, last but not least, thanks are extended to my parents and my family for their support during my studies. Their encouragement was and is greatly appreciated.

Table of Contents

List of Figures

List of Tables

Nomenclature

A_D	Developed Area Ratio
A_E	Expanded Area Ratio
A_O	Area of erosion
a_S	Gas content ratio
c/C	Blade chord fraction (0 is at L.E., 1 is at T.E.)
D	Propeller diameter
dDg	Elemental drag force
dF_R	Elemental resultant force
dL	Elemental lift force
dQ	Elemental torque
dr	Elemental width
dT	Elemental thrust
dx	Elemental length
f(x)	Shape of an eroded surface along the x-direction
F_N	Froude number
g	Gravitational acceleration
J	Advance coefficient
k	Surface roughness
k_t	Thrust coefficient
L.E.	Leading edge
MDD	Mean depth of deformation
MDDR	Mean depth of deformation rate
N	Number of propeller blades
n	Propeller revolution rate
P	Propeller pitch
P_l	Local pressure
P_{ATM}	Atmospheric pressure
P_o	Ambient water pressure (at the propeller shaft centerline)
P_v	Vapour pressure of water (at the ambient temperature)
Q	Propeller torque
q	Stagnation pressure
r	Annular radius
R	Propeller radius
r/R	Blade radius fraction (0 is at hub; 1 is at blade tip)

R_N	Reynold's number
s	Surface tension
T	Propeller thrust
t	Test duration
T.E.	Trailing edge
U_l	Local flow velocity
U_O	Ambient flow velocity
V_A	Speed of advance (axial velocity)
v_R	Resultant velocity
W_N	Weber number
z	Clearance between propeller blade and blockage
α	Gas content of water
α_s	Gas content of saturated water
β_i	Hydrodynamic pitch angle
ϕ	1) Geometric pitch angle; 2) "...a function of..." (used with dimensional analysis)
γ	Angle of incidence
λ	Length scale
μ	Absolute viscosity
ν	Kinematic viscosity
θ	Blade pass angle
ρ_w	Mass density of water
σ	Cavitation number

Chapter 1
Introduction

1.1 Historical Perspective

Mankind has made use of the water as a means of transportation for many thousands of years. The earliest "boat" may have been nothing more than a floating log which provided a means of travelling across a stream or a narrow river. Once it was realized that a person could cross a body of water rather than having to go around it, the movement of goods in the same fashion probably followed shortly thereafter.

As time progressed, it was desirable to move more people and more goods during one voyage. The result was that boats gradually became larger and more sophisticated. Large logs could have been hollowed out to create canoes, or many logs may have been lashed together to create rafts or barges. The exact nature of the first boats is unknown to us in the present day.

Of course, if one could not land the passengers and cargo at the desired shore destination, then much effort would be required to move the same over land to the required location. A means of propelling and guiding the primitive craft to specific shore sites was needed. The earliest propulsion device was probably nothing more than a long

stick or a small log which was used to push the craft through shallow water. This had certain limitations: one could not venture into deep water, and the "propulsive power" was only available as long as the person providing it did not tire.

As time progressed, boats evolved into ships. Sails were used for many hundreds of years as a means of propulsion, and indeed, are still used today on some large ships to augment mechanical propulsion devices. For their invention of a device that made use of the principle of jet propulsion, a patent was granted to Toogood and Hayes of Great Britain in 1661. This was the first propulsive device to use mechanical power (van Manen and van Oossanen, 1988). With the advent of steam power, paddle wheels were also used for a short while, but they proved to be fragile in the rough waters of the stormy North Atlantic.

While the first proposal to make use of a marine screw propeller was put forward in England in 1680 by Hooke, the first actual use is generally attributed to Colonel Stevens, who propelled a steam driven boat at New York in 1804 (van Manen and van Oossanen, 1988). It was during the early nineteenth century that the marine screw propeller was first used as a practical means of propulsion. Its prominence grew steadily as a means of propelling a vessel through the seas and oceans.

Speed continued, as always, to be an important factor in the operation of ships. The advent of the propeller, combined with improvements in mechanical power, meant that higher vessel speeds could be attained. It was at this time that cavitation became a factor in vessel propulsion.

> One of the earliest references to cavitation on marine propellers was made by Osborne Reynolds, who in 1875 referred to the effect of racing of propellers. The first fully recorded case of its occurrence on a ship is that of the British destroyer *Daring* in 1894. With the original twin three-bladed propellers, the ship on trial only reached a speed of 24 knots instead of the desired 27. When these screws were replaced by another pair with 45 percent more blade area, not only was 24 knots achieved with 17 percent less power, but a top speed of 29.25 knots was reached, with the elimination of much of the vibration previously experienced. (van Manen and van Oossanen, 1988)

Also, at this time, the Englishman Sir Charles Parsons was building the vessel *Turbinia*. He also experienced disappointing results while on ship's trials. During his attempts to understand the poor trials' results, he concluded that the propeller on his vessel was unable to achieve the required thrust due to cavitation. During his investigations, he constructed the world's first cavitation tunnel and became the first cavitation researcher (Knapp, 1970). This cavitation tunnel still exists and is presently located at the University of Newcastle-Upon-Tyne, Newcastle, England.

Since the first cavitation experiments were performed by Parsons one hundred years ago, much research pertaining to this phenomenon has been undertaken. There is still much to be learned. One specific problem related to the violent nature of cavitation is propeller erosion. It is this topic which is the focus of this thesis.

1.2 Rationale for Study

Ships that operate in the iced waters of Arctic and sub-Arctic conditions often experience increased propeller cavitation when compared to vessels that operate in open

water. During the operation of a propeller in ice-strewn waters, the presence of a relatively large ice piece in close proximity upstream of the propeller can lead to a region of stalled flow downstream of the ice piece.

In the case of an open propeller, this ice piece will ultimately move through the propeller during an ice milling event. However, before the milling event occurs, the propeller will experience momentary cloud cavitation as a result of the extreme wake and the proximity of the ice piece. Video records also show that cloud cavitation occurs during the milling event (Transport Development Centre, 1995). Cavitation in blocked flow of an open ice class propeller has been demonstrated at model scale (Walker and Bose, 1994; Walker et al., 1994).

With a ducted propeller, ice pieces can become lodged in the duct until the propeller is reversed to clear the blockage. On multi-screw vessels, in particular, clearing of the blockage is not done until vibration is excessive or forward thrust is severely impaired. This leads to periods of several minutes duration when the propeller operates in these harsh conditions. During this time, the propeller is exposed to violent cloud cavitation, again as a result of the extreme wake and the proximity of the ice piece. This phenomenon has been documented for both full scale and model scale ice class propellers in nozzles (Lindroos and Björkestam, 1986).

Regions of the propeller which experience this violent cloud cavitation may be subject to some form of erosion damage. Repeated exposure to intense cavitation may cause severe pitting on the blade surfaces (e.g. see van Manen and van Oossanen, 1988,

page 180). Increased maintenance costs for the upkeep of the propeller will be incurred, in addition to the fact that the propeller will no longer be able to provide thrust at its optimum efficiency. In an extreme case, the propeller material may be weakened to the point that parts of the blades may break off.

If at all possible, it is desirable to prevent cavitation erosion because of the severe damage which may occur. For propellers which do not operate in ice, erosion may be minimized or prevented by ensuring that the propeller does not operate in conditions which favour cavitation, through the proper selection of propeller materials, or by applying protective coverings. The best way to prevent erosion is to ensure that cavitation does not occur. However, for propellers which operate in ice, it is impossible to avoid the conditions which lead to such violent cavitation. As a result, these propellers are at risk of suffering from erosion damage.

Due to the consequences which may result if cavitation erosion affects the propeller, it is useful to be able to make an estimate of the damage that may occur. Since the nature of cavitation erosion is a complex combination of both the hydrodynamics of multi-phase flows and metallurgy, the present state of knowledge does not yet allow for the location or extent of erosion to be determined accurately by theoretical means, thus making the use of model tests of prime importance (Kato, 1992).

1.3 Objectives and Scope of Study

One method of determining the amount and severity of erosion to which a particular propeller may be subjected is to perform model experiments. Ideally, one

would prefer to test a full scale propeller. However, this is not practical because of both the fabrication costs and the lack of facilities large enough to test full scale propellers (although there are a few sites in the world which can work with some small full scale propellers).

The possibility of erosion damage is normally assessed at model scale through tests with soft paint films. Such films are applied to the surface of the model which is then tested at the required operating conditions. These tests provide information on the location and extent of erosion which the model experiences, and also provide limited information on the severity of the cavitation which causes the erosion (Lindgren and Bjärne, 1976). Secondly, to provide more quantitative information on the severity of cavitation erosion, tests may be performed with pressure sensitive films attached to the blades. The results of such tests may then be scaled to approximate the pressures which the full scale propeller may experience (Kato et al., 1981). A third method of assessing erosion damage is to perform model tests with aluminium films applied to the model (Kato, 1975b; Kato et al., 1981). Since aluminium is a soft metal, it will easily be pitted during a cavitation erosion experiment. The results from such tests provide information on the depth of erosion pits, as well as the density of pits per unit area which were formed during the test. In some cases, the rate of pit formation is also determined from the experiments. These results may then be used to estimate the material attack which the full scale propeller may experience (Kato, 1975a).

At the beginning of January 1994, work was initiated on a project to study the effects of cavitation on marine propellers in ice-blocked flow (Bose and Jones, 1993).

This work was part of a three year Natural Sciences and Engineering Research Council of Canada (NSERC) Strategic Grant which was awarded to Memorial University of Newfoundland in October 1993. A portion of this research project was devoted to performing an erosion study.

The work reported here presents the results of the erosion study that was completed in the cavitation tunnel at the Institute for Marine Dynamics, NRC. This study involved the use of two propeller models: the first was an open, fixed pitch propeller, and the second was a ducted, variable pitch propeller.

The focus of this study was to ascertain the extent of erosion which the previously mentioned ice-class propellers may experience as a result of blockage. To predict the erosion patterns on the propellers and to allow the areas of erosion to be measured, paint tests were used as the study medium.

During the experiments, a simulated ice blockage was installed upstream of the model such that the nominal blade to blockage clearance was approximately 1 mm. Experiments were carried out over a range of advance coefficients for various test conditions, including tests at reduced pressure and at atmospheric pressure. Proximity effects were also examined. A test was performed in open flow for each propeller to provide a baseline for the erosion results. For each experiment, the resulting types of cavitation were documented and the erosion patterns were photographed. In subsequent analysis, the areas of erosion were estimated using image analysis software and comparisons between each test were made.

Additionally, a limited number of tests were performed using pressure sensitive film. The results from the paint tests indicated the blade locations where the pressure sensitive film was attached for a given test condition.

Tests with aluminium films were not completed for this study. For aluminium test specimens to be used, it would have been necessary to mill holes in the propeller blades so that the specimens could be mounted flush to the blade surfaces. Since the propeller models had been accurately machined, it was desirable to leave them unmodified. Additionally, to measure pit depth and density, it would have been necessary to use a microscope for the analysis. Such measurements are time consuming and were deemed beyond the scope of the study. In practice, it is also difficult to accurately scale such results to full scale (e.g. see Kato, 1992; Franc et al., 1992).

Chapter 2
The Problem of Cavitation Erosion

2.1 Propeller Basics

Presently, the most common device used to propel a ship is the marine screw propeller. The propeller converts the power produced by an engine into a thrust force which causes the vessel to move. When a torque is applied via the engine and the shaft, causing the propeller to rotate, a thrust force is generated since water is accelerated past the airfoil shaped blades. The thrust and torque forces which act on a propeller blade are illustrated in Figure 1.

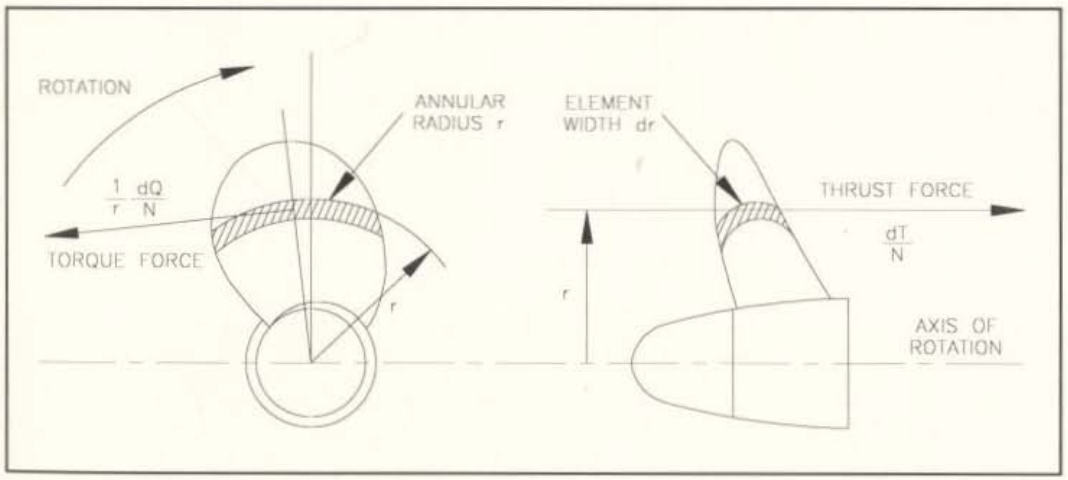

Figure 1: Thrust and Torque Forces on an Annular Blade Sectional Element (from O'Brien, 1962)

During the propeller rotation, lift and drag forces are generated over the blades. Forward motion (i.e. forward thrust) results since the lift force is greater than the drag force. Figure 2 illustrates the velocities and forces which act on a blade sectional element. When the water is accelerated, the pressure distribution on the surface of the propeller blade changes. As shown in Figure 3, there is a pressure reduction on the back of the blade and a pressure increase on the face of the blade relative to the pressure of the nearby fluid. The pressure distributions are significant not only with regard to the lift generated by the propeller, but also in relation to cavitation. Descriptions of propeller geometry, blade forces and pressure distributions are given by Carlton (1994), van Manen and van Oossanen (1988), Harvald (1983) and O'Brien (1962).

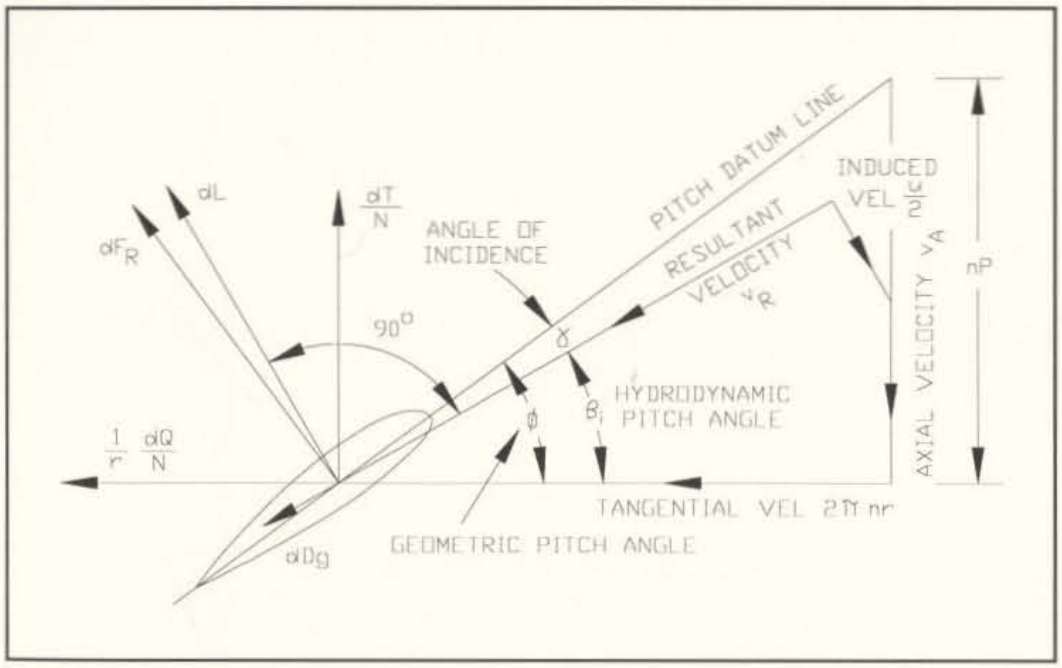

Figure 2: Velocities and Forces on an Expanded Blade Sectional Element (from O'Brien, 1962)

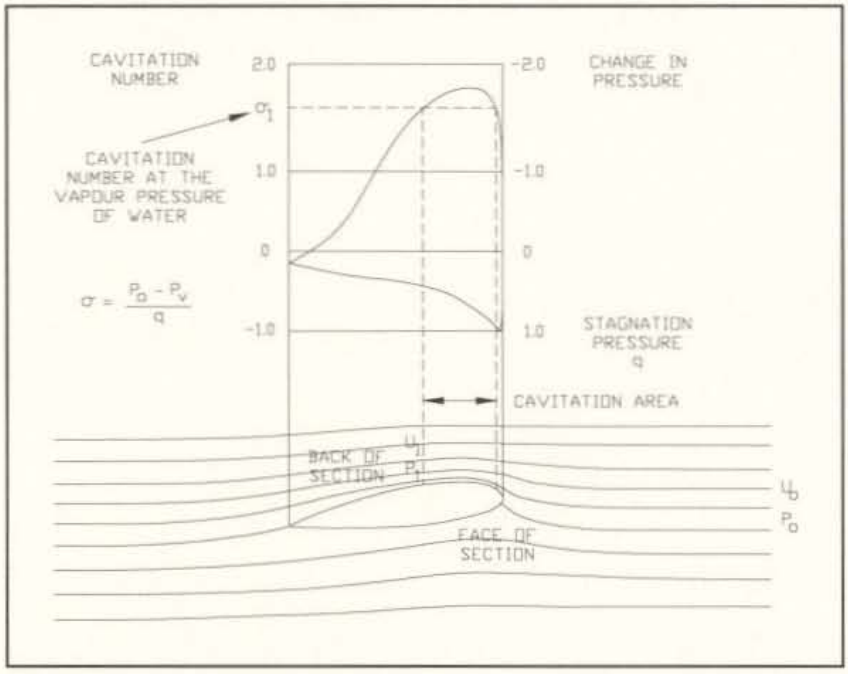

Figure 3: Flow and Pressure Around an Airfoil (from Harvald, 1983)

2.2 Overview of Cavitation and Erosion Mechanisms

Basic descriptions of cavitation are given by Carlton (1994), van Manen and van Oossanen (1988), Harvald (1983) and O'Brien (1962). Items discussed by these authors include cavitating flows, types of propeller cavitation, detrimental effects of cavitation, cavitation tunnel model testing, theory of propeller design and criteria for the prevention of cavitation. Detailed discussions of the cavitation phenomenon are given by Hammitt (1980) and Knapp et al. (1970). In Hammitt (1980), there is also a section which discusses background literature and past research.

The International Towing Tank Conference (ITTC) is devoted to advancing the state of knowledge concerning marine model testing (vessel models as well as propulsion models). ITTC members are active in the field of cavitation research and their conference

proceedings, produced every three years, include a cavitation committee report. This encompasses information pertaining to nuclei, propeller induced hull pressures, noise, erosion, high speed propulsion, scale effects and practical aspects of cavitation testing.

Cavitation is a violent phenomenon that can affect all marine propellers, particularly those which are heavily loaded. It is a dynamic process in which vapour cavities are formed at a particular location once the local pressure drops to the vapour pressure of the fluid. The vapour cavities take time to form and it is also necessary for nuclei to be present. These nuclei are small bubbles, often microscopic in size, which contain permanent gas and/or the vapour of the liquid medium.

Once a propeller reaches a certain critical revolution speed and cavitation occurs, the presence of vapour cavities causes a breakdown in the flow around the blades. As a result, the propeller will experience a subsequent loss of thrust and efficiency. Propeller cavitation may prevent a vessel from achieving its designed speed and it may also manifest itself in the form of noise, vibration and erosion (Harvald, 1983).

Noise and vibration can be a serious problem. Silence is of the utmost importance for naval vessels as undetected movement, particularly for submarines, is extremely important. For passenger vessels, propeller induced noise and vibration will detract from the overall comfort level of the passengers. Generally, as ship size increases, propeller size and loading also increases in order to produce the required thrust. As a result, incidences of cavitation and erosion also increase due to the heightened blade loading. Propellers of small, high speed craft are also heavily loaded and, therefore, also subject to cavitation.

Originally, erosion of marine propellers was believed to be the result of corrosion. Due to the pioneering work of researchers like Parsons (Knapp, 1970), it is now realized that erosion occurs as a result of cavitation. However, corrosion is a phenomenon which is closely linked with erosion since both may occur simultaneously. Therefore, some consideration must be given to the effects of corrosion. To this end, some aspects of corrosion are mentioned in the next section to provide background information, however, detailed examination of corrosion effects was beyond the scope of this study.

It is generally believed that erosion of propellers occurs when vapour bubbles in the flow collapse and return to their liquid state. When these bubbles reach locations where the fluid pressure is greater than the vapour pressure, they collapse with explosive force. If the bubble collapse occurs near a blade, then erosion of that surface may occur.

Erosion that occurs as a result of bubble collapse is believed to be caused by two principal mechanisms. These mechanisms are: i) the impingement of liquid microjets that are formed in collapsing bubbles, and, ii) the impingement of shock waves that rebound from collapsing bubbles (Suhrbier et al., 1987). Figure 4 illustrates these mechanisms.

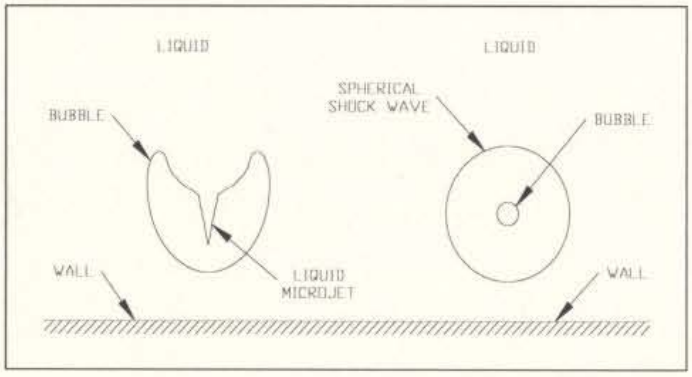

Figure 4: Erosion Mechanisms (from Suhrbier et al., 1987)

In the first case, as the bubble collapses, a microjet of water forms and shoots through the bubble, striking the nearby boundary with tremendous force. The geometry of this situation is similarly described by pushing one's finger into an inflated balloon. For the second case, the bubble implodes in a uniform manner and a spherical shock wave is sent out. The shock wave impinges on the nearby boundary, again with tremendous force.

When these microjets and shock waves strike the propeller, they do so with such force that microscopic pits are formed on the surface and material is removed from the blades. Eventually, after the millions of impacts which may occur during cavitation events, visible signs of erosion will appear on the propeller.

It was suggested by Chen and Israelachvili (1991) that cavitation erosion may also result from a different mechanism. In their study, the elasto-hydrodynamic deformations which occurred when two curved surfaces were moved towards or away from each other were examined. The rapid growth and disappearance of vapour cavities, along with their effects on nearby surfaces, was monitored. It was found that the inception of cavities was related to the simultaneous relaxation of high local strain energies on the nearby surfaces. As a result, it was concluded that damage was more likely to occur during the formation, rather than the collapse, of the cavities. Once bubbles had formed, it was noted that they usually moved to a different location before disappearing. Damage appeared only at the bubble inception locations.

Burton and Burton (1992) reported on cavitation and cavitation damage in viscous films, such as the lubricating oils that are used with bearings. The analysis given showed

that shock waves from implosions of cavities were not expected to produce damage as there would not be enough kinetic energy to cause erosion (in a thin viscous film). Application of crack theory accounted for a source of transient high surface stress during cavity formation, which indicated that damage would occur at this time. Their calculations and observations were also offered to support the findings of Chen and Israelachvili (1991) with regards to damage occurring during bubble formation.

For marine propellers, the first two erosion mechanisms mentioned above appear to be the governing mechanisms as cavitation erosion is predominant in locations where cloud cavitation occurs. This is because the areas of higher pressure where the vapour bubbles collapse are usually near a boundary. However, if the bubbles collapse far enough away from the boundary, then erosion will not occur. This principle, for example, is employed in the propulsion of high speed vessels through the use of super cavitating propellers. These propellers are designed so that the entire suction side of the blades will cavitate and the bubbles will subsequently collapse downstream of the propeller.

2.3 Erosion and Corrosion: Material Considerations

Even though erosion and corrosion are different phenomena, it is possible for interaction between these processes to occur. Once erosion affects a smooth surface, the breakdown of the material is accelerated by corrosion since more surface area is available for corrosive attack and fresh metal is continually being exposed. Also, if corrosion roughens the surface of the blades, then cavitation inception, and hence cavitation erosion, may readily occur at these locations due to irregular pressure distributions and low pressures caused by the irregular surface. Therefore, if the material selected for the

propeller is resistant to erosion damage, corrosion may also be reduced. Despite the fact that much research has been completed concerning the selection of materials, it is still possible for corrosion to be a problem, as discussed below.

Owing to the in-service failure of a seawater pump in the Persian Gulf, Al-Hashem et al. (1995) studied the cavitation behaviour of nickel aluminium bronze (NAB) in seawater. (NAB alloys are used in the manufacture of some propellers.) The failure of the pump was found to result from cavitation damage and erosion-corrosion grooves. During testing, the presence of cavitation, induced with a 20 kHz ultrasonic vibratory apparatus, increased the rate of corrosion. This rate increase resulted because fresh metal surfaces were continually being formed during the erosion proce .s. When the cavitation was stopped, a protective film quickly formed over the material, thereby preventing further corrosion. When cathodic protection was used, it was found that the rate of mass loss for the cavitated specimens decreased by 47%. This reduction was attributed to diminished electrochemical dissolution and the fact that the collapse of cavitation bubbles was cushioned by cathodic gas.

The pump failure mentioned above was also discussed by Shalaby et al. (1995). Essentially, this paper provided the same conclusions as outlined by Al-Hashem et al. (1995), however, more detail was provided regarding the on-site investigation before the experimental study was completed.

Nainar and Pola (1976), using a rotating disk test apparatus, evaluated some of the materials that are used for hydraulic machinery. The test specimens were attached to the disk which then had a water jet directed towards it. It was found that alloys based on

cobalt, with chromium, tungsten and molybdenum (known as "stellite"), are in the category of materials with the highest resistance to cavitation erosion. Manganese chromium steels also fall into this category. Alloying of stainless steel (12 % chromium) with nickel will improve the erosion resistance of the material and that resistance can be further heightened by heat treating the metal to increase the hardness. Metals of high hardness, such as weld overlays, were noted to be susceptible to cracking during testing. Also, it was noted that the use of nitridation and chrome plating did not improve erosion resistance. According to Avner (1974), nitriding will also reduce the corrosion resistance of stainless steel.

Kenkeremath and Thiruvengadam (1976) studied the size and shape of eroded particles (microscopic) which were collected following cavitation experiments in a closed system. Cavitation was induced using a vibratory test apparatus. Aluminium and steel specimens were studied in both oil and distilled water. The objective of the study was to analyze the mechanisms which cause erosion and to develop methods to identify and prevent the erosion phenomenon. The majority of the observed particles were irregular in shape and showed signs of plastic deformation. Attempts to study steel particles which were eroded in distilled water were unsuccessful as the particles suffered quick and excessive corrosion once they were removed from the water. The study demonstrated that the average size of the particles decreased with increasing cavitation intensity.

For a closed system, knowledge of the wear particles in the circulating fluid can lead to the early detection of erosion without requiring the system to be disassembled. While this is not directly applicable to marine propellers, since their operation occurs in

an open environment, knowledge of erosion mechanisms and wear particles can be used to aid in the selection of materials for new propellers.

2.4 Model Testing, Scaling Laws and Scale Effects

2.4.1 Overview

Early work dealing with the mechanics of cavitation and cavitation damage was completed by Knapp (1955). Using high speed motion pictures, detailed observations were made of the cavitation patterns that affected stationary test bodies. Damage probes (material easily damaged by cavitation) were employed to study the development of erosion damage. Use of this combination of techniques permitted surface damage to be related to different parts of the cavitation cycle. It was noted that the initial surface damage consisted of plastic deformations, with no material removal. The effect of exposure time on the pitting rate was studied for the maximum damage zone, and it was noted that the pitting rate dropped rapidly outside the maximum damage zone. Also, all other factors remaining constant, Knapp found that the pitting rate fell rapidly with decreasing flow speed such that the pitting rate varied with the 6^{th} power of the flow velocity. He suggested that standardized specimens should be used for future testing. Items identified that required additional research included: the variation of cavity size and shape and their effects on the intensity of cavitation; additional study of the effect of velocity on the pitting rate; and, correlation between the pitting rate and pit size for standardized specimens.

At about the same time, Plesset and Ellis (1955) performed cavitation damage tests in which no mechanical accelerations were used to cause cavitation. By exciting a

resonant frequency in the water, alternating pressures were generated over the test specimens to cause cavitation. (At the time, this type of testing was relatively new.) Zinc monocrystals and polycrystalline specimens were tested and then examined using photomicrographs and X-ray analysis. The specimens were studied from a metallurgical point of view, with particular emphasis on crystal structures. This work provided a relative determination of the resistance of various materials to cavitation damage. Roughly speaking, hard materials of high tensile strength are the most resistant to damage (Titanium 150-A and tungsten are in this category.) For soft materials such as nickel, brass and pure titanium, plastic deformations set in almost immediately.

Emerson and Patience (1976) pointed out that the objective of all of this research was to be able to predict and prevent cavitation erosion. Statistics given, based upon ITTC investigations, indicated that visual observation of cavitation patterns allowed for about an 85% success rate in predicting the occurrence of cavitation erosion. However, the success rate in determining the actual location of that erosion was only about 33%. Using two model propellers, it was illustrated that paint tests were quite accurate in locating the area of erosive attack, thus dramatically improving the success rate in determining the erosion location. The results of the model test program were compared with the full scale propellers (which had experienced 8 months of service).

Even now, paint tests are still being used successfully to accomplish the goals stated by Emerson and Patience (1976). The work of Bjärne (1995) provides evidence of the practical application of the paint test method. In 1992, the SSPA cavitation laboratory in Sweden was contracted to study the problem of blade root erosion on the 5-bladed

controllable pitch propellers of the *Cunard Line* vessel *Queen Elizabeth II*. Paint tests at model scale provided good correlation with the full scale erosion. When boss fins were fitted at model scale, ensuing paints tests indicated that blade root cavitation erosion did not occur. Following installation of the fins on the vessel, subsequent examination indicated that this erosion problem had been eliminated.

Kato (1992) pointed out that it is still not possible to accurately determine, by theoretical means, the location, extent and severity of erosion. Despite attempts to develop theoretical models, the use of model tests is still necessary. His paper focused on the work that was completed up to 1992, including overviews of: erosion mechanisms; impulsive pressure measurements; luminescence measurements (luminous intensity seems to be related to the implosion intensity of bubbles); the importance of cavitation nuclei in the flow; and, scaling laws for the estimation of erosion at full scale. He suggested that future work should be focused towards: additional study of cavitation patterns and extent estimation; detailed investigations of the collapse region (pressure pulses, pit distribution, etc.); continued examination of erosion mechanisms and their modelling (including metallurgical considerations); and, ultimately, the development of erosion estimation methods that do not require experiments.

Consideration of the research completed by Knapp (1955) and by Plesset and Ellis (1955) illustrates that there were a number of areas that were being studied which required additional research. To this day, that research is ongoing. Improvements to research methods and test results continue to be achieved, however, model tests are still required.

When discussing erosion test methods, it is appropriate that model scale effects also be considered as these effects can greatly influence the outcome of model tests. Due to the volume of material involved, test methods and scale effects will be considered in separate sections to assist in the organization of the material. The references that are cited provide a cross section of the research that has been completed in the field.

2.4.2 Cavitation Erosion Experiments and Test Methods

Employing two propeller models for which full scale data was available, Tanibayshi and Nakanishi (1973) used paint tests to examine tip erosion on heavily loaded propellers. It was determined that erosion damage was not always accurately predicted in non-uniform flow cavitation tests since the model wake distribution was not always steep enough to simulate the full scale phenomenon. They also illustrated the importance of completing tests at the local cavitation number since modern ships have great differences in immersion between fully loaded and ballasted conditions. Once these points were taken into account, their tests accurately reported the erosion which had occurred on the full scale propellers.

The use of an aluminium specimen as a damage probe, fitted flush to the inside of a propeller duct, was discussed by Kato (1975b). The benefit of using a test of this type is that the erosive intensity can be measured, whereas paint test results do not permit this type of measurement to be taken. Defined in equation (1), the *mean depth of deformation (MDD)* was considered as a means of qualitatively measuring erosion at model scale since the increase in surface roughness provided a measure of the erosive

intensity of the cavitation. (In this equation, f(x) is the shape of the surface along the x direction, as shown in Figure 5.) It was suggested that this was a better measure of erosion than weight loss since weight loss measurements must be extremely accurate. Test results indicated that roughness decreased with the revolution rate while it increased rapidly with decreasing cavitation number. Erosion of the aluminium specimen inside the duct was attributed to the collapse of tip vortex cavities which extended downstream from the blade tips. Paint tests were completed which showed that the areas affected by erosion during each type of test were in agreement.

$$MDD = \frac{1}{x} \int |f(x)| \, dx \qquad (1)$$

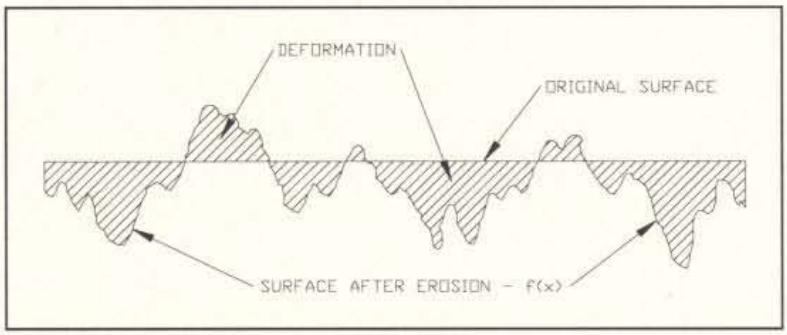

Figure 5: Mean Depth of Deformation (from Kato, 1975b)

Vibratory testing apparatus and attempts to standardize cavitation erosion tests using this type of equipment were discussed by Hobbs (1976). It was pointed out that the effects of properties such as temperature and gas content must be controlled accurately for standardized tests. The usefulness of this type of apparatus for making comparative tests of the erosion resistance of various materials was also highlighted.

Research has also been completed which attempts to relate cavitation noise to the extent of cavitation. Deeprose et al. (1976) used piezo-electric hydrophones to measure

cavitation noise from a pump and it was indicated that the same method could be used for propellers. Tests completed on a two dimensional erosion specimen indicated that maximum high frequency noise values occurred at the maximum erosion conditions. Noise from cavitation was substantially higher than fluid flow noise. Provided that background noise was low, it was suggested that noise measurements could also be used to determine the inception point of cavitation.

Shalnev et al. (1976) studied the effects of magnetic and electric fields on cavitation and erosion. With flow speed and cavitation number kept constant, cylindrical lead specimens were used to measure erosion. Magnetic fields and electric fields were applied and were noted to exert an effect on the boundary zone of cavitation and cavitation erosion. This was explained by the fact that the fields displaced the boundaries of the vapour/gas and liquid phases of the water.

A detailed examination of propeller cavitation erosion, including the usefulness of paint tests, was completed by Lindgren and Bjärne (1976). Various paint types were studied, of which *SSPA Stencil Ink* proved to be the most successful. Factors that were noted to affect test results were test duration, gas content and flow velocity. Specifically, eroded area was noted to increase with decreasing gas content. Forms of cavitation that resulted in erosion damage were discussed. Of particular interest, modifications were suggested which could reduce or avoid propeller erosion by stabilizing or reducing the amount of cavitation. These modifications included: changing the lines of the vessel if the design was not sufficiently advanced; increasing propeller blade area; and, increasing propeller pitch in the blade tip region to stabilize cavitation. For existing heavily loaded

propellers, if local modifications could not be made to reduce erosion, then the wake distribution into the propeller could be improved by applying boss fins ahead of the propeller or a new propeller could be designed for the existing wake.

Various cavitation erosion test methods were compared and evaluated by Kato et al. (1981). For paint tests, *SSPA Stencil Ink* was compared to *AOTAK*, a marking ink used at the University of Tokyo. *AOTAK* was deemed to be more useful as the adhesivity of the *SSPA Stencil Ink* was found to be more sensitive to surface conditions. The use of aluminium was again discussed as a means of providing quantitative measurements of erosive intensity. After testing, the surface of the metal could be examined, using an electron microscope, to measure pit depth and density. The rate of increase of surface roughness, the *Mean Depth of Deformation Rate (MDDR)*, could also be measured. The MDDR is simply the MDD, defined in equation (1), differentiated with respect to time. The use of pressure sensitive films *(PRESCALE)* was also discussed. These films contain microcapsules of colour developing and colour forming material, which, when exposed to a certain pressure, will break and generate a red colour. The density of the colour can be measured with a densitometer to ascertain the magnitude of the applied pressure which generated the colour. When using *PRESCALE*, five minute tests were found to be sufficient and the highest pressure measured during a model test did not exceed 100 bar.

Bjärne (1983) provided additional information on propeller cavitation erosion as an extension of the work completed by Lindgren and Bjärne (1976). Again using paint tests as the medium, a number of factors were examined which affect propeller erosion. These included blade area, angle of attack, shape of blade profile, and blade contour.

Stainless steel specimens, fitted flush to the surface of a rotating disk, were tested at high peripheral velocities by Shima et al. (1992). This type of apparatus was noted to be best suited for simulating the erosion of rotary machinery such as pumps and hydraulic turbines. Cavitation inception was stimulated by the existence of holes in the rotating disk. Erosion during these tests occurred at regions where cloud cavitation was noted to collapse. The location and extent of damage was shown to be a function of the cavitation number. An increase in the peripheral velocity caused a decrease in the cavitation number, thereby causing the erosion rate to become maximum.

2.4.3 Scaling Laws and Scale Effects

Kato (1975a) attempted to develop scaling laws which could be used to estimate full scale erosion from model test results. These attempts again made use of the previously defined MDD and MDDR. A chart, incorporating test duration, material properties and flow velocity, was developed which was used to graphically calculate full scale erosion based on the MDD. While a theoretical model of cavitation erosion was proposed and used to estimate erosion, it was stated that additional work on this model was required. Additional discussion of the erosion mechanisms was completed, including consideration of the amount of energy absorbed by the material exposed to erosive attack.

A rotating disk apparatus, towards which water jets were directed, was used by Janakiram and Rao (1976) to study the influence of jet velocity and frequency of impacts on erosion. For the aluminium specimens used, it was shown that the volume loss increased exponentially (to the power of 7.5) with increasing jet velocity. It was also

shown that the volume loss increased as the frequency of impacts increased (to the power of 5). These tests were completed in air.

The initial stages of erosion were studied by Stinebring et al. (1977). For the aluminium specimens, initial damage was in the form of indentations, with no material removal. During this stage, there was a one-to-one relationship between pit formation and bubble collapse. The rate of damage was constant for a given flow condition. The pitting rate was shown to scale with the 6^{th} power of velocity, which agreed with the results produced by Knapp (1955). Additionally, the average collapse energy absorbed by the specimens increased with the 5^{th} power of velocity. Therefore, the total cavitation bubble collapse energy absorbed per unit area per second was found to scale to the 11^{th} power of velocity. It was also shown that damage rates generally increase with decreasing air content. Also, pits at lower air content seemed to be larger than their counterparts at higher air contents.

Following discrepancies between observed cavitation patterns for full scale and model scale tests of a VLCC (very large crude carrier) ducted propeller, Kuiper (1978) studied the effects of variations in propeller loading, model wake, fluid nuclei content and propeller boundary layers. This study dealt primarily with cavitation inception and the application of leading edge roughness. Test results indicated that viscous effects were responsible for the discrepancies between full scale and model scale. Application of leading edge roughness appeared to be successful in tripping turbulent flow in the boundary layer, thereby simulating a higher Reynold's number. Also, it seemed impossible to define a critical Reynold's number above which the propeller boundary

layer would be small. Application of electrolysis did not seem to affect inception and cavitation.

Using two-dimensional erosion tests with aluminium specimens, Kato et al. (1979) again illustrated the use of the MDDR as a Cavitation Erosion Index. The tests were completed at various velocities and cavitation numbers to obtain a correspondence between the erosion and the hydrodynamic characteristics of the cavitation pattern. It was noted that the MDDR had a peak value at a certain cavitation number, and, as the cavitation number was decreased further, the erosion was reduced. This was due to the fact that as the cavitation number decreased, the cavity became larger and the location of erosion shifted since bubble collapse occurred further downstream. Eventually, bubble collapse took place in the freestream and no erosion of the test specimens was recorded.

Erosion tests on two geometrically similar venturis of different sizes were completed in a mercury tunnel by Franc et al. (1992). Pressure measurements were made and the Strouhal similarity law was verified. Pit size on the stainless steel specimens was noted to increase with length scale, but less rapidly than the length scale increase. A dependence of approximately $\lambda^{1/2}$ seemed correct for the results. Despite the differences in the length scale, there was good geometric similarity in the determination of the location of maximum erosion. Increases in flow velocity resulted in higher damage rates while the reduction in length scale induced a reduction in cavitation aggressiveness.

A detailed study of the influence of water air content on cavitation erosion was recently completed by Auret et al. (1993a). Using a rotating disk test rig, an increase in

total air content (including dissolved and entrained air) in the undersaturated range was found to result in bubble collapse cushioning and hence a reduction in erosion damage. When the water was oversaturated with air, large air bubbles formed in the flow and cavitation damage was dramatically reduced, probably due to both bubble collapse cushioning and shock wave attenuation. Since the existence of cavitation depends on the presence of nuclei, gas content is very important in relation to cavitation inception, bubble dynamics, bubble collapse violence and chemical reactivity of the eroded surface.

Auret et al. (1993b) also studied the effects of temperature on cavitation erosion of copper and aluminium specimens in water. Factors affected by temperature include changes in fluid properties, changes in the dissolved gas content of the fluid, and material property changes. The erosion rate was found to increase slightly with temperature up to a maximum, at which point the damage rate decreased considerably. The peak was generally found to occur midway between the freezing point and the boiling point of the cavitating liquid. It was noted that the corrosion rate also increased as the temperature increased. While the temperature range of these tests was beyond the normal operating range for a screw propeller, a number of important facts were highlighted.

An interesting point also discussed by Auret et al. (1993b) was that a distinction should be made between cavitation erosion caused by either flow testing or vibratory testing. The distinction is necessary because of different damage mechanisms and a lack of agreement between the erosion results for each category of test. The main differences between the two test types are associated with the relative importance of rectified diffusion and degasification in fluids experiencing vibratory cavitation.

2.5 Erosion of Propellers in Blocked Flow

Despite the fact that there is a fair amount of literature on the subject of cavitation and cavitation erosion, little research has been done which examines cavitation and erosion in blocked flow. Lindroos and Björkestam (1986) referred to ducted propeller blockage events that were recorded for ships travelling through ice. Subsequent model experiments examined the effects on the propeller of varying degrees of blockage. It was stated that blockage of the duct produced hydrodynamic loads which were on the same order of magnitude as impact loads that result from propeller/ice interaction. The susceptibility to cavitation while operating in blocked flow was quite obvious. While no mention of propeller erosion was made, the existence of violent cloud cavitation during a blockage event indicates that erosion is a possibility.

Laskow et al. (1986) discussed the propeller/ice interaction project that was conducted with the *MV Robert LeMeur* in the seasonal ice of the Canadian Beaufort Sea. A blade from the starboard propeller was instrumented with pressure transducers for this project. During the study, the propeller experienced single impact, milling and blockage events. Among the observations made from the collected data, hydrodynamic forces that occurred during nozzle blockage were identified as being of almost the same magnitude as ice/blade impact forces. Even though erosion was not mentioned, the fact that large magnitude hydrodynamic forces were measured indicated that the possibility of cavitation existed during the blockage events. Therefore, erosive cavitation was a possibility. The operating window for the propulsion system was well defined in the test results.

Full scale trials have been performed in first year level ice with an *R-Class* ice-breaker (Williams et al., 1992). While the main purpose of these trials was to examine vessel performance in ice and snow, and to measure ice properties, information pertaining to the full scale operation of the propulsion system was gathered. Despite the fact that cavitation and cavitation erosion were not explicitly stated or discussed in this work, the operating window for the propulsion system was well defined in the test results. (Knowledge of the propulsion system operating limits was useful for the model experiments that were completed for this thesis.)

More recently, blockage of an open propeller has been documented with video records (Transport Development Centre, 1995). This video, showing the port propeller of the *USCGS Polar Star*, clearly shows a large ice piece blocking the flow into the propeller for a period of approximately 5 to 10 seconds. Extensive cloud cavitation accompanied the blockage event. During other events, even when ice came into contact with and passed through the propeller, cavitation was still clearly visible.

Chapter 3
Experimental Program

3.1 Design of Experiments

3.1.1 Determination of Relevant Variables

If a study was to be completed in which the pitting rate was to be determined, it would be necessary to consider both hydrodynamic and metallurgical variables for the experimental analysis. However, the overall purpose of the NSERC Strategic Grant cavitation investigation was to analyze the effects of ice blockage on both the fluid flow into the propeller and the propeller's performance. Aluminium film tests were not completed for the erosion study. Therefore, metallurgical variables were not considered and only those variables related to the hydrodynamic problem were used in the following dimensional analysis. Additionally, as contact between the propeller and the blockage was not intended, there was no need to model the mechanical properties of ice.

The purpose of the experiments that were performed was to gather information pertaining to the area of erosion that the propellers would experience, under certain operating conditions, during soft film paint tests. Therefore, the area of erosion was one of the dependent variables that was examined through dimensional analysis. As a check, to ensure that the model propellers were operated at conditions similar to those which the

full scale propellers would experience, the dimensional analysis was also performed using propeller thrust as a dependent variable.

When testing model propellers in a cavitation tunnel to simulate full scale cavitation, there are a number of conditions which must be fulfilled in order to provide hydrodynamic similarity between model and full scale propellers. The conditions which must be satisfied are:

1. geometric similarity;
2. kinematic similarity; and,
3. dynamic similarity.

For these experiments, the variables which were required to model the similarity conditions listed above were divided into four groups. A summary of the variables is given in Table 1. (In Table 1, units of "L", "M", and "T" represent "length", "mass", and "time" respectively.) These groups were:

1. geometric variables;
2. motion variables;
3. fluid variables; and,
4. miscellaneous variables.

For geometric similarity, the model propellers were constructed as copies of their full scale counterparts. The geometric variables that were included in the analysis were surface roughness, diameter, and clearance between the propeller blades and the simulated ice piece.

Surface roughness was included in the analysis since cavitation is more likely to occur in the presence of a rough surface than it would if the surface was smooth. The clearance variable was included since the occurrence and severity of cavitation would be affected as the propeller was moved away from the block (i.e. as the propeller was moved out of the restricted flow region).

Relevant motion variables included propeller revolution rate and speed of advance. Ice movement was not considered in the dimensional analysis since only the hydrodynamic effects of the blockage were examined during testing.

There are a number of fluid variables which must be considered for propeller cavitation tests. The variables included in the analysis were water viscosity, mass density of water, ambient pressure of water, vapour pressure of water, surface tension, gas content of water, and, gas content of saturated water. Cavitation depends on all of these fluid variables. Water pressure in the tunnel can be varied through the use of the tunnel's vacuum pump. Surface tension was included since it is related to the collapse of vapour bubbles. Gas content was taken into account as it is a measure of cavitation nuclei present in the water. Consideration of the gas content of saturated water was important since full scale propellers generally operate in saturated water.

The miscellaneous variables which were considered for this study included gravitational acceleration and test duration. Test duration was not important for the thrust analysis, but it was relevant for the determination of the dimensionless parameters related to the area of erosion.

VARIABLE	SYMBOL	UNITS
Propeller Diameter	D	L
Surface Roughness	k	L
Clearance Between Blades & Simulated Ice Piece	z	L
Propeller Revolution Rate	n	1/T
Speed of Advance	V_A	L/T
Water Viscosity	μ	M/(LT)
Mass Density of Water	ρ_W	M/L^3
Ambient Water Pressure	P_0	$M/(LT^2)$
Vapour Pressure of Water (at ambient temperature)	P_V	$M/(LT^2)$
Surface Tension	s	M/T^2
Gas Content of Water	α	---
Gas Content of Saturated Water	α_S	---
Gravitational Acceleration	g	L/T^2
Test Duration	t	T
Propeller Thrust	T	ML/T^2
Area of Erosion	A_0	L^2

Table 1: Summary of Relevant Variables

3.1.2 Dimensional Analysis

Since both the propeller thrust and the area of erosion are dependent variables, two functional equations were developed for the analysis. Based on the variables listed in Table 1, these equations were:

$$A_0 = \phi(D, k, z, n, V_A, \mu, \rho_W, P_0, P_V, s, \alpha, \alpha_S, t, g) \quad (2)$$

$$T = \phi(D, k, z, n, V_A, \mu, \rho_W, P_0, P_V, s, \alpha, \alpha_S, g) \quad (3)$$

Due to the large number of variables included in these equations and in order to simplify the calculations, the dimensional analysis was based on the matrix method outlined by Sharp et al. (1992). For this method, dimensionless variables (e.g. gas content) are not included in the actual matrix manipulations, but are added to the dimensionless functional equation once the matrix analysis is completed.

The first step in the method was to set up the dimensional matrix. Solving first for the area of erosion as the dependent variable, all dimensional variables were written across the top row of the matrix, as shown in equation (4). The coefficients which were placed in each column corresponded to the powers of the dimensions for each variable. In this matrix, rows one, two and three were arbitrarily chosen to correspond to mass, length and time, respectively. For example, the propeller diameter involves only the length dimension. Therefore, the coefficients which were placed in the column for the diameter were "0", "1" and "0" for the mass, length and time dimensions respectively.

	ρ_w	D	V_A	k	z	n	μ	P_D	P_v	s	t	g	A_O
[M]	1	0	0	0	0	0	1	1	1	1	0	0	0
[L]	−3	1	1	1	1	0	−1	−1	−1	0	0	1	2
[T]	0	0	−1	0	0	−1	−1	−2	−2	−2	1	−2	0

(4)

It was necessary to choose three variables which, among them, encompassed each of the three dimensions. These variables, known as the pivotal variables, formed the first three columns of the matrix. The three variables chosen were the mass density of water, the propeller diameter and the speed of advance. The remaining variables were then written into the matrix.

Row operations were then performed on the matrix. This was necessary in order to obtain a unit matrix for the three pivotal variables. An intermediate step is shown in equation (5) and the final result is shown in equation (6). Since the first three columns of equation (6) form a unit matrix, the variables representing each row were the same as those variables which headed the first three columns.

	ρ_w	D	V_A	k	z	n	μ	P_o	P_v	s	t	g	A_o
[M]	1	0	0	0	0	0	1	1	1	1	0	0	0
[L]	−3	1	0	1	1	−1	−2	−3	−3	−2	1	−1	2
[T]	0	0	−1	0	0	−1	−1	−2	−2	−2	1	−2	0

(5)

	ρ_w	D	V_A	k	z	n	μ	P_o	P_v	s	t	g	A_o
ρ_w	1	0	0	0	0	0	1	1	1	1	0	0	0
D	0	1	0	1	1	−1	1	0	0	1	1	−1	2
V_A	0	0	1	0	0	1	1	2	2	2	−1	2	0

(6)

Once the unit matrix was formed, the dimensionless parameters were determined by dividing each variable in the top row by the variables in the first column, where the power of the variables in the denominator were determined from the coefficients found in the matrix. Since the rank of the matrix in equation (6) was 3, the number of π terms (dimensionless parameters) which resulted was 12 ("15 variables from equation (6)" minus "rank of 3" equals "12"). The resulting dimensionless equation is shown in equation (7). Note that the dimensionless variables which were not included in the matrix analysis (e.g. the gas content variables) have now been added to the functional equation.

$$\phi\left(\frac{k}{D},\frac{z}{D},\frac{nD}{V_A},\frac{\mu}{\rho_w D V_A},\frac{P_o}{\rho_w V_A^{\,2}},\frac{P_v}{\rho_w V_A^{\,2}},\frac{s}{\rho_w D V_A^{\,2}},\frac{tV_A}{D},\frac{gD}{V_A^{\,2}},\frac{A_o}{D^2},\alpha,\alpha_s\right)=0 \qquad (7)$$

A similar analysis was completed to obtain a propeller thrust parameter. For this analysis, the initial matrix is shown as equation (8), the final matrix is equation (9) and equation (10) shows the resulting dimensionless functional equation. The dimensionless parameters determined from this analysis were the same as those which were obtained for

the area of erosion parameter, with the exception that the solution for the thrust parameter did not include the area of erosion or time variables.

	ρ_W	D	V_A	k	z	n	μ	P_0	P_V	s	g	T
[M]	1	0	0	0	0	0	1	1	1	1	0	1
[L]	−3	1	1	1	1	0	−1	−1	−1	0	1	1
[T]	0	0	−1	0	0	−1	−1	−2	−2	−2	−2	−2

(8)

	ρ_W	D	V_A	k	z	n	μ	P_0	P_V	s	g	T
ρ_W	1	0	0	0	0	0	1	1	1	1	0	1
D	0	1	0	1	1	−1	1	0	0	1	−1	2
V_A	0	0	1	0	0	1	1	2	2	2	2	2

(9)

$$\phi\left(\frac{k}{D}, \frac{z}{D}, \frac{nD}{V_A}, \frac{\mu}{\rho_W D V_A}, \frac{P_0}{\rho_W V_A^2}, \frac{P_V}{\rho_W V_A^2}, \frac{s}{\rho_W D V_A^2}, \frac{gD}{V_A^2}, \frac{T}{\rho_W D^2 V_A^2}, \alpha, \alpha_s\right) = 0 \qquad (10)$$

Compounding and simple manipulations were then used to obtain more recognizable parameters for the solutions. When $(nD)/V_A$ was inverted, the result was the advance coefficient.

$$J = \frac{V_A}{nD} \qquad (11)$$

The Reynold's number was obtained by inverting $\mu/(\rho_W D V_A)$.

$$R_N = \frac{V_A D \rho_W}{\mu} = \frac{V_A D}{\nu} \qquad (12)$$

Through manipulation of $P_0/(\rho_W V_A^2)$ and $P_V/(\rho_W V_A^2)$, the cavitation number was acquired.

$$\sigma = \frac{P_0 - P_V}{\frac{1}{2}\rho_W V_A^2} \qquad (13)$$

The Weber number was given by inverting $s/(\rho_W D V_A^2)$.

$$W_S = \frac{\rho_w D V_A^2}{s} \qquad (14)$$

By taking the square root and then inverting $(gD)/(V_A)^2$, the Froude number was obtained.

$$F_S = \frac{V_A}{\sqrt{gD}} \qquad (15)$$

When $T/(\rho_W D^2 V_A^2)$ was compounded with $([nD]/V_A)^2$, the result was the propeller thrust coefficient.

$$k_t = \frac{T}{\rho_w n^2 D^4} \qquad (16)$$

Finally, the gas content ratio was obtained by compounding α and α_S.

$$a_S = \frac{\alpha}{\alpha_S} \qquad (17)$$

A summary of the dimensionless parameters is provided in Table 2. Based on these dimensionless parameters, equation (18) was written for the area of erosion parameter.

$$\frac{A_0}{D^2} = \phi\left(\frac{k}{D}, \frac{z}{D}, \frac{V_A}{nD}, \frac{V_A D}{\nu}, \frac{P_0 - P_v}{\frac{1}{2}\rho_w V_A^2}, \frac{P_0}{\rho_w V_A^2}, \frac{\rho_w D V_A^2}{s}, \frac{tV_A}{D}, \frac{V_A}{\sqrt{gD}}, \alpha, \frac{\alpha}{\alpha_S}\right) \qquad (18)$$

Equation (19) was written for the thrust coefficient.

$$\frac{T}{\rho_w n^2 D^4} = \phi\left(\frac{k}{D}, \frac{z}{D}, \frac{V_A}{nD}, \frac{V_A D}{\nu}, \frac{P_0 - P_v}{\frac{1}{2}\rho_w V_A^2}, \frac{P_0}{\rho_w V_A^2}, \frac{\rho_w D V_A^2}{s}, \frac{V_A}{\sqrt{gD}}, \alpha, \frac{\alpha}{\alpha_S}\right) \qquad (19)$$

DIMENSIONLESS PARAMETER	FORMULA
Roughness Parameter	k/D
Propeller Clearance Parameter	z/D
Advance Coefficient	$V_A/(nD)$
Reynold's Number	$(V_A D)/\nu$
Cavitation Number	$(P_O-P_V)/(\frac{1}{2}\rho_W V_A^2)$
Pressure Coefficient	$P_O/(\frac{1}{2}\rho_W V_A^2)$
Weber Number	$(\rho_W D V_A^2)/s$
Test Duration Parameter	$(tV_A)/D$
Froude Number	$V_A/(gD)^{1/2}$
Gas Content of Tunnel Water	α
Gas Content Ratio	α/α_S
Thrust Coefficient	$T/(\rho_W n^2 D^4)$
Area of Erosion Parameter	$A_O/(D^2)$

Table 2: Summary of Dimensionless Parameters

3.1.3 Criteria for Model Cavitation Experiments

The objective of the erosion study was to determine the area of erosion that a model propeller in blocked flow would experience as a result of the extreme wake behind the blockage. The results from these tests are relative to one another and cannot be scaled to give full scale erosion. Rather, they are used to assess the erosive characteristics of different flow conditions. Therefore, when performing model experiments, it is important to model the full scale phenomenon as closely as possible. As illustrated through the original dimensionless equations, (2) and (3), there are many variables which may affect the outcome of a cavitation erosion test (or a thrust performance test). Through the use of dimensional analysis, it was possible to combine these variables into dimensionless parameters. Therefore, the number of experiments that were required was reduced since there were fewer parameters to examine.

The relevance and importance of each dimensionless parameter listed in Table 2 was examined before the model experiments were designed. This was necessary since it is not possible to satisfy the conditions of all parameters simultaneously (i.e. the Froude number and the Reynold's number can not be simultaneously satisfied at model scale). By examining the relevance of the parameters, it was possible to reduce the required number of experiments as the effects of certain parameters were shown to be minimal. Some of these parameters have been examined previously in cavitation research and their application to cavitation testing is common knowledge (Harvald, 1983).

Geometric similarity is easily realized by using a scale model of the propeller. To minimize scale effects, the models were constructed with the largest diameter that could be accommodated in the cavitation tunnel (in this case, the diameter was 200 mm) without incurring tunnel wall blockage effects.

Kinematic similarity during a cavitation test can be achieved if the advance ratio is the same for the model and the full scale propeller. This requirement was easily met.

For dynamic similarity, both the Reynold's number and the Froude number must be satisfied. As was previously stated, it is not possible to simultaneously satisfy both of these conditions at model scale. During cavitation tests, the Reynold's number must not be allowed to fall too low ($R_N \approx 10^6$ according to Harvald, 1983), otherwise there is a risk that laminar flow will exist over the propeller blades. Therefore, to ensure that the flow over the propeller blades is entirely turbulent, equality of the Reynold's number is taken as an important test requirement and the Froude number is ignored. Also, gravitational

acceleration, and hence again, the Froude number, can be ignored since there is no free surface in the cavitation tunnel test section.

To ensure the same risk of cavitation at model scale, equality of the cavitation number with the full scale value must exist. Since the tunnel pressure was controllable, the pressure coefficient, and hence the cavitation number, were controllable. A common variation of the cavitation number (van Manen and van Oossanen, 1988), shown in equation (20), was used for the experiments that have been reported here.

$$\sigma = \frac{P_o - P_v}{\frac{1}{2} \rho n^2 D^2} \qquad (20)$$

At full scale, cavitation occurs in water that is at or near the gas saturation point. To ensure that the same risk of cavitation exists between full scale and model scale, the gas content ratio, α/α_S, should be equal to the ratio of the ambient test pressure to atmospheric pressure, P_O/P_{ATM}. Additionally, the gas content ratio must not be permitted to fall below 0.3 (Harvald, 1983). If the ratio falls below this value, there will not be enough undissolved gas in the water to stimulate cavitation inception. It has been shown experimentally that the gas content has an effect on the erosion damage rate: the gas content will influence the extent and thickness of any cavities that develop (Stinebring, 1977; Auret et al., 1993). Therefore, it is also important to ensure that the gas content is not too high relative to the pressure ratio, otherwise, cavitation may not be accurately modelled. The gas content, α, and hence α/α_S, were controlled during experimentation (see Section 3.3.3 and Section 3.3.4 for values used during testing).

Another parameter related to cavitation inception is roughness. If the tests were concerned with determining the cavitation inception point, then roughness would have been important. However, since the propeller operated in an extreme wake, there was no need to promote turbulence over the blades as cavitation occurred readily. Therefore, this parameter was ignored. Even for open flow tests, this was ignored since past experience showed that the flow would be turbulent provided that $R_N \approx 10^6$ (Harvald, 1983).

It was not possible to satisfy Weber's law, which is related to the surface tension of the cavitation bubbles, as the water velocity would not be high enough, even if the Reynold's number was satisfied. The remaining parameters, namely the propeller clearance parameter and the test duration parameter were easily complied with.

While temperature changes do indeed have an effect on viscosity and density, temperature was not included as a variable in the analysis. Despite the fact that the water temperature usually increased by one or two degrees during an experiment, it was assumed to remain constant for the duration of each test. The effect of temperature changes over such small ranges does not greatly affect test results, as was discussed by Auret et al. (1993a). Presently, there is no way to control the water temperature in the tunnel. Additionally, the temperature changes which would occur at full scale during a blockage event only cover a small range (e.g. no more than a few degrees Celsius).

Finally, the type of ink that was used as the soft film was not included in the dimensional analysis. The choice of ink was based on past knowledge from previous experiments that have been reported in the literature (Lindgren and Bjärne, 1976; Kato et al., 1981). Additionally, since the test results were relative, the important consideration

was that the same type of ink be used for each test so that the results could be compared directly with one another.

3.2 Test Apparatus

3.2.1 Cavitation Tunnel and Associated Equipment

All erosion tests for this study were completed in the cavitation tunnel at the Institute for Marine Dynamics (IMD). The cavitation tunnel facility has been described previously (Doucet, 1992b), including procedural descriptions for operation of both the water system and the vacuum system (pressure control). Principal details of the tunnel's test section are presented in Table 3. A schematic of the tunnel is shown in Figure 6.

Test Section Dimensions:	0.5 m x 0.5 m x 2.2 m
Water Speeds:	0 - 12.0 m/s
Propeller Speeds:	0 - 60 RPS
Test Section Pressures:	0.1 - 1.0 atm.

Table 3: Test Section Particulars

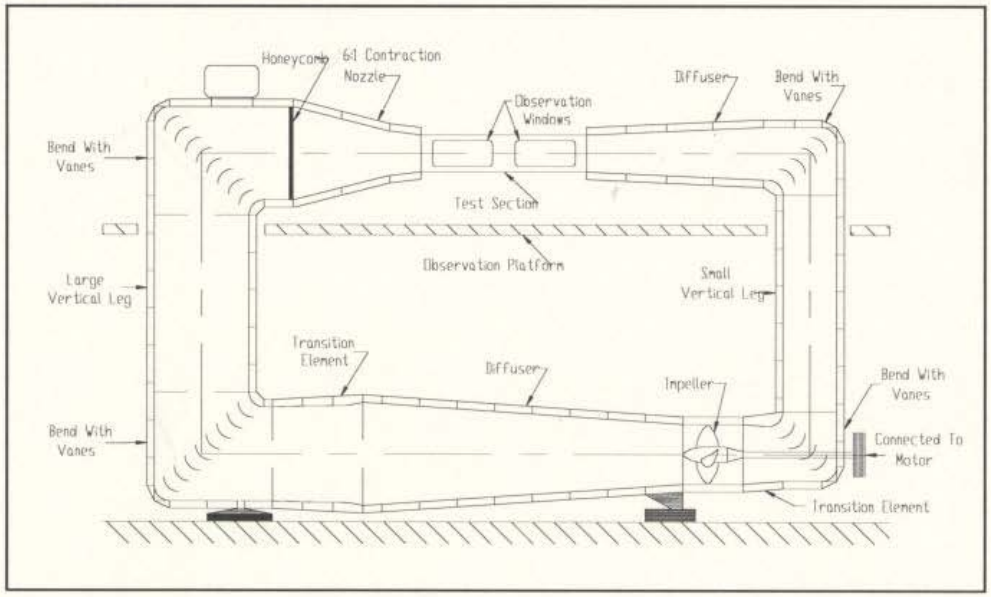

Figure 6: Cavitation Tunnel Schematic (from Doucet, 1992b)

During experimentation, the water velocity through the test section was measured using a differential mercury manometer. This device was connected across the upstream diffuser at the position of the shaft centerline, as illustrated in Figure 7. The tunnel pressure at the shaft centerline was measured using a second mercury manometer. Documentation exists which describes the calibration and operation of these instruments (Doucet, 1992a).

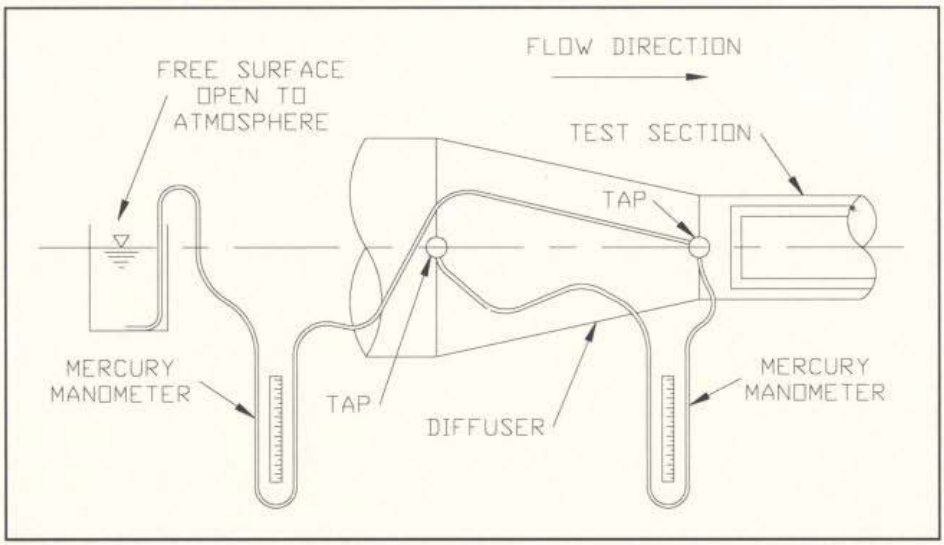

Figure 7: Test Section Velocity and Pressure Measurements

Gas content measurements were made with a *YSI Model 50B Oxygen Content Meter* (see Figure 8). Temperature measurements were also made with the *Model 50B* instrument.

All tests were documented using both 35 mm still photography and *VHS Video* equipment. The apparent motion of the propeller was slowed or frozen through the use of a variable frequency strobe light (see Figure 9). The operation manual for the strobe light is included in Doucet (1992b).

Figure 8: *YSI Model 50B* Oxygen Content Meter

Figure 9: *STROBOLUME Type 1450* Variable Frequency Strobe Light (from Doucet, 1992b)

3.2.2 Open Propeller and Blockage

The propeller used for the first series of tests was a 200 mm diameter model of the 1200-Series open propellers fitted to the Canadian *R-Class* ice-breakers. The model was constructed using CNC machining and was milled to an accuracy of ±0.05 mm. Propeller characteristics are given in Table 4 and the blade outline is shown in Figure 10.

Number of Blades:	4
Diameter:	0.2 m
Pitch/Diameter Ratio (r/R=0.75):	0.779
Expanded Area Ratio (A_E):	0.670

Table 4: Open Propeller Model Particulars

For these experiments, an ice blockage was simulated by using a rectangular block of high density polyethylene (HDPE) which measured 210 mm x 210 mm x 75 mm. To allow for different degrees of blockage to be examined during testing, the block was made with three laminates such that one or two of these could be removed for any given test. The block was attached to the top of the test section with two aluminium struts.

To simulate the flow which would exist behind an ice piece during a milling event, a 50 mm recess was cut into the block. The shape of this recess corresponded to the swept contour which would result if the propeller had partially milled a channel through the block. During testing, the propeller was operated within the recess and the minimum clearance between the blades and the block was approximately 1 mm. The orientation of the block and the propeller is illustrated in Figure 10.

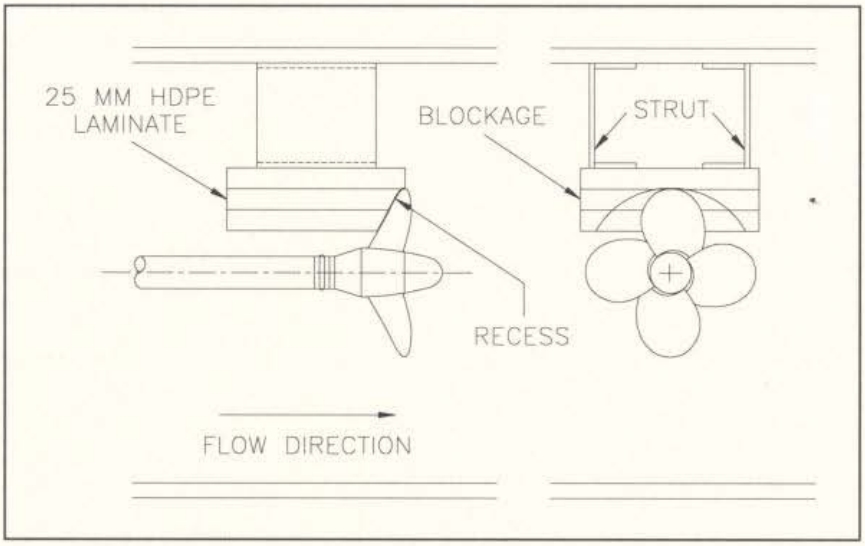

Figure 10: Open Propeller Test Apparatus (from Doucet et al., 1995a)

3.2.3 Ducted Propeller and Blockage

For the second series of experiments, the propeller used was a 200 mm diameter model of the ducted controllable pitch propeller fitted to the supply vessel *MV Robert LeMeur*. Made from brass, this model was also constructed using CNC machining and was milled to an accuracy of ±0.05 mm. This model was variable pitch, but it was necessary to set the pitch before the model was installed in the tunnel. The propeller hub consisted of two pieces which were held together in the longitudinal direction with four

screws. Machined grooves in the hub provided seating locations for the blade palms. Once the blades were positioned at the proper pitch angle (using pitch pins), the screws were tightened to prevent blade movement. There was no capability to change the blade pitch while the model was installed in the tunnel.

The model of the duct, which was attached to the top of the tunnel with a single brass strut, was constructed from clear polycarbonate to allow for observation of the cavitation patterns inside the nozzle during the experiments. Principal characteristics for the propeller and the nozzle are given in Table 5. The cross-section of the duct is illustrated in Figure 11. The blade outline for the propeller is illustrated in Figure 12.

PROPELLER PARTICULARS	
Number of Blades:	4
Diameter:	0.2 m
Pitch/Diameter Ratio (r/R=0.7; ϕ=25°):	1.096
Expanded Area Ratio (A_E):	0.604
NOZZLE PARTICULARS	
Length:	0.100 m
Inside Diameter:	0.202 m

Table 5: Ducted Propeller Model and Nozzle Model Particulars

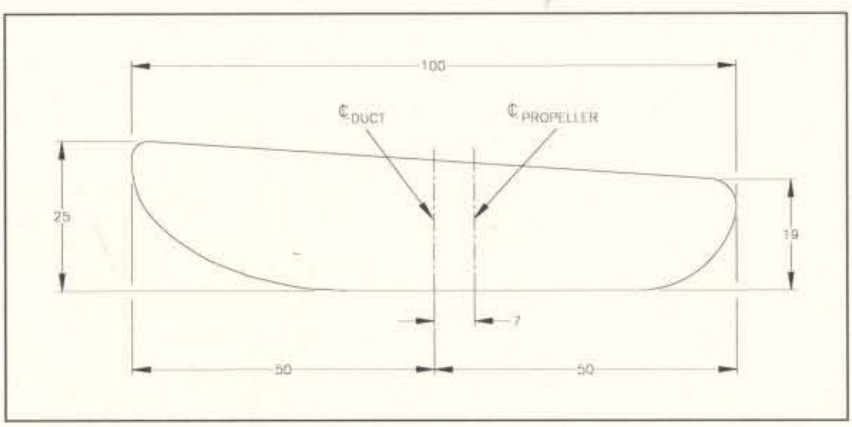

Figure 11: Nozzle Cross Section

For the ducted propeller tests, an ice blockage was simulated by using a block of HDPE with dimensions of 240 mm x 240 mm x 75 mm. This block, also a three-tiered laminate, was attached to the top of the test section with two brass struts.

The downstream portion of the block was fitted flush to the inside surface of the duct. To simulate the flow which would exist during an ice milling event, the end of the block was formed so that its shape corresponded to the swept contour which would result if the propeller had partially milled the block. During testing, the minimum clearance between the block and the extreme edge of the blades was approximately 1 mm. The orientation of the block, nozzle and propeller is illustrated in Figure 12.

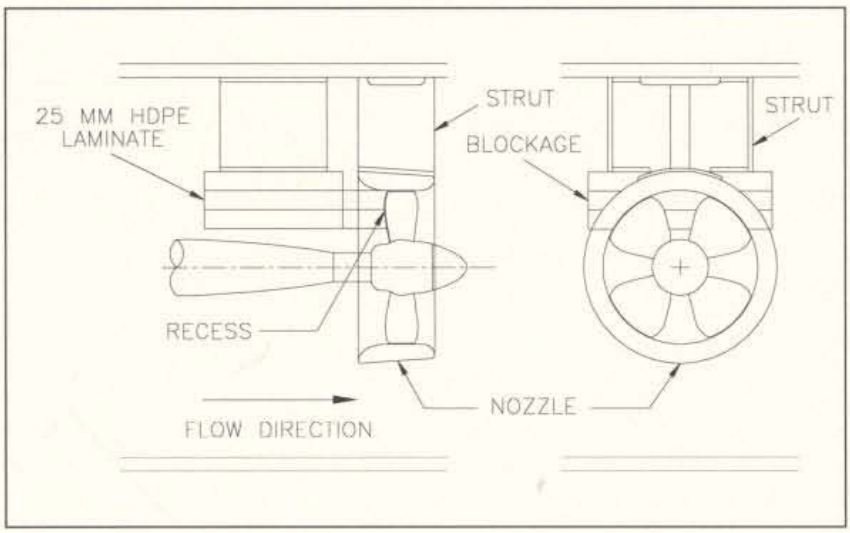

Figure 12: Ducted Propeller Test Apparatus (from Doucet et al., 1996)

3.3 Methods

3.3.1 Paint Application for Soft Film Tests

For soft film erosion testing, a standard film was proposed by the 14th ITTC Cavitation Committee and a standard procedure for its application was also proposed

(Kadoi and Sasajima, 1978). The recommendation was that roller system stencil ink should be used and applied according to stringent conditions. Unfortunately, it is necessary to let the stencil ink dry for at least twelve hours before attempting to perform an erosion test. During any large scale test program, it is quite impractical to have to wait this length of time before beginning an experiment. For this reason, it was desirable to choose another ink as the soft surface for these erosion tests.

When stencil ink is not used for erosion paint tests, lacquer based inks are often used. Initially, the soft film which was used for these tests was *Crown Blue Toolmakers Ink*. This lacquer based ink is similar to *AOTAK*, which is commonly used at the University of Tokyo for erosion tests (Yamaguchi, 1993). Results from past experiments have shown that the use of *AOTAK* provides reliable results for erosion tests (Kato et al., 1981). One of the benefits of using *Crown Blue Toolmakers Ink* was the short drying time for the product (a few minutes). For the tests reported here, a minimum of 30 minutes of drying time was allowed to elapse before the propeller was immersed in water.

Before each experiment, a strict procedure was followed for surface preparation and paint application. Before the ink was applied, the propeller was thoroughly cleaned with methanol to remove all dirt, oil and grease that may have accumulated on the surface. Methanol was also the solvent used to remove old ink from previous tests. Once the propeller was cleaned, all subsequent handling was done by holding on to the hub so as to avoid contaminating the freshly cleaned blade surfaces.

Since an aerosol was used as the application medium, the propeller was painted under a fume hood to dissipate any vapours emitted by the ink and the propellant. Ink

was applied to one side at a time since the model was resting on a small table. The idea behind the painting process was to allow tiny particles of ink to accumulate on the surface, rather than to soak the surface with a wet layer of ink. A wet layer of ink would generally run down the blade causing sags in the painted surface and resulting in non-uniform ink thickness over the blade.

Therefore, rather than using a continuous spray, a number of sweeping passes were made over each blade to allow the surface to be "speckled". During each pass, the aerosol can was held approximately 25 - 30 cm away from the model and perpendicular to the blade surface. To achieve uniform ink thickness during each pass, the spray was initiated before the ink came into contact with the blade surface and was only terminated after the ink spray had completely passed over the blade. A waiting period of a few seconds was observed before performing the next pass. This process was continued until the entire surface of the blade was covered and no metal was visible.

Crown Blue Toolmakers Ink was used for the open propeller tests. Initial tests results were acceptable, however, the ink was not ideal. Some paint peel did occur during testing, but the areas affected by paint peel were easily identified based on the nature of the eroded areas on the blades. If peel occurs, strips of paint are removed, thereby leaving identifiable marks (e.g. see Figure 39). During a proper paint test, erosion will occur as paint removal of tiny flecks of the soft surface.

Towards the end of the open propeller test program, the onhand supply of this ink ran low, necessitating the purchase of additional stock. However, the new supply proved to be unacceptable as paint peel became a significant problem. The propellant used for

the aerosol had been changed and this had adverse effects on the adhesivity of the product when it was immersed in water (e.g. see Figure 39).

Due to the paint peel problem which had developed, it was necessary to select a new ink to be used during the ducted propeller tests. Following trials with different brands of similar lacquer based marking inks, including *Starrett Kleenscribe Blue Layout Dye*, which still provided unacceptable results, a different approach was taken. A pen type, black permanent marker (*Avery Marks-A-Lot* marker), similar to that found in a stationery store, was used. Trials with this marker gave excellent results and no peel was evident, as shown in the ducted propeller test results of Figure 48 through to Figure 62.

As with the *Crown* product, a strict application procedure was followed. Surface preparation remained the same as that previously outlined. Before each test, the ink was applied to the blades in a standard manner: the edges of the blades were covered first, then starting at the tip and working towards the blade root, the marker was applied in the chordwise direction using overlapping strokes. Once the application procedure was started on any blade surface, it was not interrupted until that surface had been completely covered. Due to the quick drying time of the ink, this procedure was used to ensure that the film thickness would be as uniform as possible. To ensure that the ink was sufficiently dry before testing, a minimum of 30 minutes was allowed to elapse before the painted model was immersed in water.

3.3.2 *Pressure Sensitive Film Application*

Two experiments with pressure sensitive film were attempted using the ducted propeller model. The test results are discussed in Chapter 4. For these tests, *FUJIFILM PRESCALE* was applied to the surface of the blades based on the locations that were determined from the soft film tests. As discussed by Kato et al. (1981), *PRESCALE* has been used for propeller experiments, whereby it was secured to the model surface using an adhesive tape coated with a thin aluminium film. *PRESCALE* consists of two sheets which are superimposed on one another: one is composed of microencapsulated color forming material while the second has a layer of color developing material. Manufacturer's information is included in Appendix A.

Before the *PRESCALE* was applied, the propeller surface was cleaned as per the procedure outlined for paint tests. Following this, appropriate sizes of the *PRESCALE* sheets were cut, superimposed upon each other and positioned on the blades. Aluminium foil duct tape was used to hold the sheets in place. Since exposure to water causes the developed colour on the sheets to run, it was necessary to ensure that the sheets would be waterproof. This requirement was also to be met through the use of the duct tape. Care was taken to ensure that no air bubbles were trapped beneath the tape during application.

3.3.3 *Open Propeller Test Plan*

Based on the analysis shown previously in this chapter, a test plan was developed for the open propeller model. The actual test conditions are given in Table 6. The data sheets from each open test are found in Appendix B.

For these experiments, the gas content ratio, α/α_S, was set to within ±10% of the pressure ratio. As previously indicated, tests could be performed with the gas content ratio at a value of about 0.3 or above. The corresponding pressure ratio (P_D/P_{ATM}) would therefore be 0.3. However, due to a small air leak in the test section, the tunnel pressure could not be lowered below about 40 kPa. To do so would have introduced a large quantity of entrained air into the flow. Therefore, the lowest pressure that was used was 40 kPa and the corresponding gas content ratio was approximately 0.4.

Kadoi and Sasajima (1978) showed that a 15 minute duration test was suitable for an erosion test of this type. They reported that a 15 minute test gave almost the same results as a 30 minute test. For the experiments reported here, the test duration was set at 15 minutes once propeller speed reached the desired setting. To determine if this time frame was reasonable for the ink used, a 30 minute test was also performed.

One test was performed at atmospheric pressure to represent the non-cavitating condition (i.e. higher cavitation number). All other tests were performed at a nominal cavitation number of approximately 3.0. This value was slightly below the full scale cavitation number of 3.8 for this propeller.

The advance coefficient was varied as the full scale propeller may experience ice blockage conditions over a range of advance coefficients. Additionally, the effect of reducing the degree of blockage (two laminates instead of three) was also examined over a range of advance coefficients.

For most of the blocked tests, the nominal gap between the block and the extreme edges of the blades was 1 mm. The effect of proximity was examined by changing the gap while the advance coefficient was kept constant (J = 0.4). Additionally, one test was performed in unblocked flow (at reduced pressure) to provide a baseline for the comparison of erosion results.

Due to paint peel problems, some tests were added after the test program was underway. Test O-12 was added as a repeat of Test No. O-9 using the same ink. Test No. O-13 was a repeat of Test No. O-1, but a different ink was used (*Starrett Kleenscribe Blue Layout Dye*). Test No. O-15 was a repeat of O-14 using the *Crown* product as the soft surface. Finally, Test No. O-16 was also a repeat of O-14, but the *Starrett* dye was used instead of the *Crown* dye.

Test No.	J	σ	Degree of Blockage	Proximity (mm)	Duration (min)
O-1	0.40	2.99	3	1	15
O-2	0.20	8.36	3	1	15
O-3	0.61	3.09	3	1	15
O-4	0.20	3.13	3	1	15
O-5	0.40	3.06	3	1	30
O-6	0.20	3.12	2	1	15
O-7	0.40	3.08	2	1	15
O-8	0.61	3.10	2	1	15
O-9	0.40	3.07	3	5	15
O-10	0.39	3.13	3	10	15
O-11	0.40	3.09	3	20	15
O-12	0.40	3.16	3	5	15
O-13	0.41	3.03	3	1	15
O-14	0.39	3.00	0	-	15
O-15	0.47	2.98	0	-	15
O-16	0.43	2.98	0	-	15

Table 6: Open Propeller Test Conditions (Measured)

3.3.4 Ducted Propeller Test Plan

The test plan used for the ducted propeller experiments, as shown in Table 7, was similar to that which was developed for the open propeller. This was done to allow the test results from each model to be compared with one another. Three significant differences must be noted. First, ducted tests with a reduced degree of blockage (i.e. less than three laminates) were not performed as a result of time constraints during this phase of testing. Second, it was not necessary to repeat tests since the new ink used provided excellent results. Third, as the propeller model was variable pitch, the pitch presented an additional variable whose effects could be examined. The data sheets from each experiment are found in Appendix C.

As was the case for the open propeller, the limitations on the gas content ratio and the test section pressure were taken into account for these ducted propeller tests. Additionally, due to equipment limitations, there was an upper limit on the shaft revolutions which were used during the ducted tests.

When the test apparatus was evaluated in open flow conditions prior to block installation, duct vibration occurred at propeller speeds of approximately 1275 RPM. This factor was critical since the clearance between the blade tips and the duct was approximately 1 mm. When exposed to the extreme wake that was generated by the blockage, propeller and/or duct damage may have occurred if the propeller was operated at higher revolution rates. Therefore, the revolution rate used during testing could not be increased beyond approximately 1200 RPM. No duct vibration was noted during tests (including blockage) that were performed near 1200 RPM.

For the full scale ducted propeller, the cavitation number was determined to be approximately 1.8. However, it was not possible to achieve a cavitation number below approximately 4.5 for the ducted propeller tests. To reduce the cavitation number of the model below 4.5, it would have been necessary to either further increase the revolution rate or further decrease the test section pressure. Both of these options were unavailable as a result of the previously described limitations (see above and Section 3.3.3).

As with the open propeller tests, the gas-content ratio was set within ±10% of the pressure ratio. Nominal test time was set at 15 minutes, with a 30 minute test being performed to evaluate the new ink. One test was performed at atmospheric pressure to represent the non-cavitating condition. All other tests were performed at the same cavitation number. Variation of both advance coefficient and proximity were examined.

Test No.	J	σ	Degree of Blockage	Proximity (mm)	Duration (min)	ϕ (deg)
D-1	0.41	4.73	3	1	15	25
D-2	0.42	4.81	3	1	30	25
D-3	0.38	12.56	3	1	15	25
D-4	0.17	4.75	3	1	15	25
D-5	0.65	4.66	3	1	15	25
D-6	0.42	4.73	3	5	15	25
D-7	0.49	4.64	0	N/A	15	25
D-8	0.44	4.72	3	20	15	25
D-9	0.41	4.73	3	1	15	10

Table 7: Ducted Propeller Test Conditions (Measured)

As previously mentioned, the propeller model was of variable pitch design and the pitch had to be set before the experiments. For all tests except D-9, the pitch angle was set at 25°, which was the maximum pitch setting for the full scale propeller and

corresponded to the operational setting used when the propeller was involved in ice-breaking activities (Laskow et al., 1986). Test No. D-9 was placed at the end of the test program so that it was not necessary to change the pitch, once initially set, until all tests at $\phi = 25°$ had been completed. Two tests using pressure sensitive film were attempted, before Test No. D-9, with a blade/block gap of 20 mm. These tests are described in Chapter 4.

3.3.5 Typical Test Procedures

The procedures outlined below were followed for all cavitation tunnel tests. Particulars concerning the operation of cavitation tunnel equipment are discussed by Doucet (1992b). Additional references concerning equipment operation are provided where necessary.

In preparation for a cavitation test, the first step performed was to de-aerate the tunnel water until the gas content ratio was at the required level. To do this, water was drawn from the bottom leg of the tunnel, using the water pump, and sprayed into the air space at the top leg of the tunnel (at the upstream diffuser). While the water was sprayed into the tunnel, the vacuum pump was operating, drawing excess air and water vapour out of the tunnel. This process was continued until the gas content was at the desired level.

Once the gas content ratio was set, the water level in the tunnel was lowered and the model propeller was installed. Care was taken when handling the model to ensure that the ink surface was not damaged. If necessary, adjustments to the gap between the propeller and the block were made at this time. Water temperature was also measured.

The model was only installed immediately prior to the execution of an experiment. This was done as a precautionary measure to avoid excessive exposure of the painted model to water. Prolonged immersion may have had adverse effects on the adhesivity of the ink. During these experiments, no adverse effects, such as bubbling of the painted surface, were observed due to water immersion.

Following installation, the water level was raised and all pre-test adjustments were made. These adjustments included generator start-up, purging air bubbles from the manometer lines and removal of the air pocket in the diffuser downstream of the test section. Video and photographic equipment were also readied.

Tunnel pressure, as measured at the centreline of the test section, was then lowered to the required level using the tunnel's vacuum system. Following this, the water velocity was set, but slightly below the required value. It was not set exactly as propeller rotation had not been initiated. Operation of a propeller in the tunnel induces a slight increase in the flow velocity: since the tunnel is a closed system, propeller rotation causes some water circulation. Once the flow speed stabilized, it was necessary to increase the tunnel pressure slightly: water circulation causes a reduction in the test section dynamic pressure. After this adjustment, the propeller revolution rate was ramped up to the required value over a period of approximately 10 seconds. The slow increase in the revolution rate was used primarily to prevent shock loading of the model and the propeller shaft components. Additionally, damage to the soft surface due to sudden water acceleration (before cavitation occurred) could be avoided.

It was noted that cavitation generally commenced about half way through the ramp-up period. The timer was started as soon as the propeller reached the desired revolution rate. The tunnel pressure and the flow velocity were then re-checked and, if necessary, re-adjusted. Propeller revolution rate, water velocity and tunnel pressure were re-checked periodically to ensure that all were at the required settings.

During a test, photographs and video were taken from both sides of the test section. For illumination, a camera flash was used for photographs while the strobe light was used with the video equipment. No other light sources were active during testing. After this, observations of the cavitation patterns were made until the test was completed.

Once the required time had elapsed, the propeller revolution rate and the water velocity settings were quickly reduced and then set to their null positions. The tunnel was re-pressurized, the generator was shut-down, and the water level was lowered.

With care, the model was then removed from the test section. The model was quickly examined to determine if there was any evidence of lifted paint on the surface. (Lifted ink indicates that paint peel occurred during testing.) Gas content and water temperature were also measured. The erosion results, both face and back, were then recorded on the bench using both video and photographic equipment.

3.4 Measurement of Erosion Results

3.4.1 Overview

Upon completion of the experimental work, the images containing the test results were analyzed to provide erosion area estimates. Photographs and video records provide

only two dimensional representations of their subjects. For example, they do not account for the twist in the propeller blades (i.e. pitch angle of the blades, rake, etc.). Therefore, any areas measured using image analysis software are projected areas only: the actual areas are underestimated. To determine the actual areas, corrections must be applied to account for the blade pitch.

3.4.2 Image Processing

Since the erosion results were available as both photographic and video records, it was necessary to choose which record type would be used for area measurements. Single images could have been captured from video using a frame grabber and the appropriate software, however, the images would not have been as clear as if photographs were used.

Therefore, the photographic records were scanned into digital format as colour images and saved as computer files (PCX format). Image scanning was accomplished using *DESKSCAN II* software and a *Hewlett Packard ScanJet IICX* scanner. Once scanned, image fine-tuning was completed using *ALDUS PHOTOSTYLER* software. While fine-tuning included adjusting image focus if necessary, the primary purpose of this step was to ensure that the contrast between painted and eroded areas was great enough to be discernible on the computer screen. As a result, both brightness and contrast were adjusted if necessary.

Once the images were scanned and fine-tuning was completed, the actual measurement process was started. Area measurements were made using *MOCHA* Image Analysis Software (Jandal Scientific, 1993a, 1993b and 1994). Essentially, to measure

areas with this software, it is necessary to place an overlay on the regions to be measured. The area measurements, given for each separate section of the overlay, are then based on the number of pixels in each section of that overlay. The results are given in square pixels unless the image has been calibrated to some other unit of measure. The procedure followed to analyze an image has been outlined below.

After one of the colour images was loaded into *MOCHA*, the first step in the analysis procedure was to convert the colour image to an 8 bit-per-pixel monochrome image. Following the conversion, the image was represented as 256 shades of gray: a pixel with an intensity of "0" was black while a pixel with an intensity of "255" was white. If necessary, image cropping was done at this time.

When a colour image is converted to a monochrome image, all of the intensity values are not necessarily used. For example, an image which does not have any "white" pixels does not make use of the intensity value of 255. To improve the contrast of the image and use the entire range of gray intensities, the "*Histogram Stretch*" feature was employed. This allowed the image's pixels to be re-mapped so that the full range of gray intensity values was used.

Before any measurements could be made, it was necessary to calibrate the image. Realizing that there was a "depth difference" in the image between the top and bottom edges of the blades, calibration was done using points which were known to be at a depth midway between the extreme top and bottom edges of the propeller blades. A two point calibration was utilized: using opposite blades, a point was chosen at the middle of each

blade tip and the propeller diameter (0.2 m) was used as the calibration value (see Figure 13). Even using this calibration value, there was still an error associated with measuring any area that was not at the same depth as the two points. No correction was applied for this error. This magnitude of this error was estimated to be approximately ± 5%.

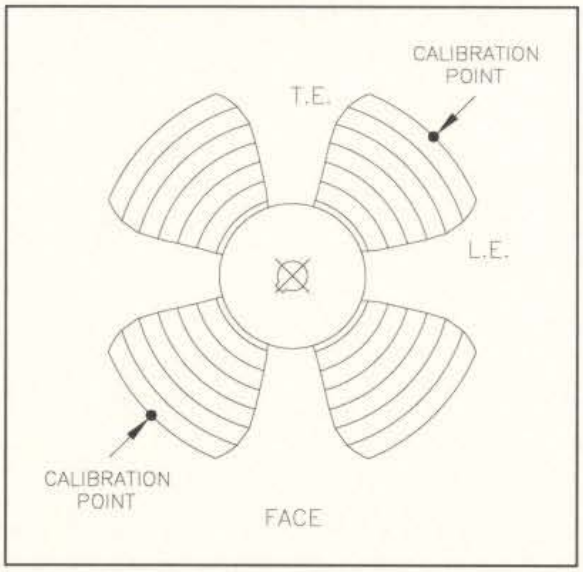

Figure 13: Location of Calibration Points (ducted propeller model)

When the test results were photographed, every attempt was made to ensure that the camera was located directly above the centre of the propeller hub. If the camera was not centred, then the lens would not be parallel to the propeller plane since the field of view for all photographs always centred on the propeller hub. Therefore, subsequent measurements would be underestimated as a result of the non-parallel planes. No correction was applied for this error. The magnitude of this error was estimated to be ± 3% (This corresponds to the lens being tilted at a 10° angle from the horizontal.)

Following image calibration, an overlay was applied to the eroded areas. *MOCHA* has four overlay levels that can be used. Adding overlays to an image does not alter the

image file unless the user indicates that permanent alterations are to be made. The overlays are saved with the same file name, but with different extensions for each overlay level. Since only one of these overlays can be referred to when measurements are made, all eroded areas had to be represented on the Level 1 overlay.

Using the "*Threshold Overlay*" feature, the threshold level was chosen such that all pixels above the threshold intensity (i.e. eroded areas) were covered with an overlay while all other pixels were unaffected. If necessary, pixels could then be manually removed from or added to the overlay to ensure that the proper regions were covered. Since lighting conditions were not ideal when the test results were photographed, each blade was illuminated to a different degree. Therefore, in most cases, it was necessary to apply the overlays to each blade separately. As a result, portions of overlays were first sized in the Level 2 overlay and then added to the Level 1 overlay using the "*Overlay Math*" feature.

Another possible source of error in estimating areas with *MOCHA* was related to image resolution. There was no clear dividing line between the eroded areas and the non-eroded areas, but rather, there was a gray transition zone between these light and dark regions. Since the image would have to be examined on the "pixel" level (i.e. magnified) in order to view the transition, it was felt that this error would be minimal. No correction was made for this error nor was an error value calculated.

Once all eroded areas had been represented on the Level 1 overlay, the area measurements were made. *MOCHA* assigned a number (saved on the Level 3 overlay) to each separate area that was measured, recorded the area measurements (in square

millimetres), and also calculated the major and minor axes lengths for each area. The major and minor axes were saved on the Level 4 overlay.

3.4.3 Area Corrections

Once the projected areas were measured with *MOCHA*, it was necessary to apply correction factors to account for the propeller pitch. For almost all propellers, the pitch angle is not constant and varies radially over the blade. The geometric pitch angle, ϕ, at any given radius is defined in equation (21) and is illustrated in Figure 2. The area correction calculation is shown in equation (22).

$$\phi = \mathrm{TAN}^{-1}\frac{P}{2\pi r} \qquad (21)$$

$$A_{Corrected} = \frac{A_{Projected}}{\mathrm{COS}\,\phi} \qquad (22)$$

Therefore, for a given projected area measurement, it was necessary to determine the radial location of the eroded region relative to the centre of the model. This was done by using *MOCHA* to measure the distance from the centre of the hub to the approximate centre of each eroded region. All r/R measurements were rounded to the nearest 0.05R. Once these were estimated, the area correction was applied using the appropriate pitch angle for that radial position. A sample table illustrating the calculation is shown in Table 8. The corresponding photograph (with overlays) is shown in Figure 14.

Ideally, an eroded area could have been discretized such that a pitch angle could have been applied for each elemental radii position. However, this would have been time

consuming. Additionally, based on the previously discussed errors, the additional level of accuracy achieved through discretization would have been questionable.

Once the actual areas had been determined for all eroded regions, calculations were completed which provided total eroded area measurements for each blade and for the entire propeller. Due to the paint problems that were alluded to earlier, it was necessary to ensure that regions affected by paint peel were not included in these area measurements. Therefore, a provision was included in the *EXCEL* spreadsheet to indicate whether or not a region was included in the blade area calculations.

		Propeller Model:		R-Class			
		Test No.:		O-1			
		Propeller Side:		Back			
Eroded Area No.	Blade No.	Measured Projected Area (mm^2)	r/R (Avg.)	Pitch Angle (ϕ) for r/R (deg)	Corrected Area (mm^2)	Included in Total Area Calc.	Inc. in Blade Erosion Calc.
1	2	136.8	0.75	18.3	151.7	Y	2
2	3	133.3	0.75	18.3	147.9	Y	3
3	4	304.3	0.60	22.1	354.4	N	Not Inc.
4	1	88.5	0.70	19.4	99.4	Y	1
5	4	163.7	0.75	18.3	181.6	Y	4
		Blade 1 Eroded Area (mm^2):			99.4		
		Blade 2 Eroded Area (mm^2):			151.7		
		Blade 3 Eroded Area (mm^2):			147.9		
		Blade 4 Eroded Area (mm^2):			181.6		
		Total Eroded Area (mm^2):			580.7		

Table 8: Sample Table Illustrating Area Calculations

In Chapter 4, the test results are presented as "% erosion" rather than actual area measurements (e.g. see Figure 41). The total blade surface area was required for this calculation. For each propeller, the corresponding expanded area coefficients (A_E) were used to determine the total blade surface area (one side) for each propeller. For the plots

which show "% erosion" of individual blades, the total blade surface area was divided by the number of blades (i.e. "4") for the calculation. While it was recognized that a more accurate determination of blade surface area would have resulted if the developed area coefficient (A_D) was used, A_E was used since the values for each propeller were readily available. Additionally, since neither of these coefficients account for blade thickness, the actual surface area can never be determined with 100% accuracy using coefficients.

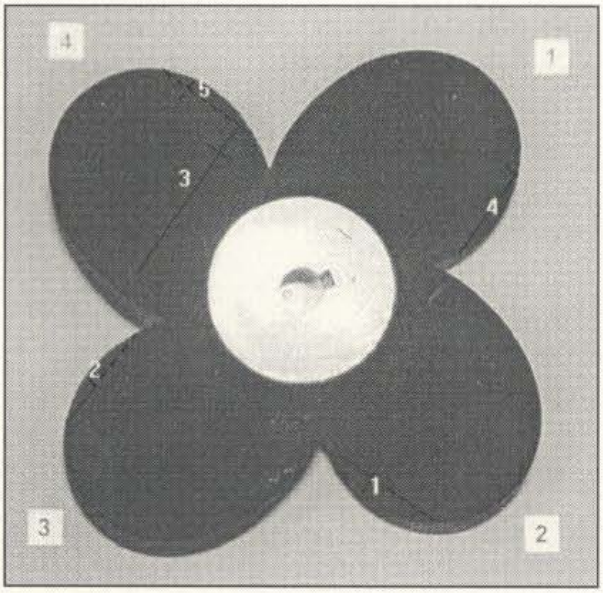

Figure 14: Test No. O-1 (Back) Showing Overlays

As a final note related to area measurements, it must be re-iterated that such results provide information on the extent of erosion which a propeller may experience. The results can not be scaled to give full scale erosion (i.e. depth or density of pits). However, the tests, and the results, are all relative and they are used as a guide to indicate which operating conditions are the least favourable. Therefore, in the next chapter, the area measurements, in conjunction with the cavitation descriptions, were used to assess the effects of proximity and to determine which conditions were the most severe.

Chapter 4
Test Results and Discussion

4.1 Open Propeller

4.1.1 Descriptions of Cavitation and Blade Erosion

Operation of the open propeller model in close proximity to the block resulted in violent cloud cavitation. This was accompanied by a substantial amount of noise and vibration. Cavitation descriptions for a generic ice-class propeller operating in similar conditions are reported by Walker and Bose (1994a). The cavitation patterns which were observed during Test No. O-1 are illustrated in Figure 15 and are described below. This description also relates blade erosion to the cavitation patterns. Preliminary erosion experiments with this propeller were reported previously (Doucet et al., 1995a). The cavitation patterns shown in Figure 15 are basically similar for all open propeller tests, with any differences being noted for subsequent experiments. For all erosion experiments, both open and ducted, the blade notation used in the erosion photographs is shown in Figure 16. The actual tests conditions are listed in Table 6 (see Section 3.3.3).

As the reference blade approached the block, but had not yet entered the recess, at an angle of $\theta = -90°$ (measured with respect to the vertical), there was no cavitation visible on the blade which could be attributed to propeller-ice interaction. A small,

unattached tip vortex was present which was similar to the cavitation that occurs in uniform flow.

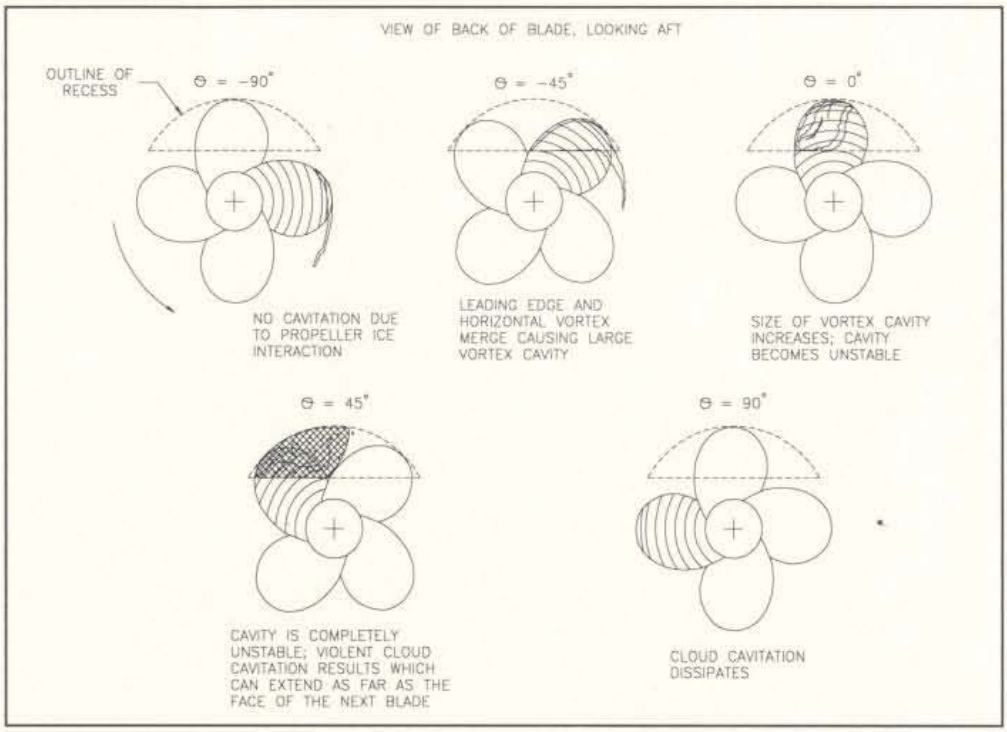

Figure 15: Typical Cavitation Patterns on Open Propeller in Blocked Flow (from Doucet et al., 1995a)

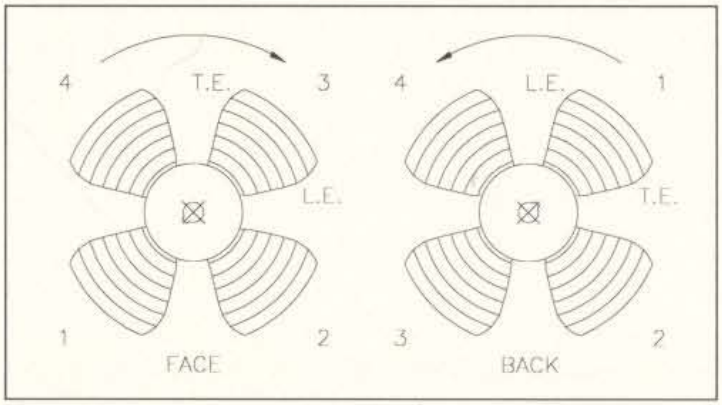

Figure 16: Blade Notation (from Doucet et al., 1996)

At $\theta \approx -80°$, the leading edge of the blade, near $r/R \approx 0.75$, entered the recess. On the face, a small amount of cavitation was present at this region. This was shed from the

cavity that was attached to the back of the previous blade which was passing through the recess. On the back of the reference blade, a stable sheet formed at the leading edge and covered the portion of the blade which was in the shadow of the block. Once the tip entered the recess, the tip vortex merged with the sheet and aided in its growth.

As the blade progressed from $\theta \approx -80°$ to $\theta \approx -45°$, the amount of leading edge face cavitation increased. When the blade reached $\theta \approx -65°$, the cavity shed from the back of the previous blade extended completely to the face of the reference blade, contacting the surface near the leading edge. On the back, the sheet cavity continued to grow. The cavity size fluctuated in an oscillatory manner such that it covered anywhere from half to all of the blade portion that was in the shadow of the block. Its stability continually degraded as the blade progressed through the recess.

Between $\theta \approx -45°$ and $\theta \approx 0°$, the amount of cavitation affecting the leading edge of the face continued to increase. Erosion of this region (see erosion in Figure 17) began near $\theta \approx -20°$ due to the impingement of violent cloud cavitation. The cloud was not causing erosion over the entire region simultaneously. As the blade progressed through the recess, the impinging cloud moved inwards along the chord towards the centre of the blade. On the back, the cavity size continued to increase, however, at $\theta \approx 0°$, it had almost completely broken down into cloud cavitation.

Leading edge erosion on the face continued until $\theta \approx 25°$, at which point the erosive cloud jumped to the mid-span region. On the back, the cavity continued to grow and extended from the back of the reference blade to the face of the following blade.

Impinging cavitation continued to move steadily across the face as the blade progressed through the recess. Face erosion of the mid-span region continued until the trailing edge left the recess at $\theta \approx 80°$. The impinging cloud then jumped to the trailing edge region, causing erosion until the cloud dissipated at $\theta \approx 95°$. As the blade left the recess, the cavity shed by the back separated and shrunk into two distinct entities: one influenced the back of the reference blade while the other impinged on the face of the following blade. Trailing edge back erosion began as the blade left the recess and continued until $\theta \approx 105°$, at which point the cloud cavitation had dissipated and transformed itself back into a tip vortex.

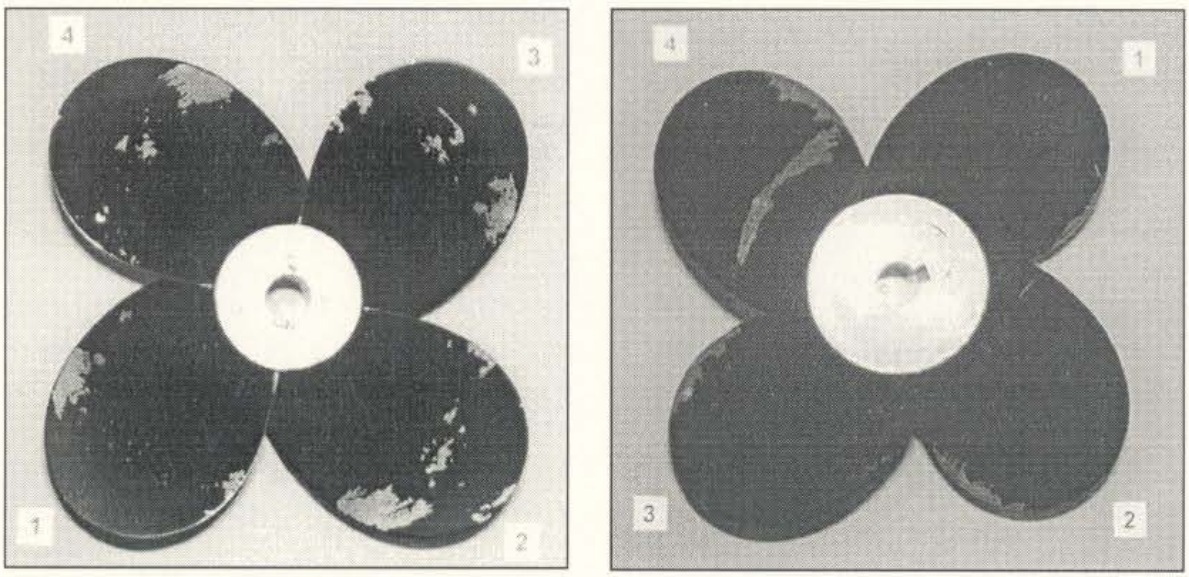

Figure 17: Erosion Results for O-1 (Face and Back: J = 0.40, σ = 2.99)

Experiment O-1, which was described above, was conducted at an advance coefficient, J, of 0.40 and a cavitation number, σ, of 2.99. Test results are illustrated in Figure 17. The outcome of Test No. O-2, performed at J = 0.20 and σ = 8.36, is

illustrated in Figure 18. This test, performed at atmospheric pressure, represented the "non-cavitating" condition. Back cavitation occurred when the reference blade was in the recess, but the cavity was not large enough to extend to the face of the following blade (see Figure 19). A small vortex was shed by the cavity, but it did not impinge on the face. Therefore, no face erosion occurred. The apparent erosion present on blade 1 was the result of paint peel (see Figure 18).

On the back, the cavity which formed when the blade entered the block's shadow did not fill the recess and was focused on the blade tip. This cavity became unstable near $\theta \approx 0°$, at which point erosion began. Erosion continued until the trailing edge left the recess, at $\theta \approx 80°$, and the remaining cavitation quickly dissipated. Paint peel was evident on blades 2, 3 and 4. Only the tip erosion should be present.

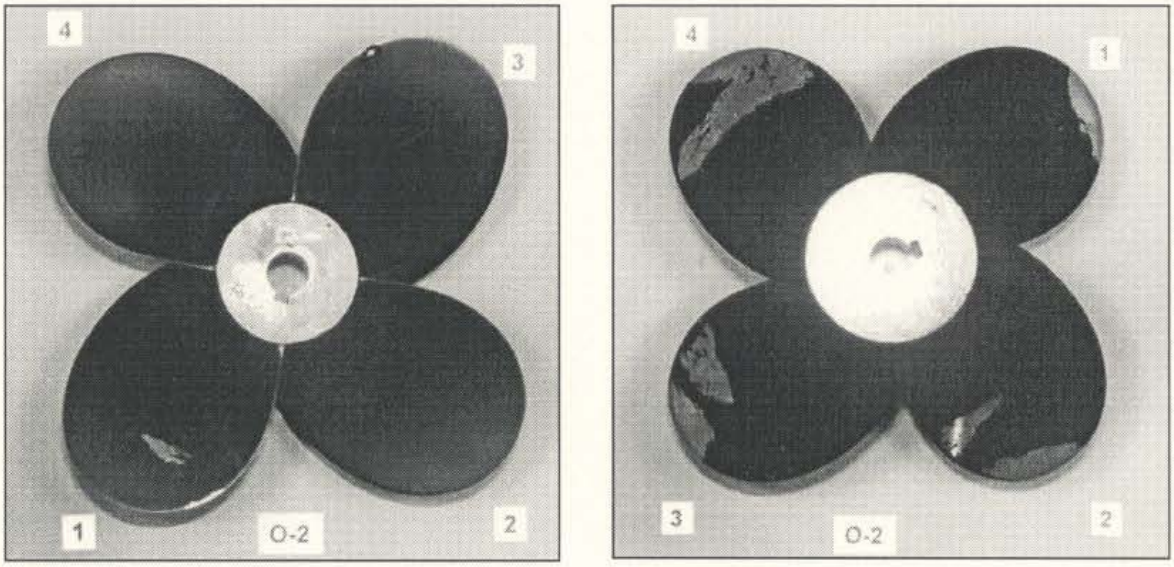

Figure 18: Erosion Results for O-2 (Face and Back: J = 0.20, σ = 8.36)

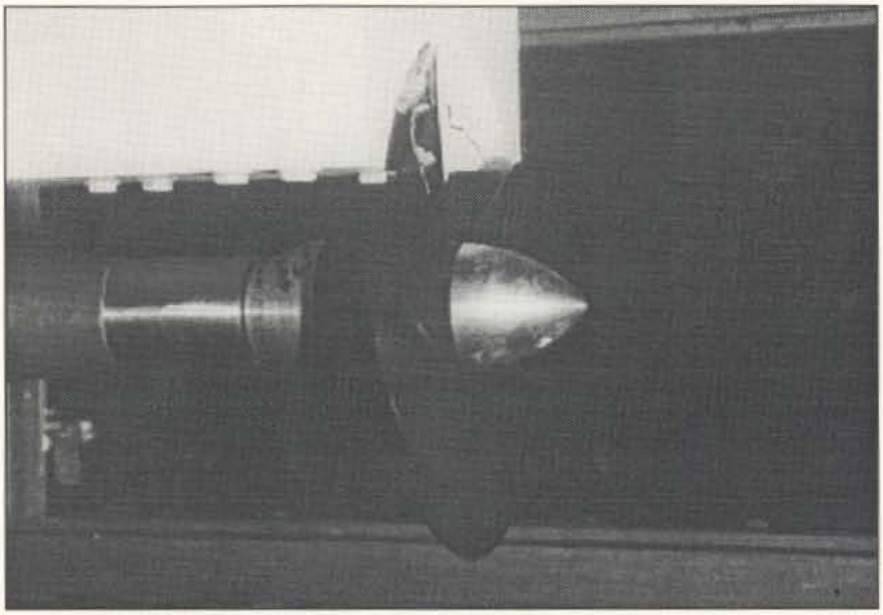

Figure 19: Cavitation During Test No. O-2

Cavitation during Test No. O-3, conducted at J = 0.61 and σ = 3.09, is shown in Figure 20 and the test results are presented in Figure 21. During this test, some entrained air bubbles were visible in the test section. The resulting locations of face erosion were similar to those from O-1, but more erosion was present. This increase in erosion was attributed to the higher advance coefficient: the differences between the blocked flow region and the unblocked flow region, as each blade operated within and outside the wake of the blockage, were greater than they were for O-1 (J = 0.40). The amount of back erosion was marginally less than that of O-1, but the same locations were affected. Some paint peel did occur during this test as the shape of the eroded regions on the face differed significantly from blade to blade. Back erosion should be present only along the trailing edges. Spots on the leading edges and the mid-span regions were attributed to paint peel.

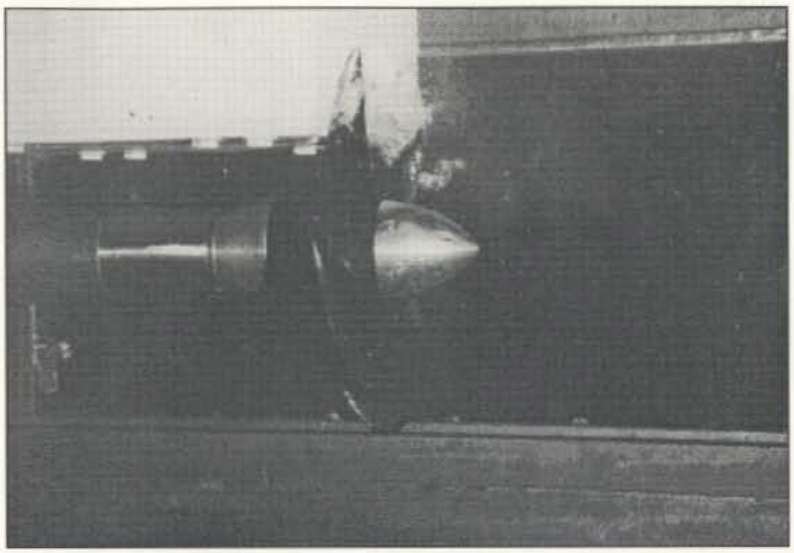

Figure 20: Cavitation During Test No. O-3

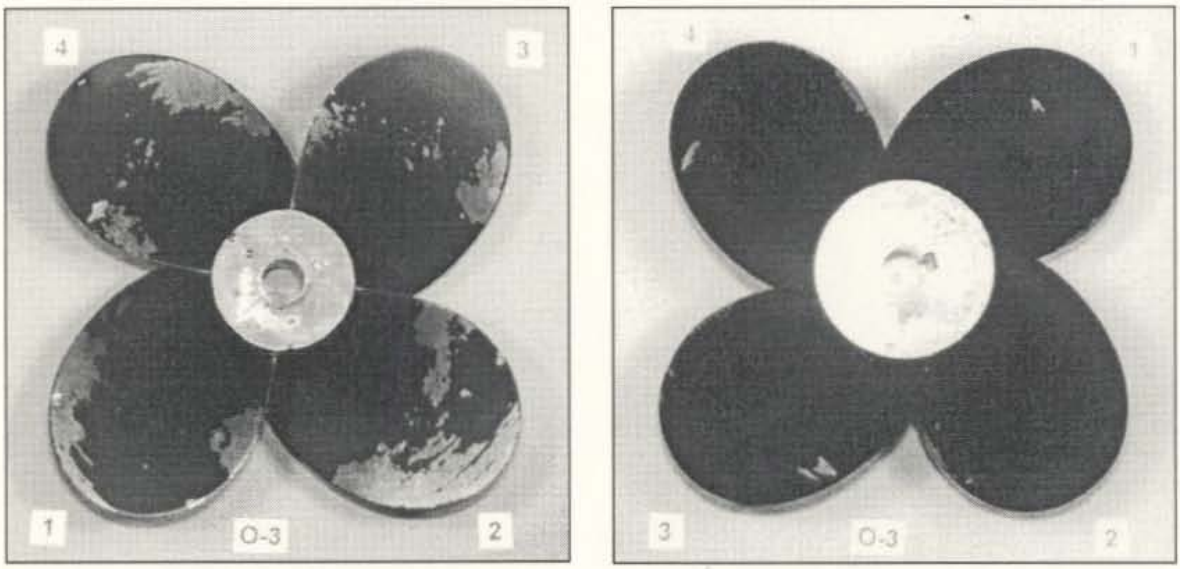

Figure 21: Erosion Results for O-3 (Face and Back: J = 0.61, σ = 3.09)

Figure 22 shows the results from Test No. O-4, which was conducted at J = 0.20 and σ = 3.13. During this test, an attached tip vortex was present when the propeller was operating in unblocked flow (see Figure 23). The regions of the face that were affected by erosion were the same as in O-1, but less erosion occurred. Face cavitation did not begin to affect the leading edge until $\theta \approx 0°$ and the amount of cavitation which was

observed was marginally less than that which occurred during O-1. Trailing edge back erosion was similar in location to that from O-1, but the amount was reduced. Blade 2 on the face and blade 4 on the back exhibited obvious paint peel.

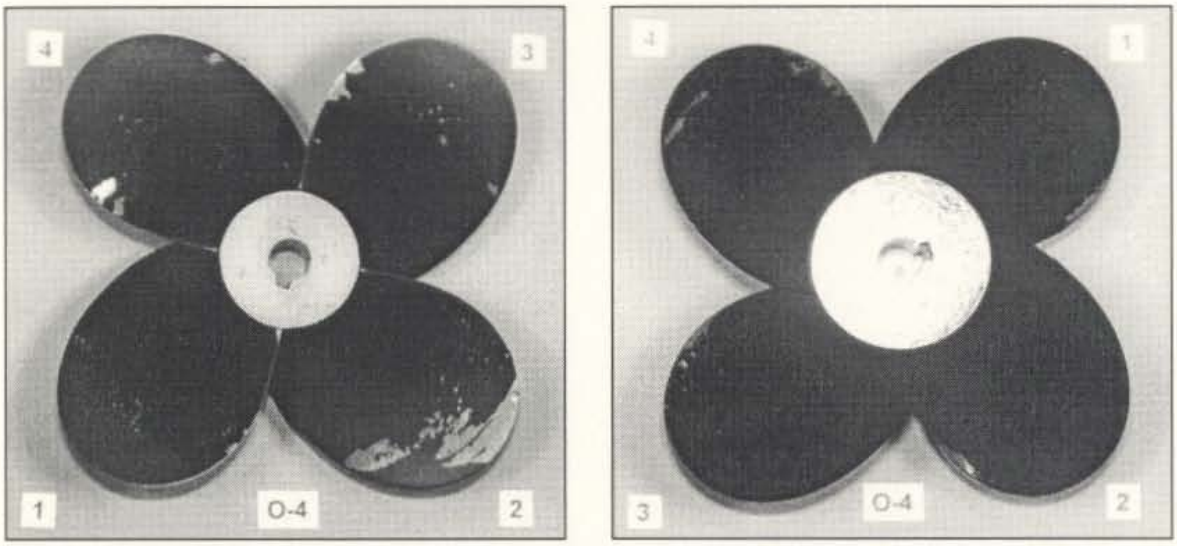

Figure 22: Erosion Results for O-4 (Face and Back: J = 0.20, σ = 3.13)

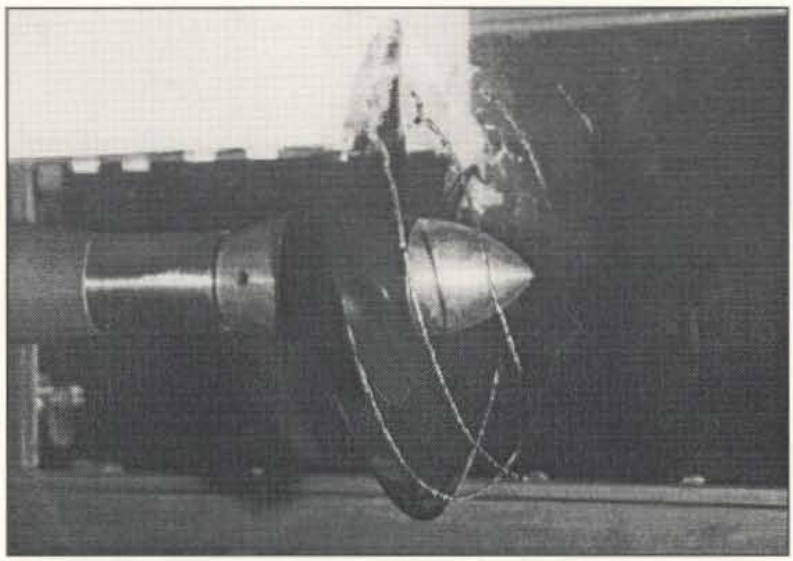

Figure 23: Cavitation During Test No. O-4

Test No. O-5 erosion results are illustrated in Figure 24 and propeller cavitation is shown in Figure 25 and Figure 26. With J = 0.40 and σ = 3.06, this test was similar to

O-1, except that the duration was 30 minutes instead of 15 minutes. The locations of face erosion between these two tests were similar, with the 30 minute test showing slightly more erosion, especially in the mid-span region. However, as the affected region was clearly indicated after a 15 minute test, a duration of 15 minutes was acceptable for the remaining tests. Back erosion from these two tests was almost identical. As before, spots of paint peel were easily identified (i.e. leading edge on back of blades 1 and 4).

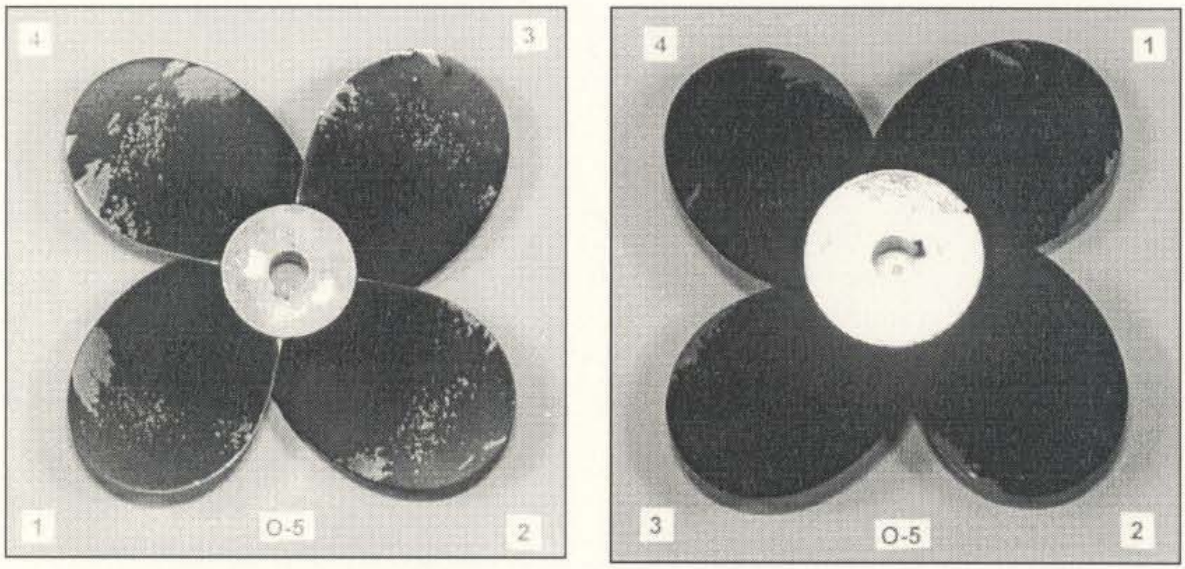

Figure 24: Erosion Results for O-5 (Face and Back: J = 0.40, σ = 3.06)

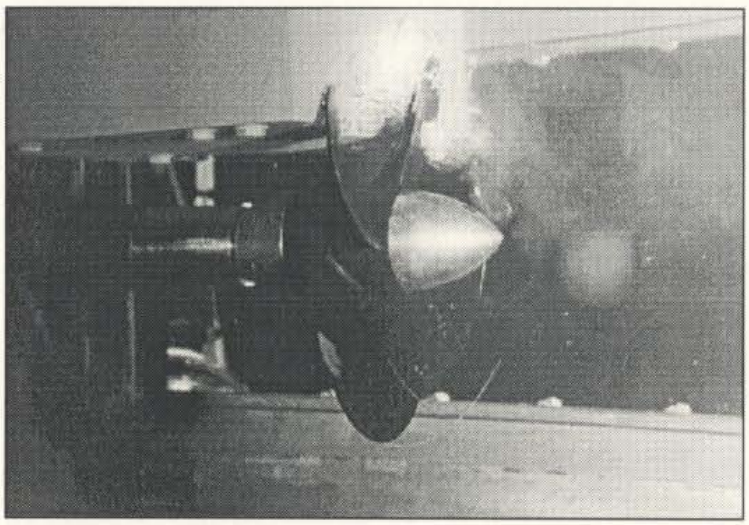

Figure 25: Cavitation During Test No. O-5

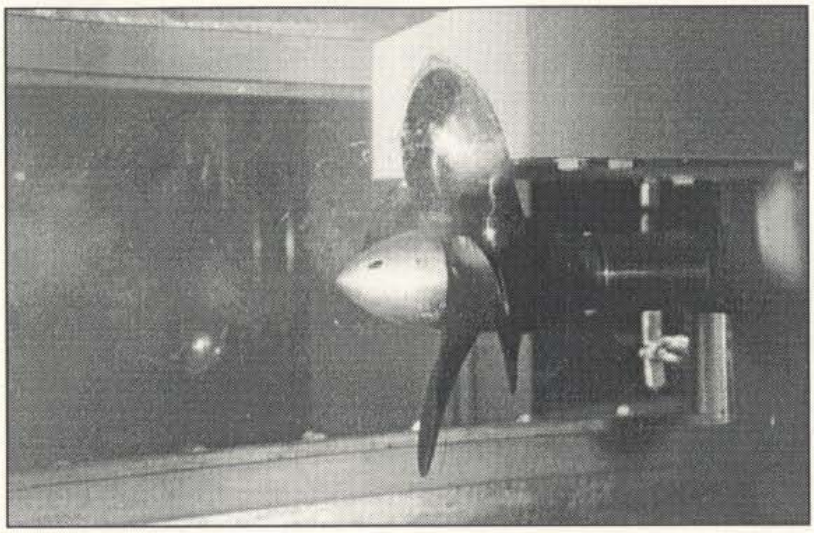

Figure 26: Cavitation During Test No. O-5 (opposite side)

The results for Test No. O-6, where J = 0.20 and σ = 3.12, are presented in Figure 27. As this test was completed to study the effects of reduced blockage, only two of the three laminates were used. A large hub vortex was present and an attached tip vortex was visible during blade operation in unblocked flow (see Figure 28).

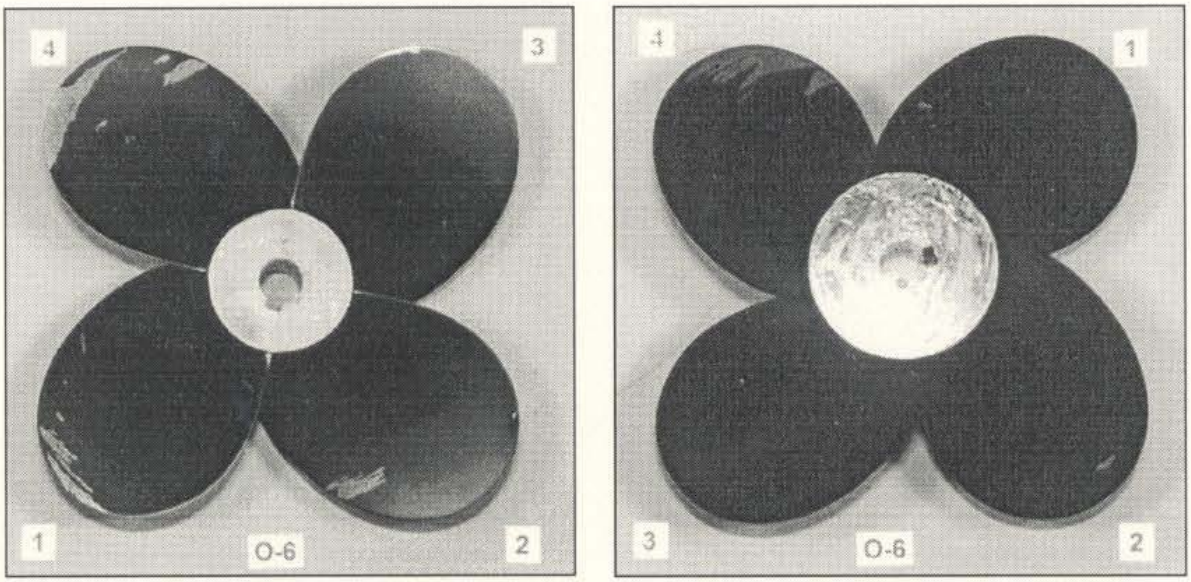

Figure 27: Erosion Results for O-6 (Face and Back: J = 0.20, σ = 3.12)

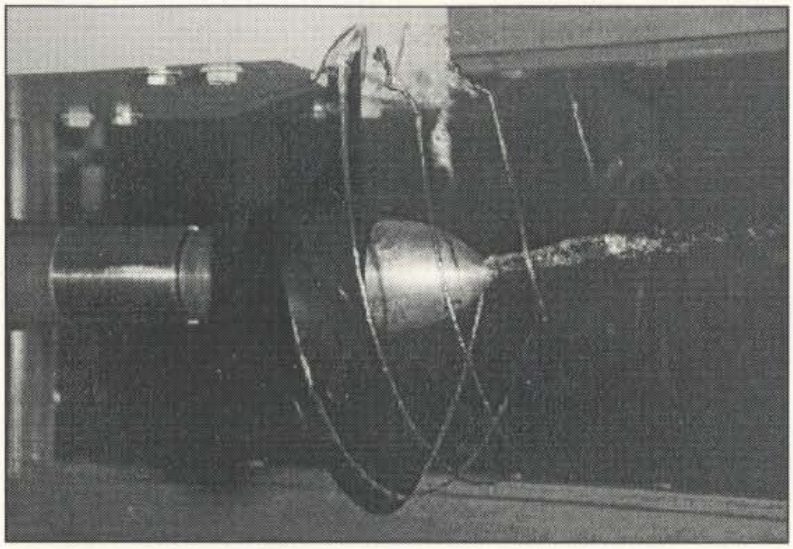

Figure 28: Cavitation During Test No. O-6

As the reference blade entered the recess, at $\theta \approx -50°$, the tip vortex expanded to form a cavity on the back of the blade. During blade progression through the recess, the cavity increased in size and continued to shed an unstable vortex/cloud. However, as this passed over the face, there was no erosion since impingement did not occur. On the back, a cloud developed from the cavity just as the blade left the recess. This affected only the extreme tip and dissipated quickly. All regions of film removal during this test were attributed to paint peel.

Test No. O-7 was also conducted to examine the effects of reduced blockage. Figure 29 illustrates the results of this test, which was performed at $J = 0.40$ and $\sigma = 3.08$. A small, unattached tip vortex was present during this test. There was no hub vortex. As with O-7, there was no impingement on the face. On the back, the cloud at the trailing edge caused a small amount of erosion as the blade left the recess. All other erosion, both face and back, was the result of paint peel.

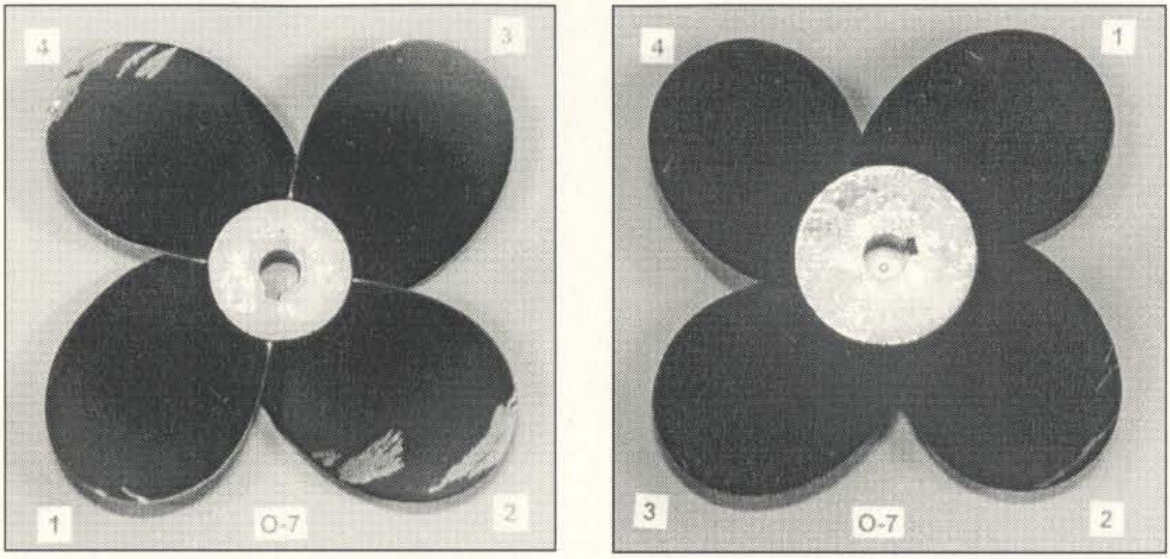

Figure 29: Erosion Results for O-7 (Face and Back: J = 0.40, σ = 3.08)

A third test, with J = 0.61 and σ = 3.10, was conducted to investigate reduced blockage effects. The results of this test, O-8, are presented in Figure 30. A small amount of entrained air was observed in the flow during this test. Tip vortex cavitation was not present. Cloud impingement on the leading edge appeared to occur from $\theta \approx 0°$ until the blade left the recess.

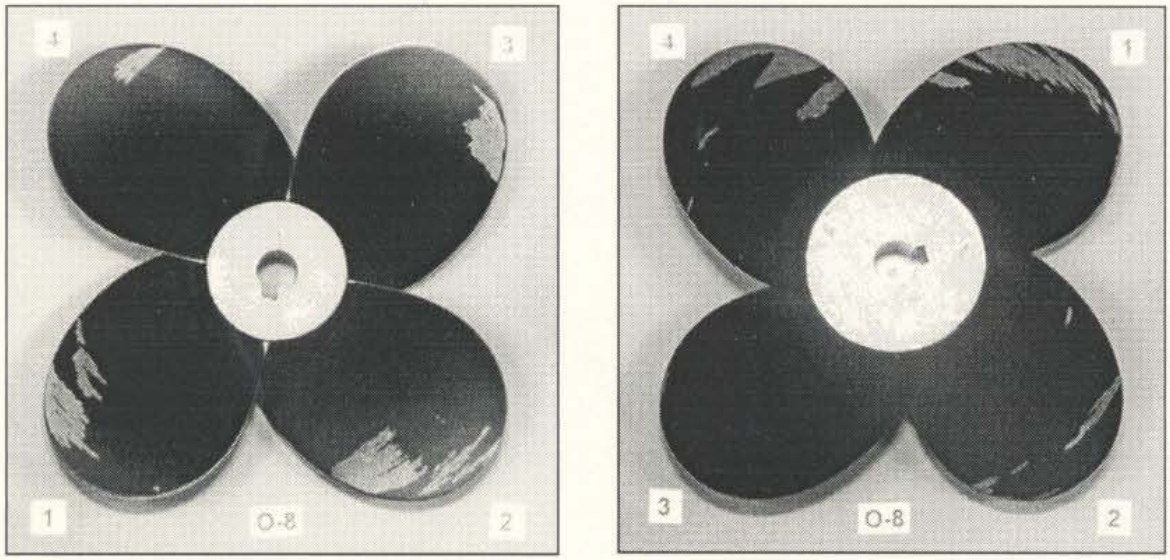

Figure 30: Erosion Results for O-8 (Face and Back: J = 0.61, σ = 3.10)

Even though the locations of face erosion were common for O-8, evidence of paint peel was strong since the eroded region sizes differed from blade to blade. A small amount of back erosion did occur on the trailing edge as it left the recess. All other back erosion was the result of paint peel.

Experiment O-9, with maximum blockage re-installed and a blade/block clearance of 5 mm, was conducted to study proximity effects. A small unattached tip vortex was present during the test. Cavitation during this experiment, with $J = 0.40$ and $\sigma = 3.07$, was violent (see Figure 31 and Figure 32). Face impingement was similar to that observed during O-1. As illustrated in Figure 33, the paint removal appeared to be excessive. Additionally, the erosion patterns were different from blade to blade. On the back (see Figure 33), trailing edge erosion was common between all blades, however, the streaks emanating from the leading edges were caused by paint peel.

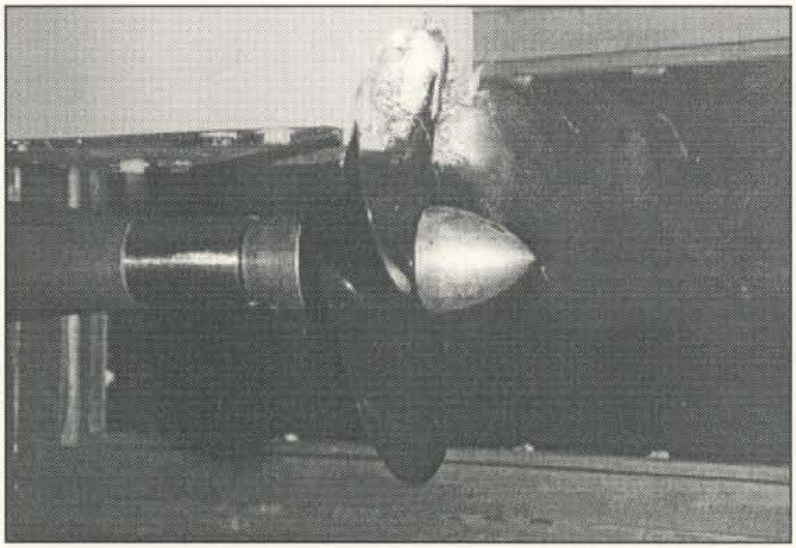

Figure 31: Cavitation During Test No. O-9

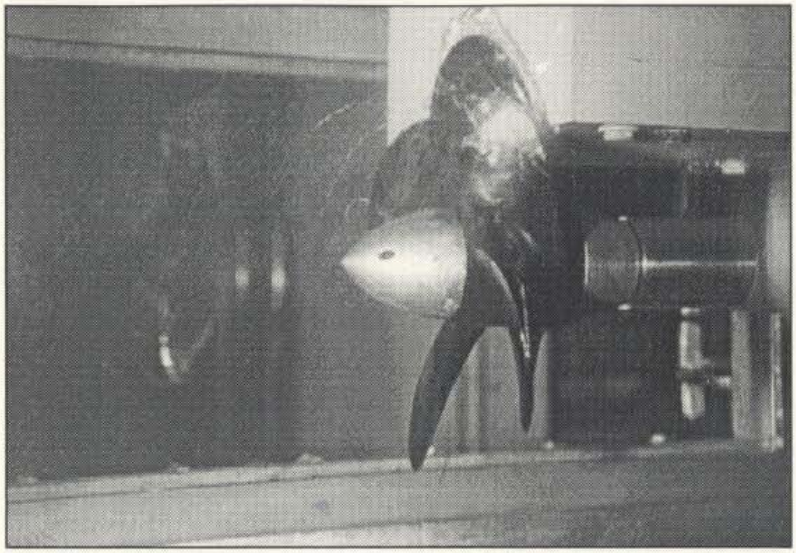

Figure 32: Cavitation During Test No. O-9 (opposite side)

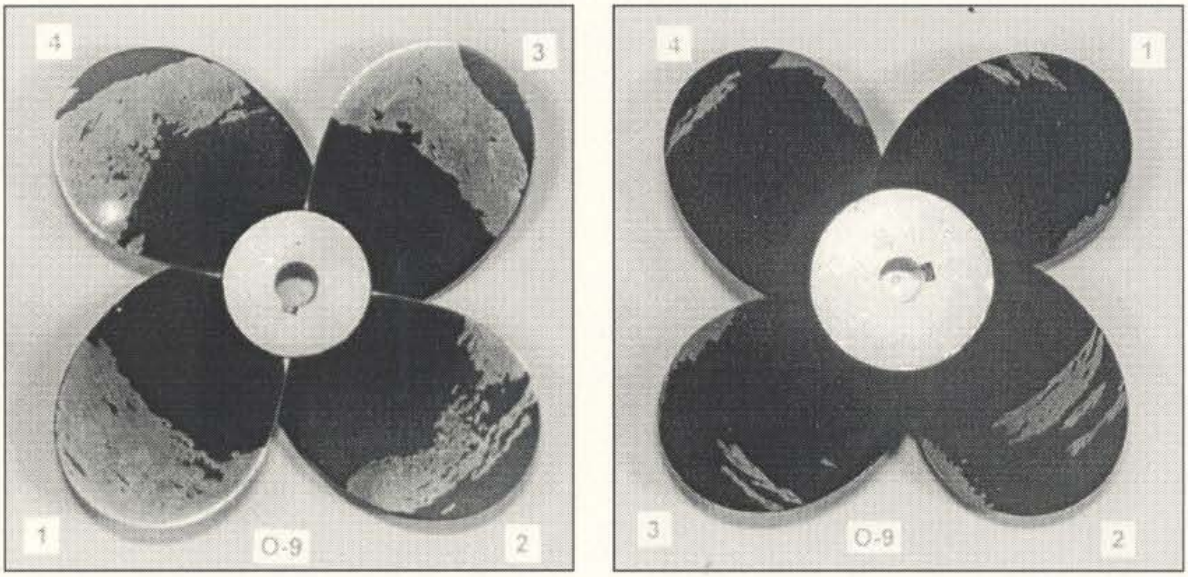

Figure 33: Erosion Results for O-9 (Face and Back: J = 0.40, σ = 3.07)

Test No. O-10, conducted with J = 0.39 and σ = 3.13, was also performed to study proximity effects. With a blade/block clearance of 10 mm, the amount of cavitation that was present, although still substantial, was reduced compared to O-9. A small, unattached tip vortex was present when the blade was in unblocked flow. The cavity shed by the back of the previous blade never completely extended to the face of the

following blade at any time during a revolution. Tiny clouds were shed from the cavity and were directed towards the face, but these dissipated before they impinged on the surface. No face erosion occurred (see Figure 34). On the back (see Figure 34), erosion occurred at the trailing edge as the blade left the shadow of the block.

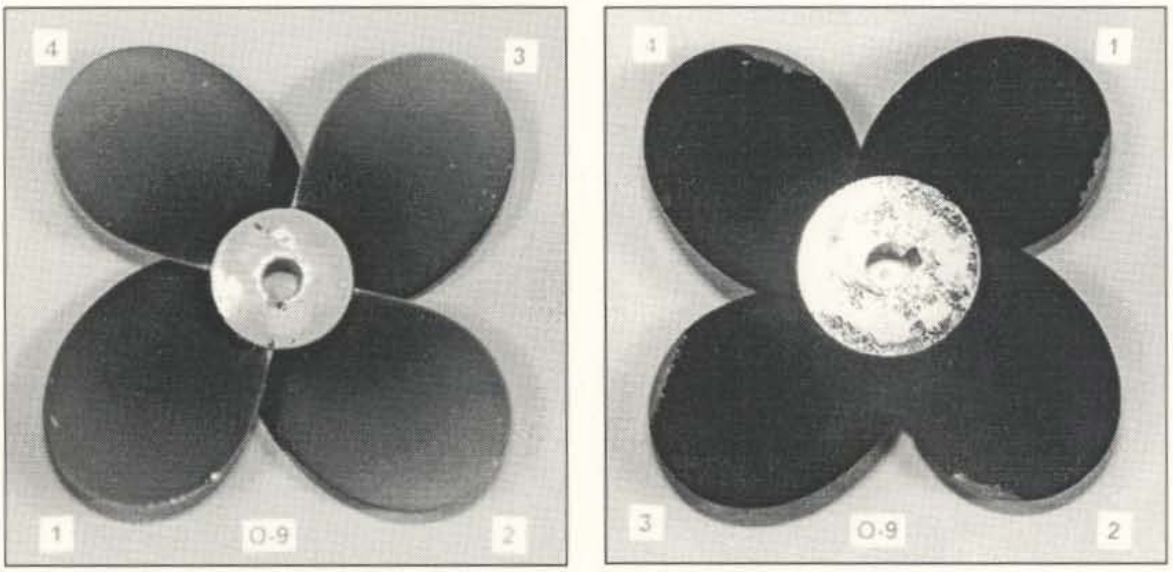

Figure 34: Erosion Results for O-10 (Face and Back: J = 0.39, σ = 3.13)

A third test, with J = 0.40 and σ = 3.09, was completed to further study proximity effects. Experiment O-11, with a blade/block clearance of 20 mm, showed no erosion on either the face or the back that could be attributed to cavitation: film removal was the result of paint peel (see Figure 35). The amount of cavitation present during this test (see Figure 36) was dramatically reduced compared to those tests with smaller blade/block clearances. A small, unattached tip vortex was present when the blade was in unblocked flow. An intermittent hub vortex was also observed. A small cavity was present on the back as the blade was in the shadow of the block. Even though this became a cloud as the blade entered unblocked flow, it dissipated quickly and caused no erosion.

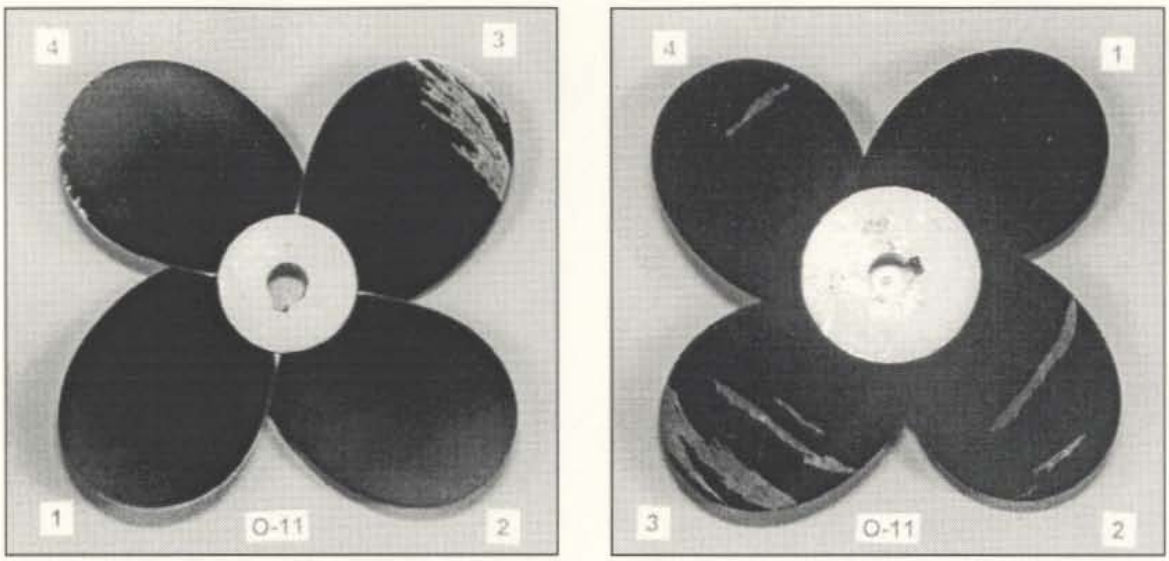

Figure 35: Erosion Results for O-11 (Face and Back: J = 0.40, σ = 3.09)

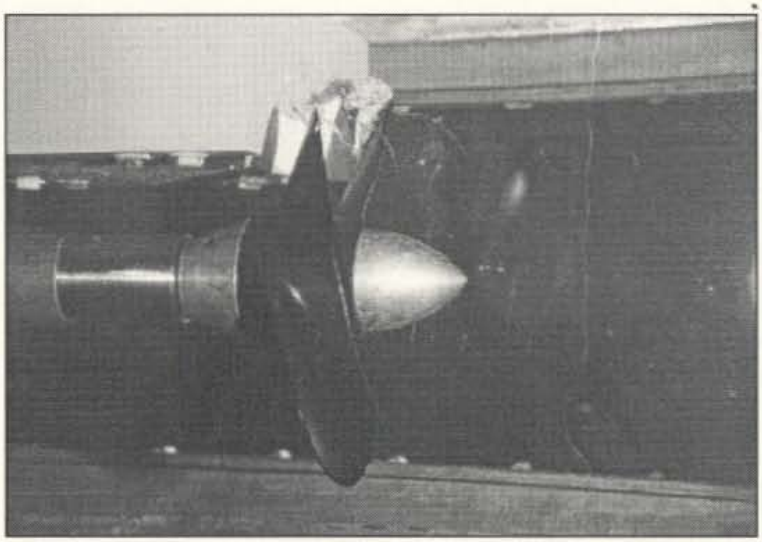

Figure 36: Cavitation During Test No. O-11

Since the erosion which occurred during Test No. O-9 seemed excessive and paint peel was evident, this test was repeated as Test No. O-12. The results, illustrated in Figure 37, again show that paint peel was a problem. As for O-9, a large amount of erosion did occur on the face, but, the patterns did not correspond between blades, nor were they repeatable between tests. What this does indicate, however, is that the

cavitation which occurred at the blade/block clearance of 5 mm was extremely violent. No other test showed this much film removal. Back erosion at the trailing edges was predicted more consistently, but paint peel was also evident as streaks on the blades.

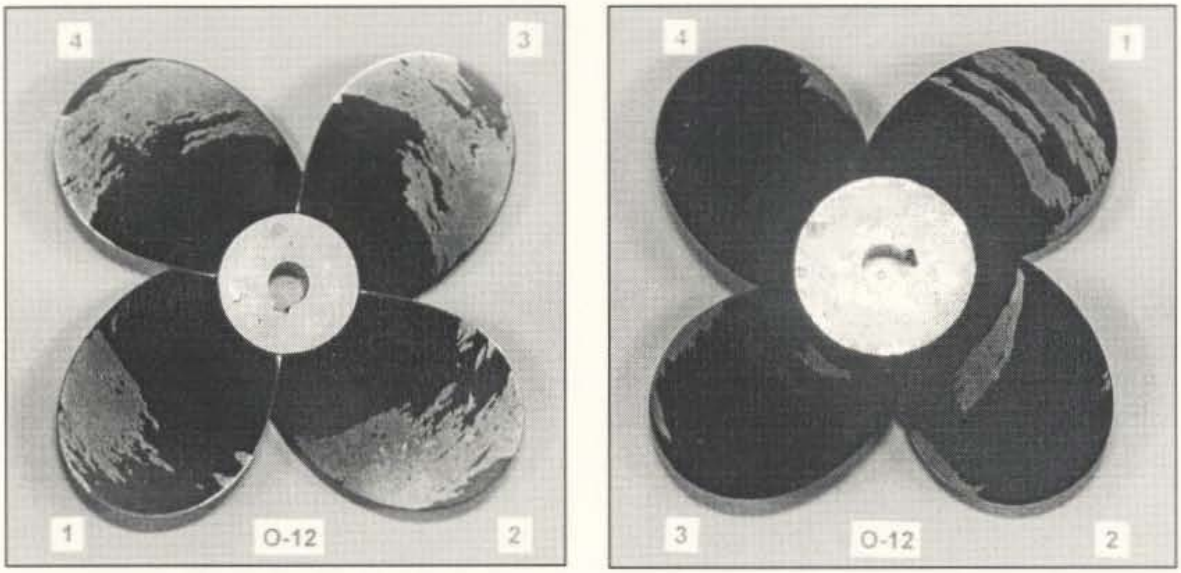

Figure 37: Erosion Results for O-12 (Face and Back: J = 0.40, σ = 3.16)

Due to the obvious occurrence of paint peel, Test No. O-13 was added to assess a different ink (*Starrett Kleenscribe Blue Layout Dye*). This test, a repeat of O-1, also allowed for examination of test repeatability. The results are illustrated in Figure 38. Minimal paint peel occurred during this test, as can be determined by comparing the size and shape of the eroded regions.

Test No O-14, conducted at J = 0.39 and σ = 3.00, was performed in uniform flow. Figure 39 shows the erosion results. During this test, a small, unattached tip vortex was the only form of cavitation that affected the blades. Therefore, no erosion should have occurred on the propeller. Paint peel was evident. (The *Crown* ink was used for this experiment).

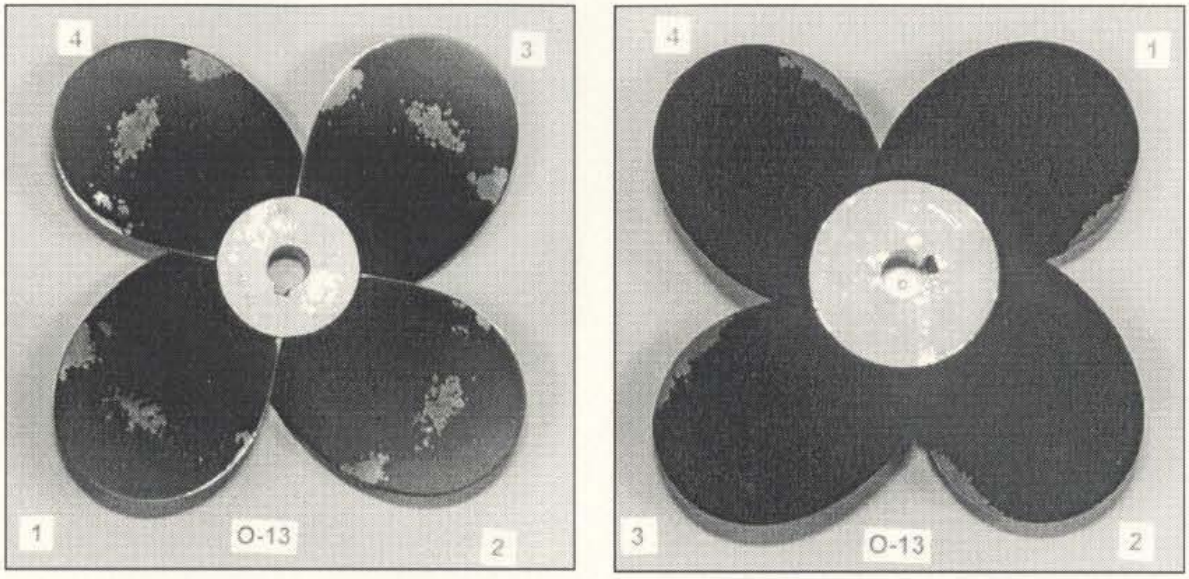

Figure 38: Erosion Results for O-13 (Face and Back: J = 0.41, σ = 3.03)

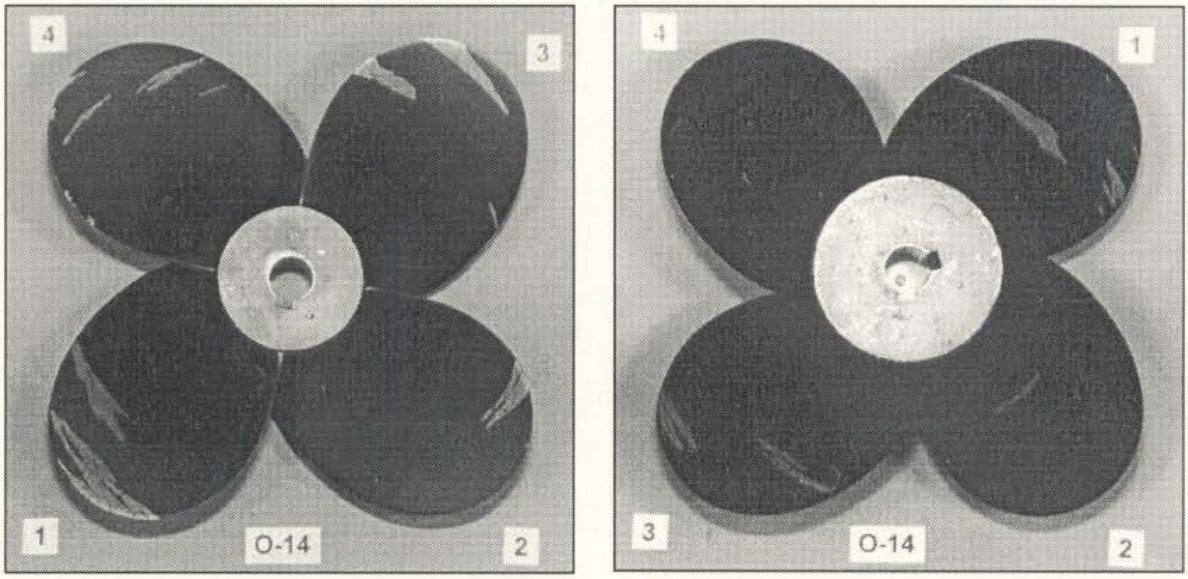

Figure 39: Erosion Results for O-14 (Face and Back: J = 0.39, σ = 3.00)

Due to the poor results from Test No. O-14, the test was repeated as O-15 using the *Crown* ink. During surface preparation and paint application, additional care was taken to ensure that the application was done in a uniform manner on a clean surface. As during O-14, paint peel occurred. The results of Test No. O-15 were not photographed.

Test No. O-14 was again repeated as O-16, but *Starrett Kleenscribe Blue Layout Dye* was used as the soft surface. As expected for open flow, the test results show that no erosion appeared on the blades during this test (see Figure 40).

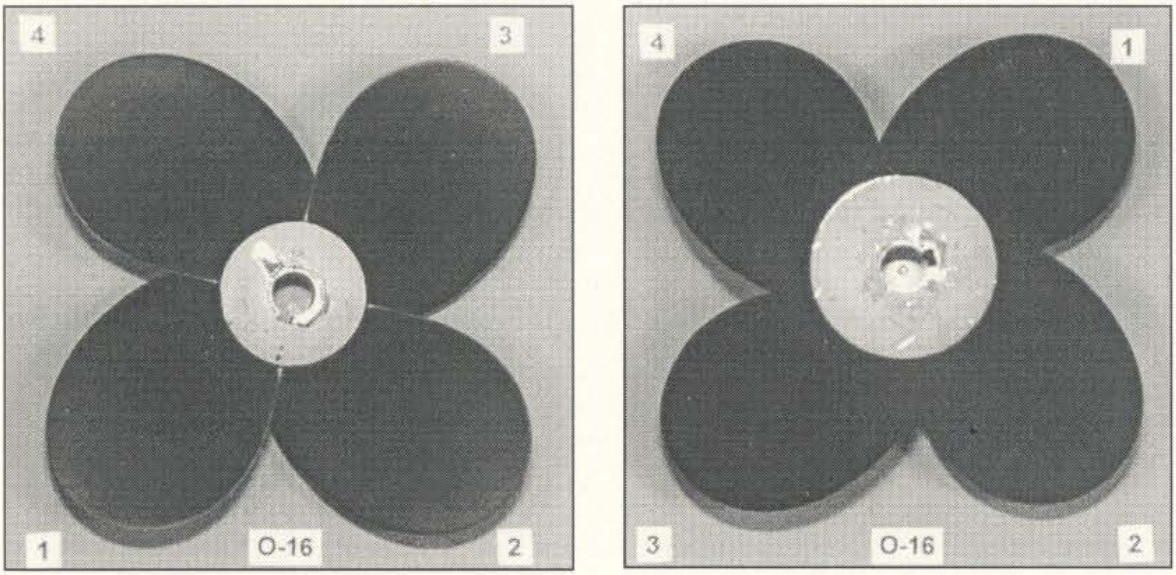

Figure 40: Erosion Results for O-16 (Face and Back: J = 0.43, σ = 2.98)

4.1.2 Erosion Results

Before making detailed comments on the open propeller area measurements, paint peel must be discussed briefly. From the descriptions and the photographs that were presented in the previous section, the occurrence of paint peel during these tests has been documented. Generally, any erosion pattern that was not common to all blades could be attributed to paint peel. These regions were easily distinguished from true results.

However, for eroded regions which were common between blades, paint peel may have still been a problem. For example, cavitation may have caused a certain amount of erosion at a given blade location, but that erosion could have been exaggerated if paint

peel occurred. This type of problem was harder to distinguish, and, if it occurred, the true result was masked. For some of these tests, eroded regions which were common between blades may have been affected by paint peel. Close examination of these eroded region boundaries showed tears that would be typical of paint peel.

For the results which are reported here, only those regions that were not common between blades have been excluded from the area measurements. All common regions were included. Bearing this fact in mind, the measured results which are presented below may actually be greater than the actual erosion which occurred.

As previously mentioned, the test duration that was chosen for these experiments was 15 minutes. As a check, a 30 minute test was performed with all other test conditions remaining the same. The results of the check, both face and back, showed slightly more erosion during the 30 minute test (see Figure 41). However, interpretation is necessary. While more erosion did occur during the 30 minute test, the regions and extent of erosion were well defined during the 15 minute test. More erosion was measured for the 30 minute test since more film removal occurred within the defined regions. As a result, it was decided that 15 minute tests were acceptable since the extent of erosion would be well defined after this time.

An important observation from these experiments was that the amount of face erosion increased with increasing advance coefficient (see Figure 42, face). One would normally expect more cavitation, and hence more erosion, at lower advance coefficients since the propeller loading is normally increased at the lower J values. The reason for this reversal is likely related to the non-uniform wake which occurred behind the block.

At higher J values, the difference in flow conditions between the blocked flow region and the unblocked flow region, as each blade operated within and outside the wake of the blockage, would be greater than they would be at the lower advance coefficients. Clouds passed from the back of blades to the face of the following blades in a different manner as the advance coefficient was changed.

The effect of increasing advance coefficient on back erosion was minimal (see Figure 42, back). At J = 0.4, slightly more erosion was noted than at the other advance coefficients, however, this increase was slight when compared to the overall blade area. Even though the amount of cavitation seemed to increase with increasing J, this did not substantially affect back erosion. For cavities which affected the back, the majority of the resulting cloud cavitation collapsed on the face of the following blade. Back erosion occurred predominantly as a blade was leaving the recess. As the blade entered unblocked flow, the portion of the back cavity which remained attached to the blade quickly collapsed into a small cloud. Focused over a small area near the tip and the trailing edge, this cloud dissipated quickly as the blade moved away from the block.

Investigation of proximity effects indicated that erosion initially increased as the propeller was moved away from the block and then decreased with further increases in the blade/block clearance (see Figure 43). Gaps of 1, 5, 10 and 20 millimetres were tested at J = 0.4. The largest amount of erosion occurred at a 5 mm gap. Since the resulting face erosion from the first 5 mm test seemed excessive and there was some evidence of paint peel, this test was repeated, with almost identical results. (It is certain that paint peel exaggerated these two results, but increased erosion at this gap was also

certain.) Once a maximum value for face erosion was reached, the amount of erosion dropped steeply with further increases in gap. Back erosion appeared to follow the same trend as face erosion: there was a slight increase at 5 mm and then a decrease. However, due to the limited number of data points, an accurate representation of the trend could not be determined. Further tests are required to define the trends in more detail.

When the cavitation number was compared to percent erosion, an anomalous result was found. Normally, the amount of cavitation, and hence erosion, should decrease with increasing cavitation number, assuming that all other conditions remain the same. The amount of cavitation which was observed at the higher cavitation number was indeed reduced (compare Figure 19 and Figure 23). Face erosion did decrease for the higher cavitation number (see Figure 44, face). However, back erosion increased, rather than decreased (see Figure 44, back). While there is a common eroded area between each of the blades for the test at atmospheric pressure (see Figure 18), the shapes are not the same and the edge boundaries exhibit characteristics that are typical of paint peel. Therefore, this result is questionable.

Additionally, for each test, percent erosion was plotted for each blade to determine if there were any noticeable trends. For example, if there were geometric differences between blades, then one blade may always show more or less erosion than the others. Only the results for Test No. O-1 have been shown here as an example (see Figure 45). Plots of "% erosion vs. blade number" for the remaining tests have been included in Appendix D. Inspection of these plots revealed that there was a fair bit of scatter in the amount of erosion between blades. For these experiments, the scatter was

attributed to paint peel. Examination of the erosion photographs showed that paint peel was evident during these tests.

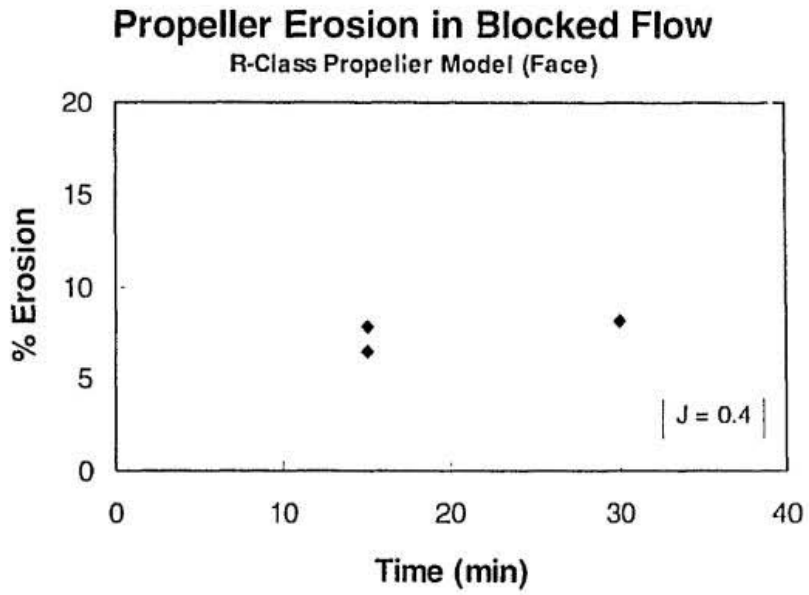

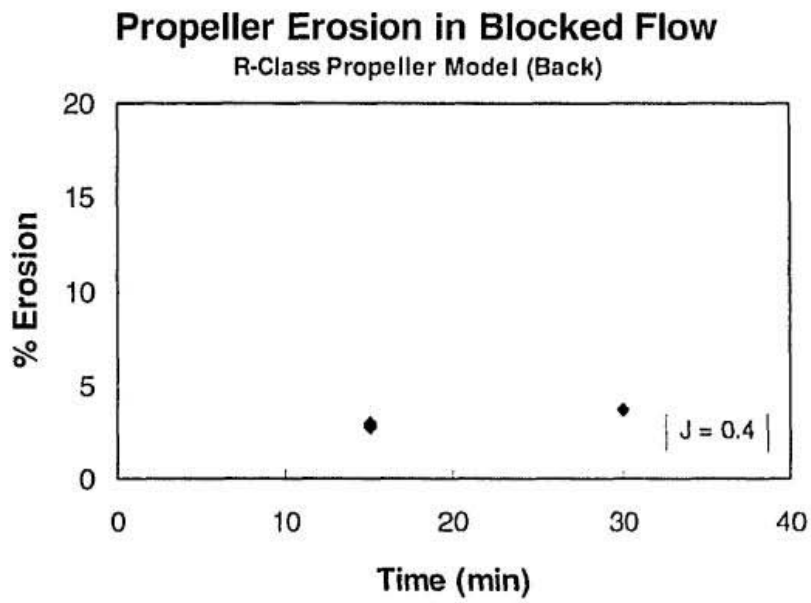

Figure 41: Open Propeller Erosion Results (Face and Back: % Erosion vs. Time)

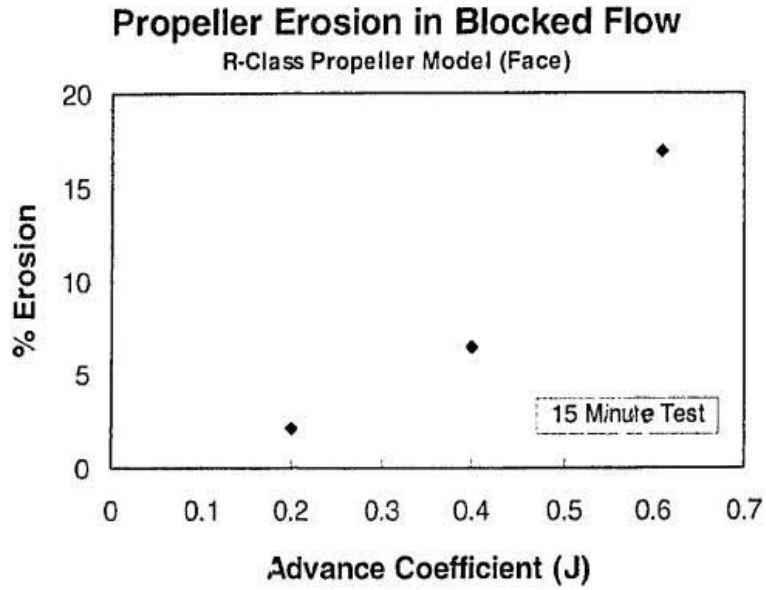

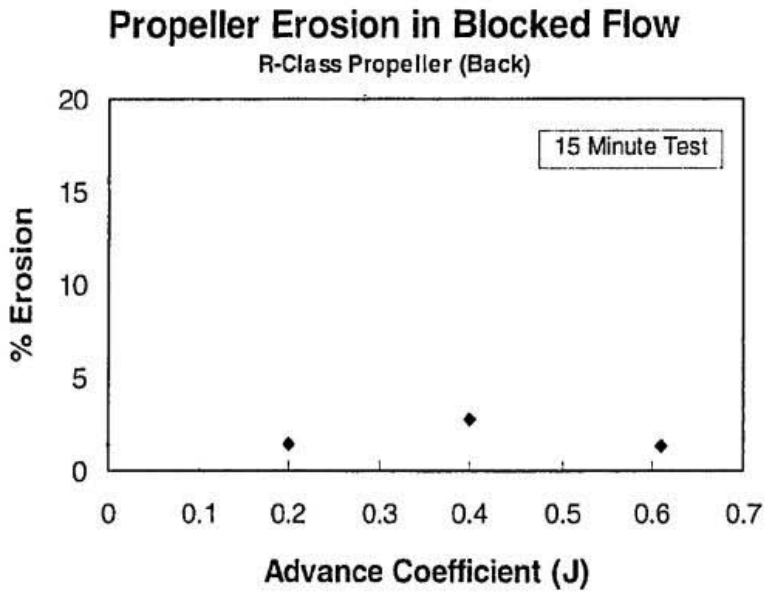

Figure 42: Open Propeller Erosion Results (Face and Back: % Erosion vs. Advance Coefficient)

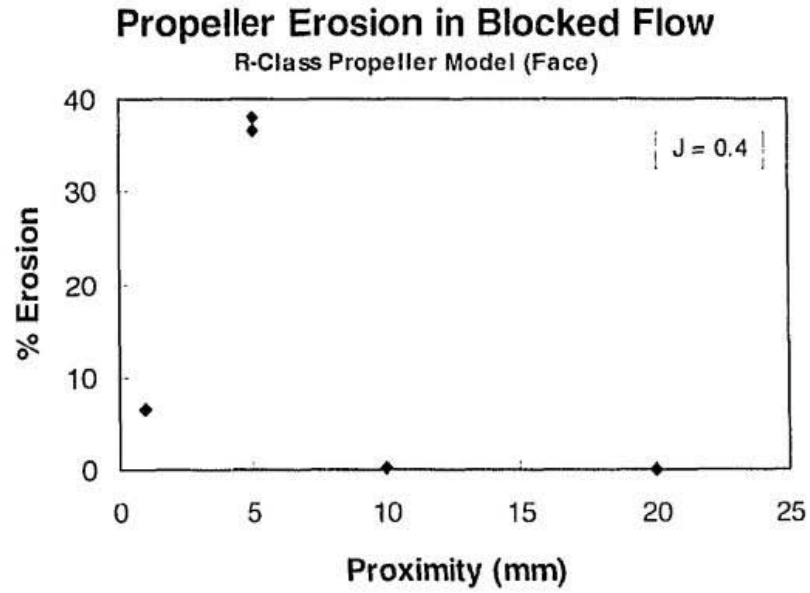

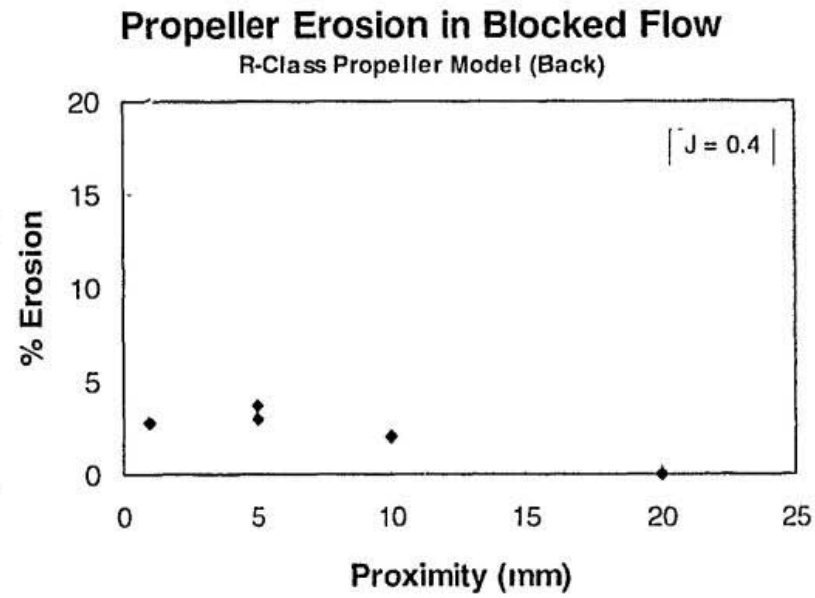

Figure 43: Open Propeller Erosion Results (Face and Back: % Erosion vs. Proximity)

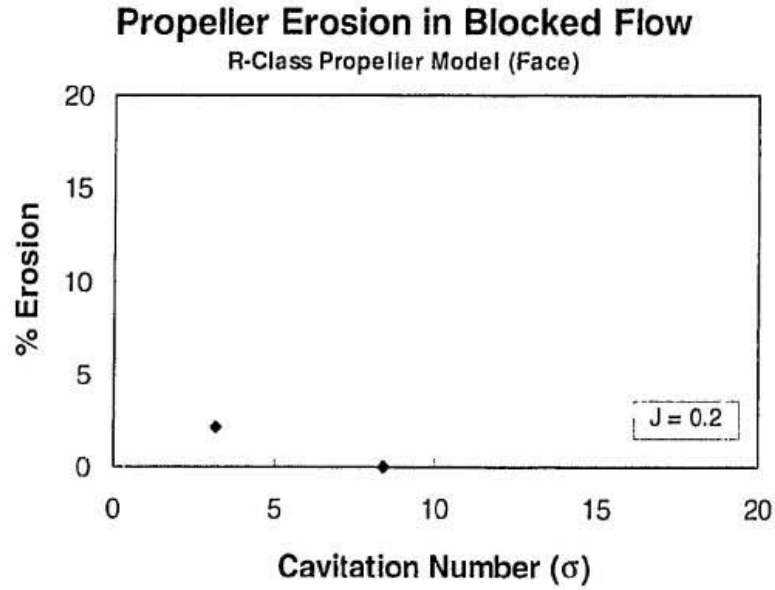

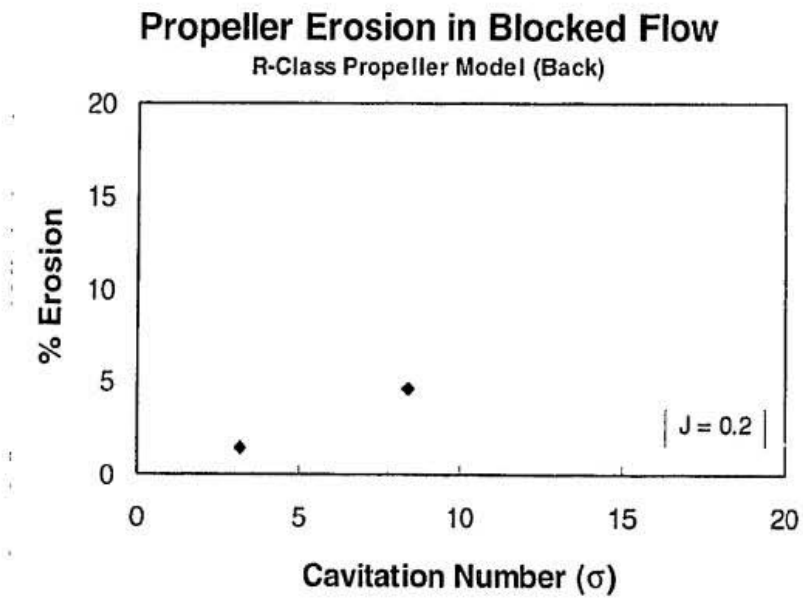

Figure 44: Open Propeller Erosion Results (Face and Back: % Erosion vs. Cavitation Number)

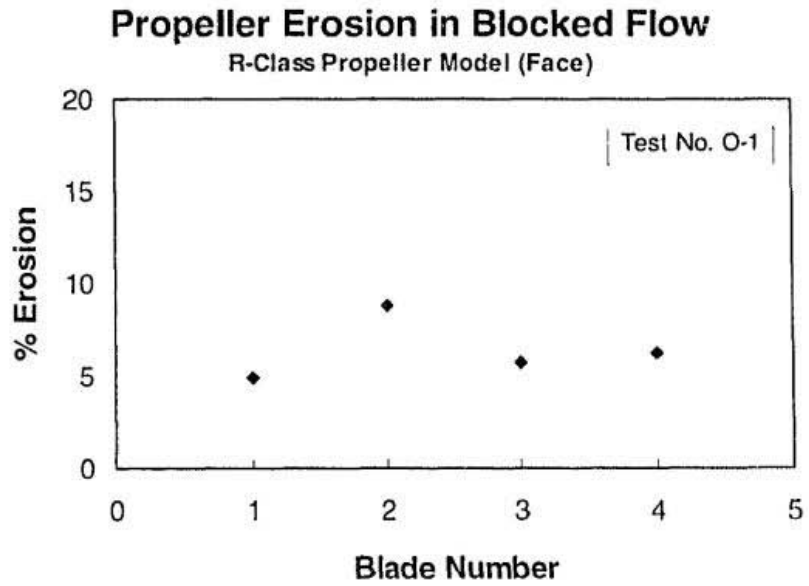

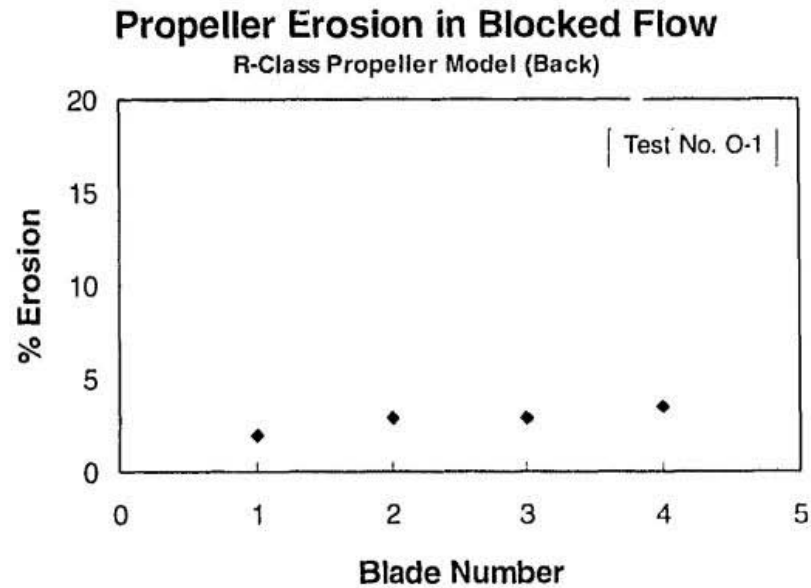

Figure 45: Open Propeller Erosion Results for Test No. O-1 (Face and Back: % Erosion vs. Blade Number)

4.2 Ducted Propeller

4.2.1 Descriptions of Cavitation and Blade Erosion

When the ducted propeller model was operated in close proximity to the block, violent cloud cavitation, noise and vibration occurred. Cavitation patterns for a ducted ice-class propeller (with Kaplan type blades) operating in similar conditions are reported by Walker and Bose (1994a). Some of the erosion experiments presented here have also been reported previously (Doucet et al., 1996). The cavitation patterns that occurred during Test No. D-1 are described below and are summarized in Figure 46. This description also relates the erosion on the blades to the cavitation patterns. These cavitation patterns are basically the same for all ducted experiments, with any differences being noted for each of the subsequent tests. The actual experimental conditions are listed in Table 7 (see Section 3.3.4).

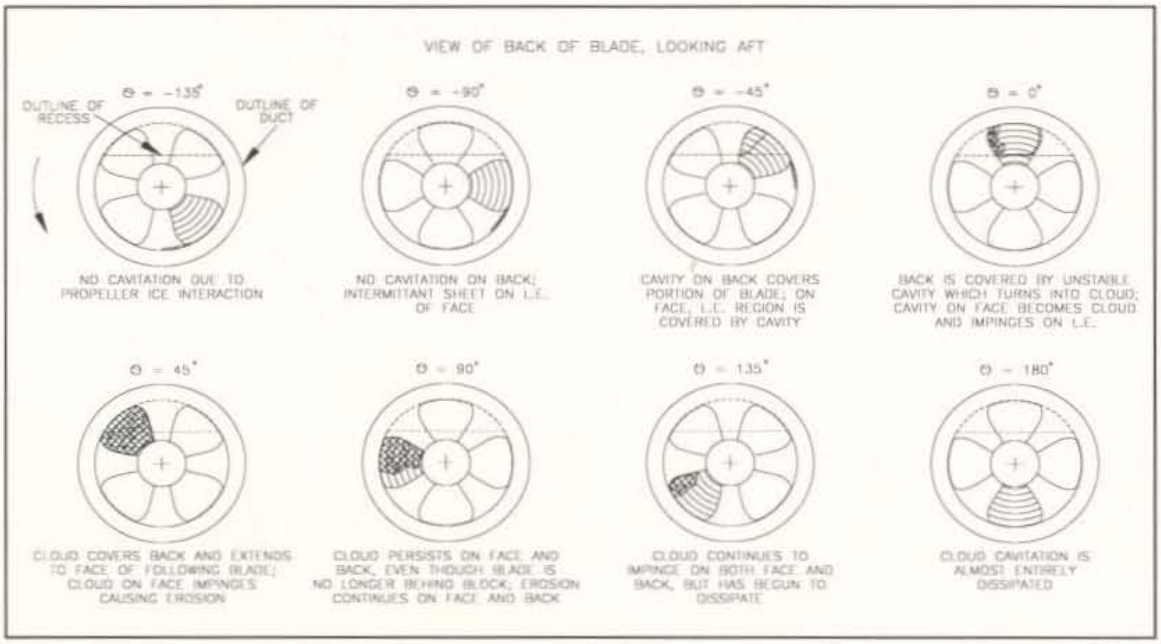

Figure 46: Typical Cavitation Patterns on Ducted Propeller in Blocked Flow (from Doucet et al., 1996)

As the reference blade approached the block, but was still operating in a region of unblocked flow, at an angle of $\theta = -135°$ (measured with respect to the vertical), no cavitation that could be attributed to propeller-ice interaction was visible on the blade. There was a vapor cavity immediately downstream of the block that was shed by the previous blade passing through the blocked flow. This cavity, which was present during the entire revolution of the propeller, is clearly visible in Figure 47.

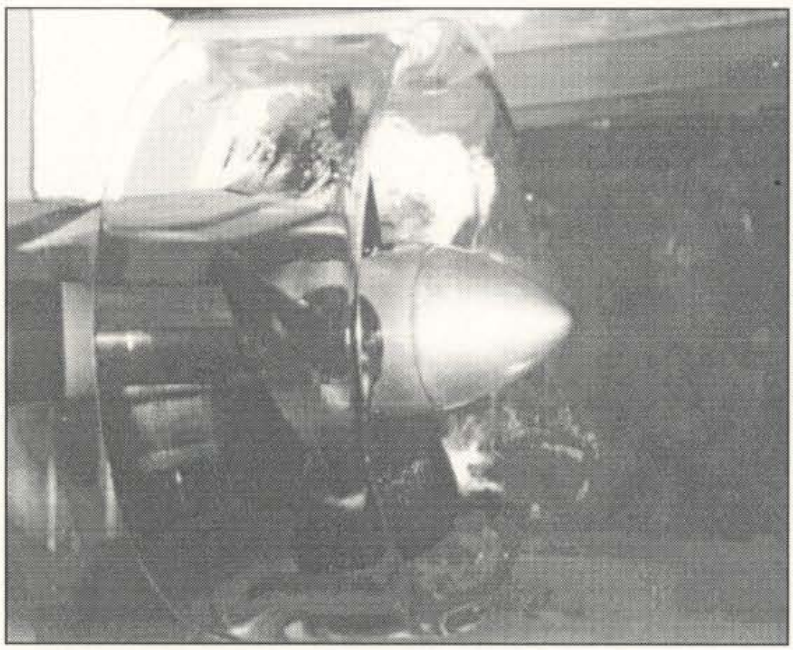

Figure 47: Cavitation During Test No. D-1

At an angle of $\theta = -90°$, the leading edge of the reference blade was almost within the recess. On the face, intermittent sheet cavitation began along the entire leading edge. There was no cavitation on the back. At $\theta \approx -85°$, the leading edge, at $r/R \approx 0.90$, entered the recess and the blade sliced into the cavity that was present behind the block. The sheet cavitation on the leading edge of the face merged with this cavity. On the back, a cavity covered the portion of the blade that was within the recess.

As the reference blade progressed from $\theta \approx -85°$ to $\theta \approx -45°$, the size of the cavity on the face grew in the chordwise direction, but at the same time, it also moved inward along the blade radii, leaving the tip of the blade cavitation free. At $\theta \approx -45°$, this cavity extended from $r/R \approx 0.85$ and $c/C \approx 0.25$ all the way down to the root with $c/C \approx 0.10$. On the back, the cavity grew along the chord until at $\theta \approx -45°$, it extended to $c/C \approx 0.25$. The remainder of the back was still cavitation free.

Between $\theta = -45°$ and $\theta = 0°$, the size of the cavities on both the face and the back continued to grow. The cavity affecting the face of the reference blade extended from the back of the previous blade (see Figure 47). On the face, the cavity grew in a chordwise direction while moving away from the tip of the blade. At $\theta = 0°$, this cavity began to turn into cloud cavitation. Erosion began to take place on the face as the cloud impinged on the edge of the first region near the leading edge (see erosion at $0.1 < c/C < 0.5$ in Figure 48, face). On the back, only the trailing edge was unaffected by the cavity, which at $\theta = 0°$ began to break down into cloud cavitation.

As the reference blade progressed past $\theta = 0°$, the cavities on both the face and the back broke down completely into violent cloud cavitation. When the reference blade reached $\theta \approx 10°$, the previous blade was no longer in blocked flow. The cloud between the two blades separated and shrunk into two distinct entities: one continued to influence the face of the reference blade while the other affected the back of the previous blade. Cloud impingement on the face of the reference blade caused erosion on the region nearest to the leading edge (see Figure 48, face). The cloud was not causing erosion on

the entire region simultaneously. As the blade progressed through the recess, the impinging cloud moved inwards along the chord towards the center of the blade. The outline of this eroded region was very well defined, which indicated that the impinging cavitation was highly focused.

On the back of the reference blade, at an angle of $\theta = 20°$, cloud cavitation was collapsing near the trailing edge, causing erosion near $r/R = 0.6$ (see Figure 48, back); this region was almost outside of the recess. Within the recess, cavitation still covered the back of the reference blade and extended to the face of the following blade. At θ 35°, the leading edge was completely out of the recess. The cloud that impinged at r/R 0.6 steadily moved outwards along the radii and was focused on the trailing edge region that was leaving the recess.

At $\theta \approx 60°$, the cloud on the face jumped slightly in the chordwise direction and began impinging on the second area (see face erosion at $0.55 < c/C < 0.9$ in Figure 48). Here, the outline of the eroded region was not as well defined as that of the first region. This indicated that the cavitation which affected the second region was not as focused as it had been when the first region was affected. Cavitation on the back continued to cause erosion near the mid-radii of the trailing edge.

Once the reference blade reached an angle of $\theta = 85°$, the trailing edge of the blade had just left the recess. At $\theta \approx 100°$, the cloud on the face rapidly shrunk, but still impinged violently on the second region, moving toward the trailing edge as the blade continued its revolution. The cloud on the back separated into two distinct entities: the

first continued to affect the back of the reference blade while the second impinged on the face of the following blade. At this point, the cloud on the back was collapsing violently on the region near the tip of the trailing edge (see Figure 48, back). The cloud cavitation on both the face and the back persisted until, and finally dissipated when, the blade reached an angle of $\theta \approx 180°$.

As was previously discussed in Chapter 3, paint peel problems necessitated the selection of a new ink for the erosion tests. The *Avery* ink that was subsequently chosen provided excellent results. Paint peel did not occur, as can be seen from the erosion results shown in this section.

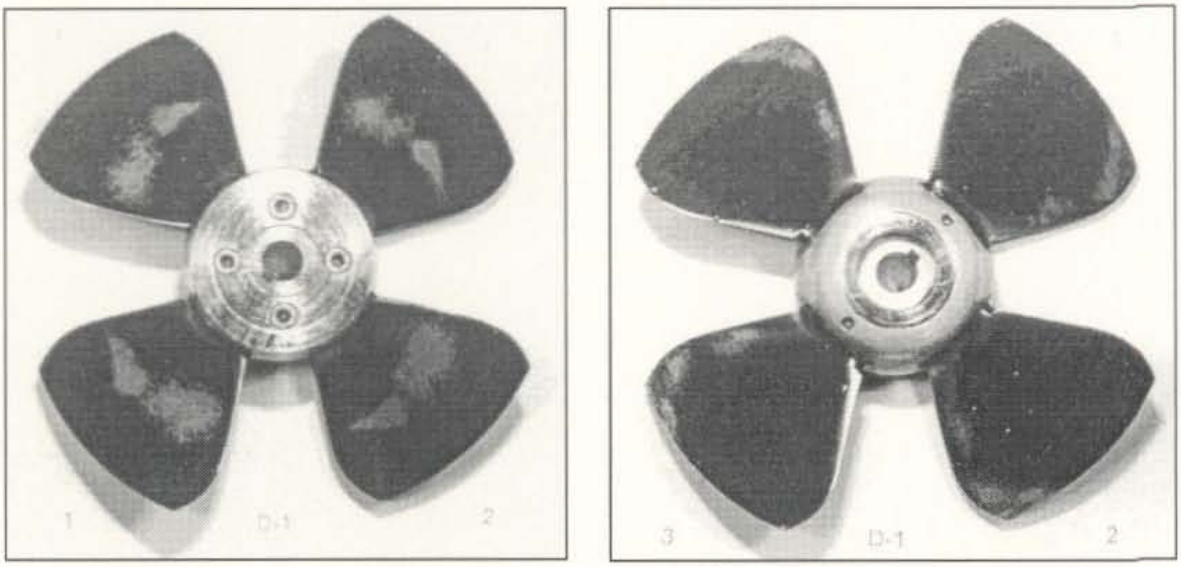

Figure 48: Erosion Results for D-1 (Face and Back: J = 0.41, σ = 4.73)

The results of Test No. D-1, which was described above, are shown in Figure 48. The test conditions for D-2, conducted at an advance coefficient, J, of 0.42 and a cavitation number, σ, of 4.81, were similar to those for D-1, except that the duration was 30 minutes instead of 15 minutes. D-2 erosion is illustrated in Figure 49. The results

from these two experiments were almost identical: the erosion for the 30 minute test was only marginally greater than that of the 15 minute test. This indicated that a 15 minute test duration was suitable for the remaining experiments.

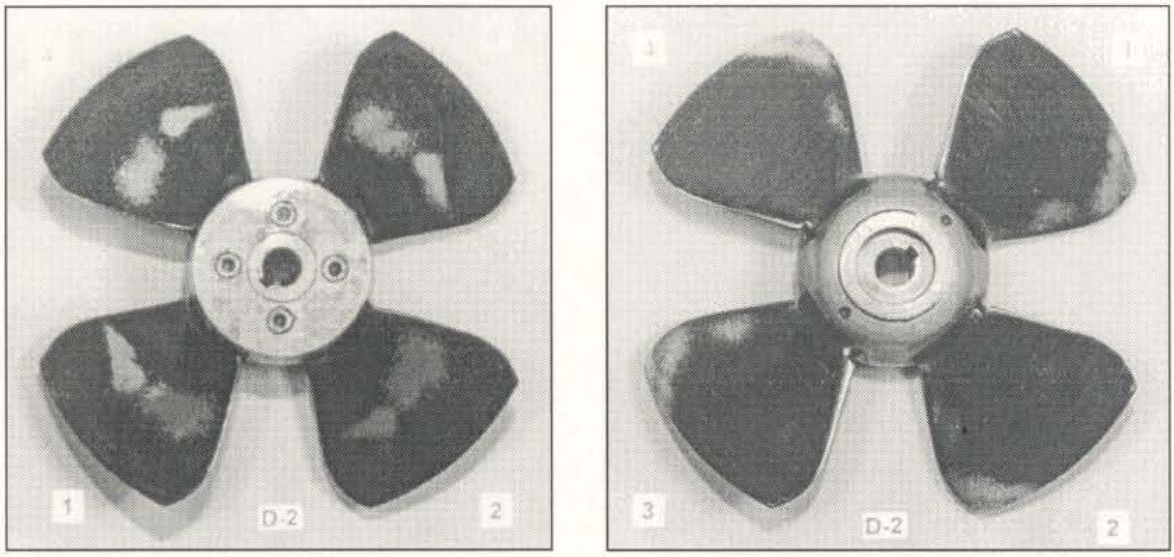

Figure 49: Erosion Results for D-2 (Face and Back: J = 0.42, σ = 4.81)

The outcome of Test No. D-3 is shown in Figure 50. This test, performed at J = 0.38 and σ = 12.56, represented the "non-cavitating condition". Even at atmospheric pressure, cavitation was still visible (see Figure 51) and erosion did occur. However, the extent and severity of the cavitation was greatly reduced compared to D-1. On the face, the erosion occurred while the blade was within the recess, between $\theta \approx 0°$ and $\theta \approx 45°$. Since almost all of the cavitation had dissipated once the blade left the recess, at $\theta \approx 90°$, there was no opportunity for erosion to occur farther back along the chord, as was the case in the first two tests. The resulting erosion on the back, which was focused near the tip only, was more clearly defined than it was for D-1 because of the intense cloud cavitation which impinged on the small area.

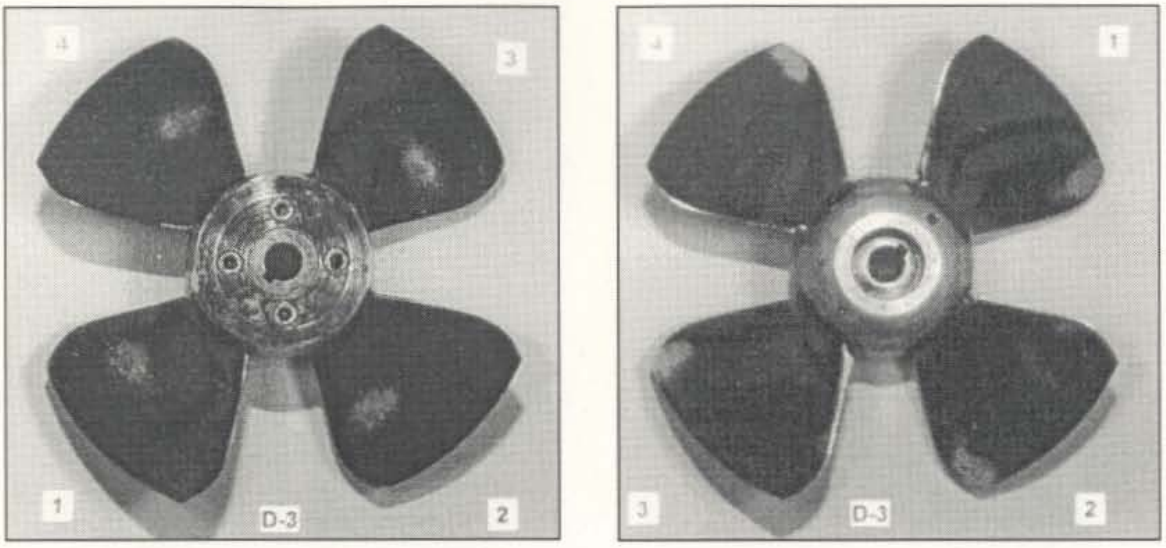

Figure 50: Erosion Results for D-3 (Face and Back: J = 0.38, σ = 12.56)

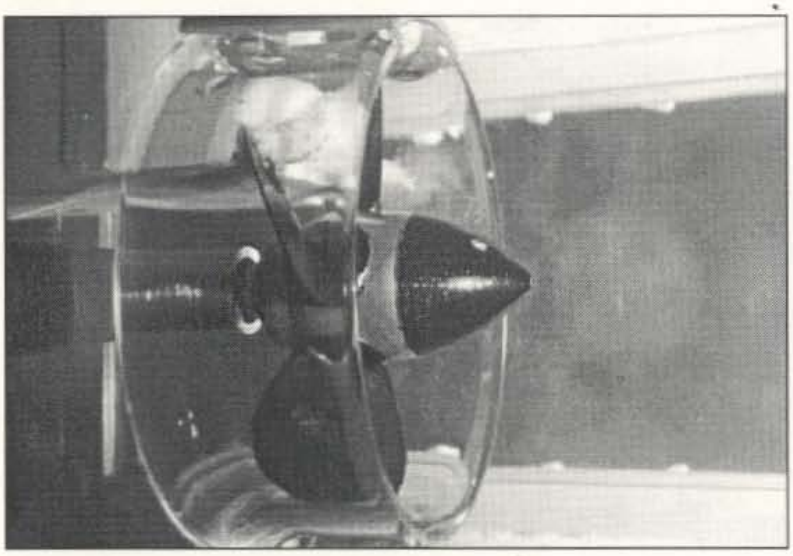

Figure 51: Cavitation During Test No. D-3

Figure 52 shows the results for Test No. D-4, which was conducted at J = 0.17 and σ = 4.75. The erosion patterns on the face were in approximately the same location as for D-1. However, there were differences. For the first region, located nearest to the leading edge, the size of the region was smaller than it was for D-1. Also, the non-eroded gap between the two eroded areas was reduced as the second region was shifted farther

away from the trailing edge than it had been for D-1. Since the flow speed was relatively low for this test, the flow conditions between the blocked flow region and the unblocked flow region, as each blade operated within and outside the wake of the blockage, were not as great as they were for D-1. This lower dynamic difference may explain why the cloud affecting the second region did not shift further along the chord as it had during the first two tests.

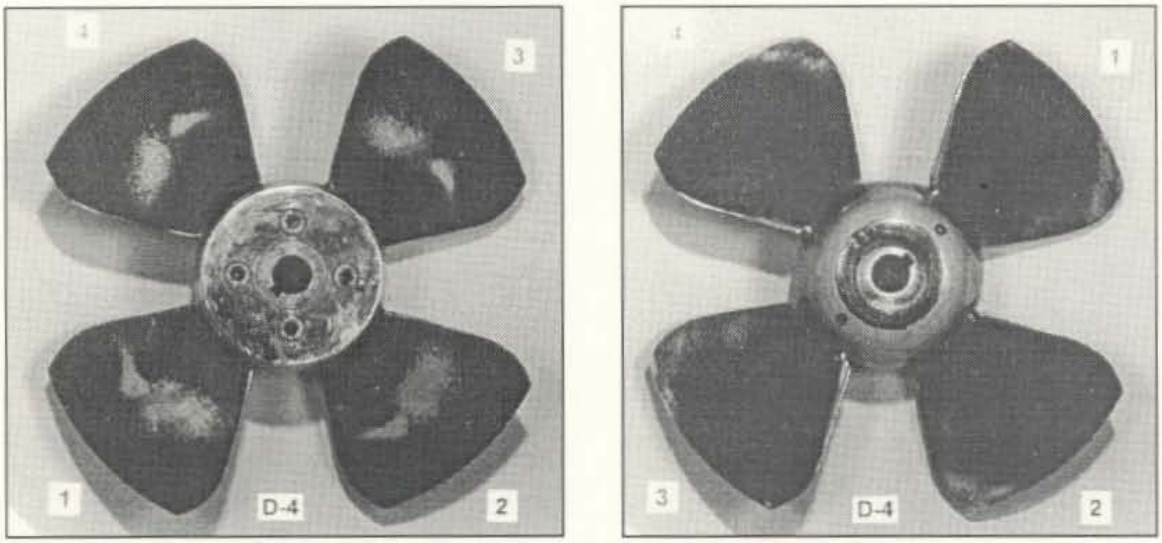

Figure 52: Erosion Results for D-4 (Face and Back: J = 0.17, σ = 4.75)

The erosion patterns and locations on the back were similar to those shown for D-1, but the erosion was not as complete. On the trailing edge tip region, film removal on the eroded areas was approximately 25%, whereas it was near 75% for D-1. While there was an eroded region on the trailing edge, near r/R $\approx$ 0.6, for D-1, erosion was almost non-existent at that region for this test.

Figure 53 and Figure 54 clearly shows the cloud cavitation affecting both the face and the back of the propeller blades during Test No. D-4. Throughout this test, a small,

unattached tip vortex was present when the propeller was operating in open, undisturbed flow (i.e. before the blade entered the recess).

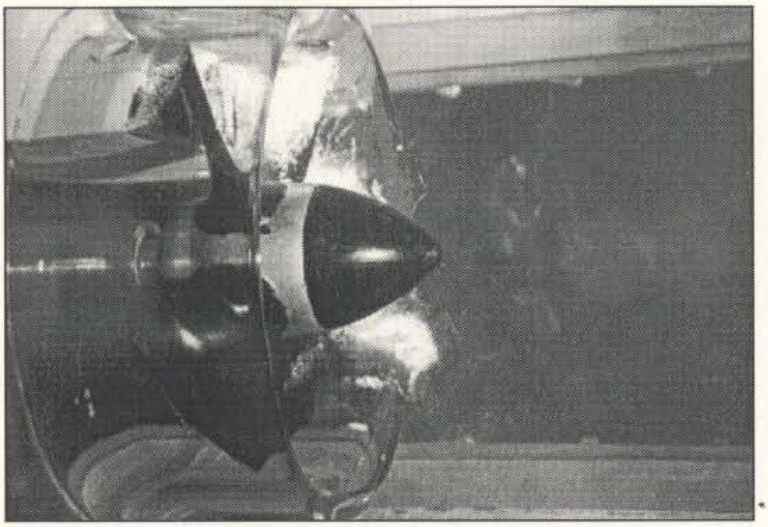

Figure 53: Cavitation During Test No. D-4

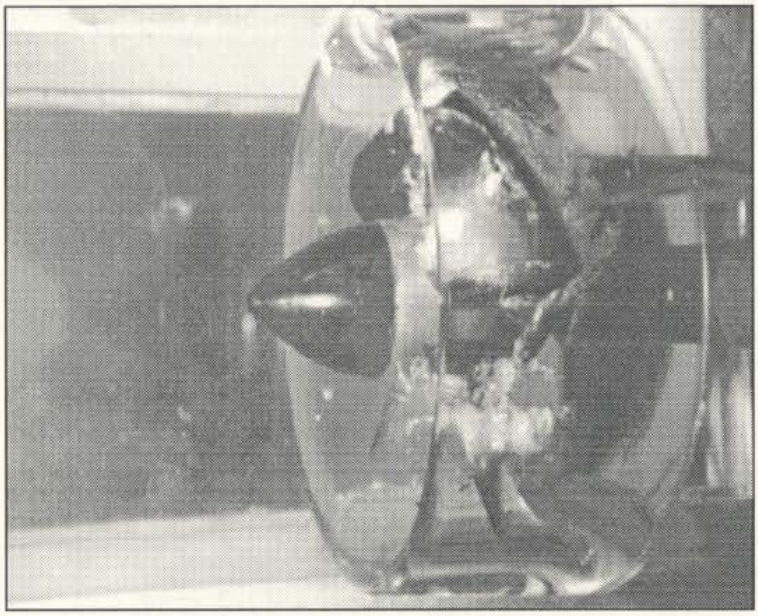

Figure 54: Cavitation During Test No. D-4 (opposite side)

The results for Test No. D-5, performed at J = 0.65 and σ = 4.66, are shown in Figure 55. Cavitation during the experiment is shown in Figure 56. For this test, there

was an additional region of erosion on the face: erosion occurred near the leading edge at $r/R \approx 0.5$ as cloud cavitation affected this region between blade angles of approximately -25° and 0°. The second region, extending from $0.15 < c/C < 0.45$, near $r/R \approx 0.7$, was marginally larger than it was for D-1. The non-eroded gap between this region and the third region was larger than it was for the previous tests as the erosion in the third region had shifted towards the trailing edge. For this test, the flow speed was substantially higher than it had been for D-1: the differences between blocked and unblocked flow were greater than they had been for D-1. The erosion at the third region occurred as the blade was moving from blocked to unblocked flow.

On the back, the trailing edge tip erosion was well defined. This was similar in location and pattern to that shown for D-1, but the erosion was more pronounced: the film removal on the area was approximately 95%. Near $r/R \approx 0.6$ along the trailing edge, erosion was almost non-existent, while it had been apparent for D-1.

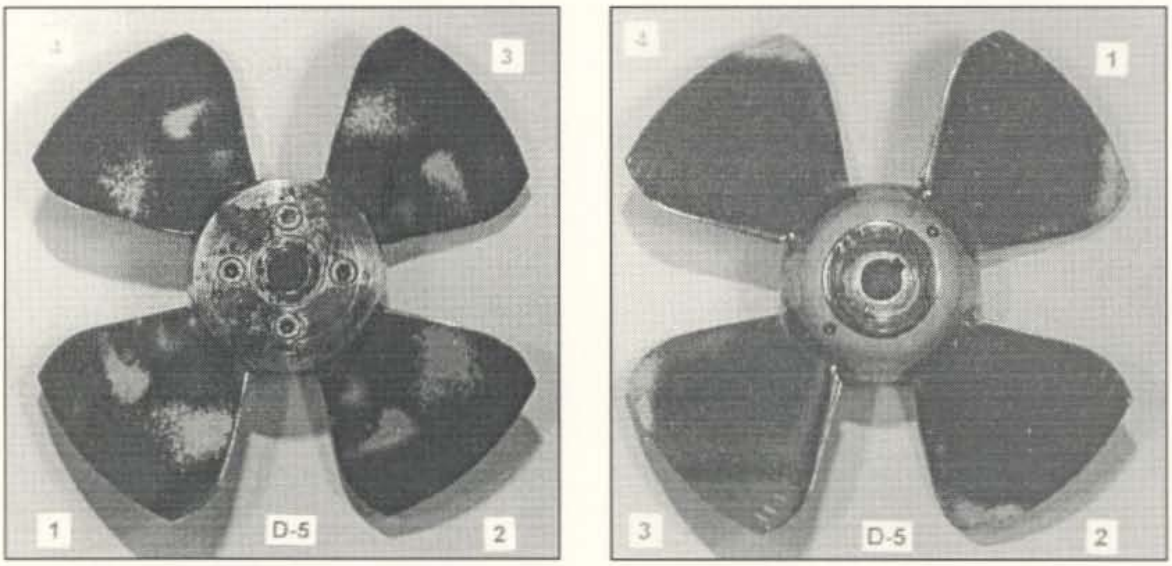

Figure 55: Erosion Results for D-5 (Face and Back: $J = 0.65$, $\sigma = 4.66$)

Figure 56: Cavitation During Test No. D-5

Test No. D-6, completed with J = 0.42 and σ = 4.73, was conducted to study proximity effects: the gap for this test was 5 mm. Test results are illustrated in Figure 57. Despite the increase in the blade/block clearance, the resulting cavitation (see Figure 58) was as aggressive as that observed during D-1. The extent of the eroded regions was greater for this test (D-6) than for any other ducted test.

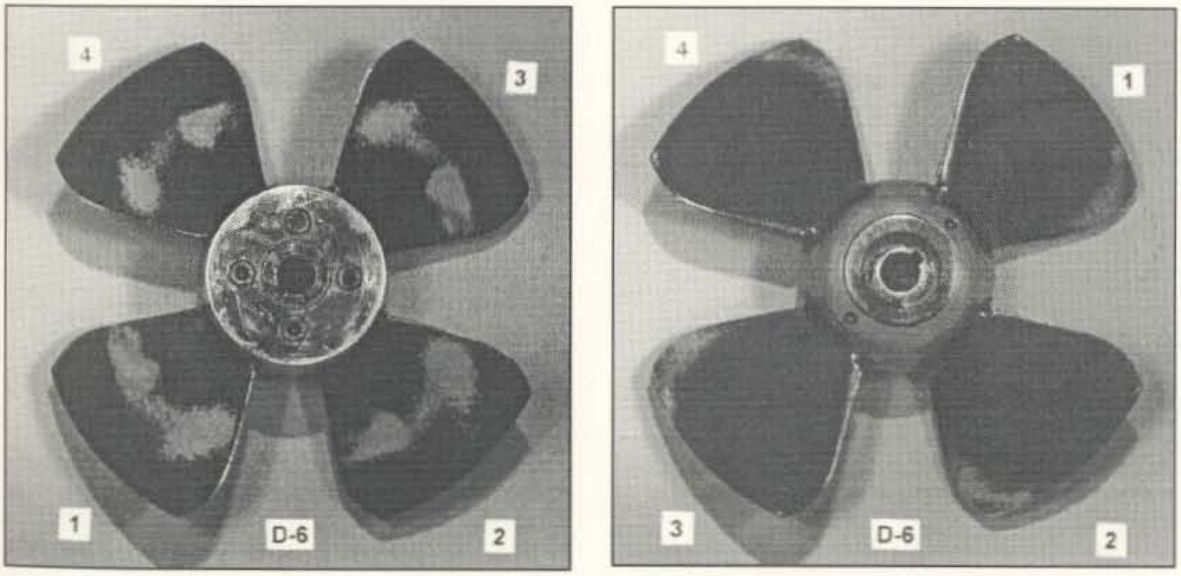

Figure 57: Erosion Results for D-6 (Face and Back: J = 0.42, σ = 4.73)

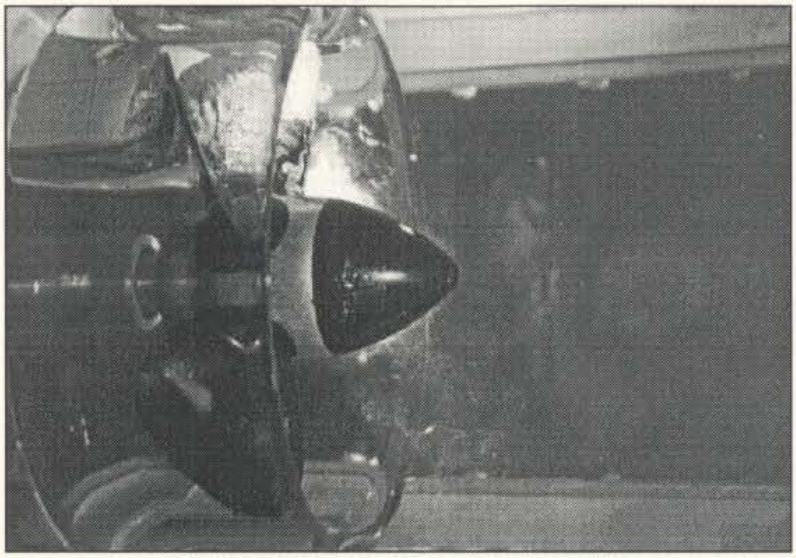

Figure 58: Cavitation During Test No. D-6

There were three distinct regions of erosion on the face. The cavitation description from D-1 applies for the erosion which occurred in the region nearest to the leading edge. Erosion on the mid-span region occurred between $\theta \approx 60°$ and $\theta \approx 95°$: the impinging cloud did not jump across the blade as in D-1. Through these blade pass angles, the blade experienced a transition between blocked and unblocked flow. At $\theta \approx 60°$, about 15 to 20% of the blade was behind the block, while at $\theta \approx 85°$, the tip of the trailing edge had just left the recess. Erosion on the trailing edge region occurred from $\theta \approx 95°$ to the end of the cavitation cycle. The difference in shape for all three eroded regions indicates that there was a transition in the type of cloud that impinged on each region.

Back erosion during this test was greater than that which occurred during D-1. Erosion covered the trailing edge from the blade tip to $r/R \approx 0.65$, whereas, for D-1, there was a non-eroded region between the mid-radii erosion and the tip region erosion. Also,

the film removal over the region was more complete than it had been for D-1. The back erosion occurred from $\theta \approx 25°$ through to $\theta \approx 180°$.

Test No. D-7 was conducted at J = 0.49 and $\sigma = 4.64$, but was in unblocked flow. During this test, the only cavitation that was present was a small, unattached tip vortex. As illustrated in Figure 59, there was no blade erosion.

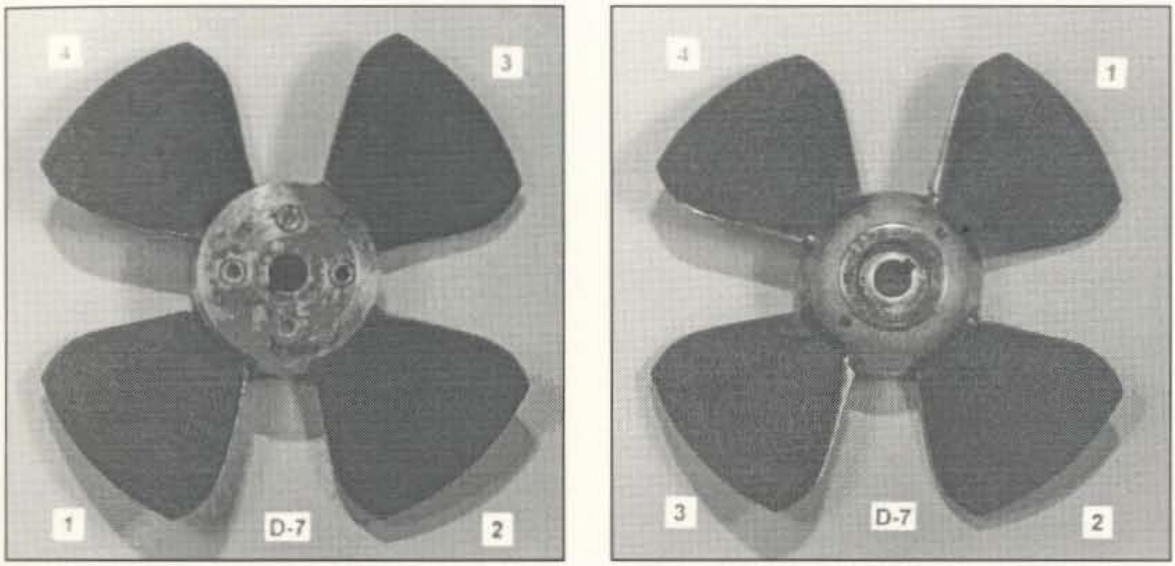

Figure 59: Erosion Results for D-7 (Face and Back: J = 0.49, $\sigma = 4.64$)

Test No. D-8, with J = 0.44 and $\sigma = 4.72$, was also performed to study proximity effects: a gap of 20 mm was used. As illustrated in Figure 60, the erosion patterns were different compared to those tests with smaller blade/block clearances. The amount of cavitation observed during this test (Figure 61) was also less compared to previous tests.

As in D-1, there was a cavity immediately downstream of the block. However, due to the increased clearance, a blade entering the recess did not "slice through" as much of this cavity as, say, during Test No. D-1. Therefore, face cavitation was reduced.

Erosion of the leading edge region appeared to begin near $\theta \approx -20°$ and it ended near $\theta \approx 45°$. It is likely that the mid-span erosion occurred between $\theta \approx 0°$ and $\theta \approx 90°$. This was difficult to judge as cavitation obscured that region of the blade during observations. Tip erosion near the trailing edge occurred between $\theta \approx 85°$ and $\theta \approx 100°$: back cavitation "spilled" over the blade edge onto this region.

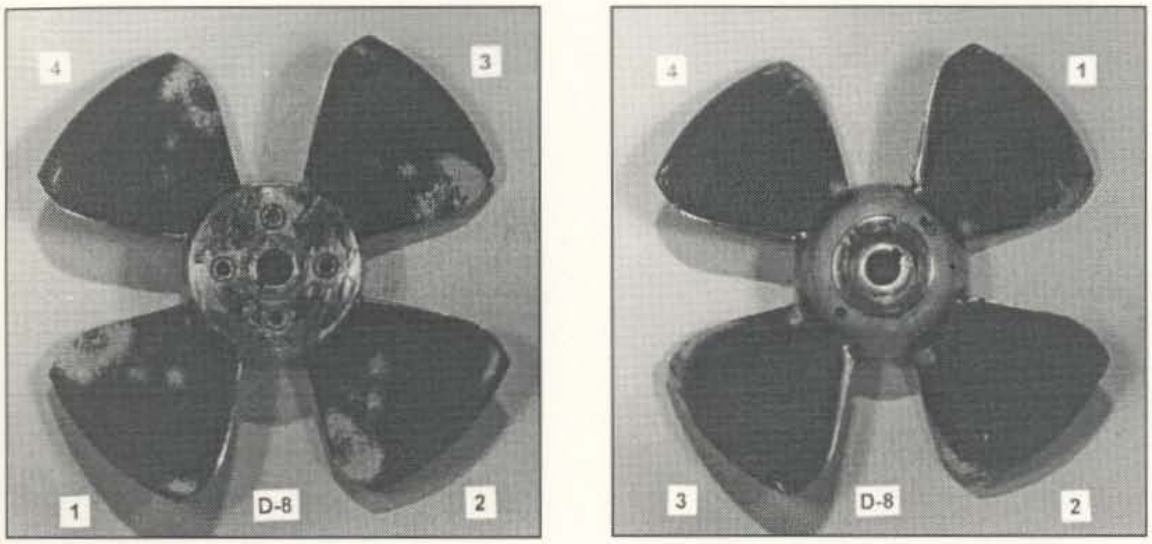

Figure 60: Erosion Results for D-8 (Face and Back: J = 0.44, $\sigma = 4.72$)

Back erosion along the trailing edge and the blade tip for D-8 was less than, but similar to, that reported for D-6. At $\theta \approx -45°$, only the leading edge was affected by cavitation. At $\theta \approx 0°$, the cavity covered the leading edge half of the blade that was within the recess. Once the blade reached $\theta \approx 45°$, the entire back of the blade within the recess was affected by cavitation. Cloud cavitation began impinging near the mid-radii leading edge region and moved radially outward as the blade progressed through the recess. By the time the blade reached $\theta \approx 85°$, the cloud impinged heavily on the trailing edge tip region. This cavitation persisted until $\theta \approx 135°$. There was also a region of

erosion near the trailing edge blade root. Vortex cavitation, which appeared to be shed from the main cavity on the back, impinged on this region from $\theta \approx 45°$ to approximately $\theta \approx 85°$ (i.e. when the blade left the recess). Since this region of the blade was near the hub, it was never behind the block during a propeller revolution.

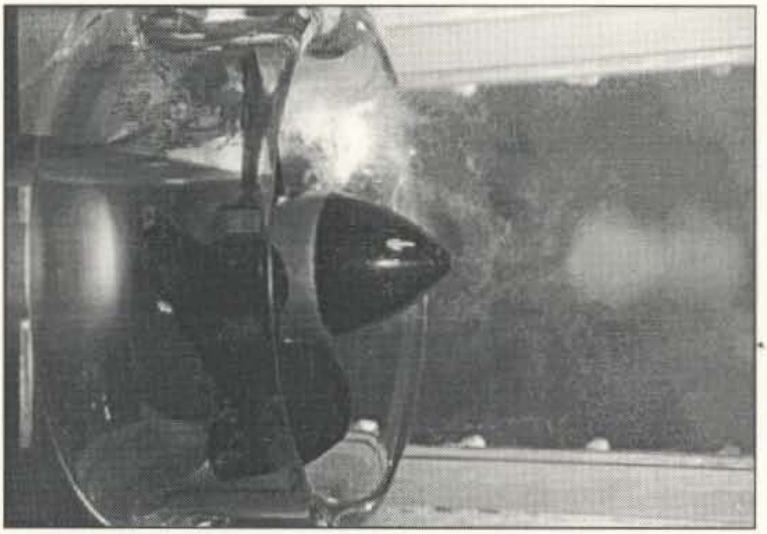

Figure 61: Cavitation During Test No. D-8

The final experiment, Test No. D-9 was conducted at $J = 0.41$ and $\sigma = 4.73$, but the pitch angle was 10° instead of 25°. As illustrated in Figure 62, the blade erosion was quite different from previous tests. The size of the cavity behind the block was smaller compared to all other ducted tests (see Figure 63). Generally, all cavitation was reduced. Since the geometric pitch angle was lessened, the propeller was not as heavily loaded as during similar tests at the same advance coefficient (with $\phi = 25°$).

When the reference blade was at $\theta \approx 135°$, an intermittent sheet was visible along the leading edge of the face, covering approximately 5% of the chord length. For previous tests, this sheet cavitation only appeared near $\theta \approx -135°$. Leading edge erosion

near the tip occurred between $\theta \approx 0°$ and $\theta \approx 45°$ as a result of impingement by intermittent vortex cavitation. The vortex was shed from a larger cloud which impinged on the inner radii of the leading edge region. This larger cloud caused erosion from $\theta \approx 0°$ to $\theta \approx 60°$. At $\theta \approx 60°$, the cloud jumped and began eroding the mid-span region of the blade, although less vigorously than it had when the leading edge was affected. This persisted to $\theta \approx 90°$, at which point it had almost entirely dissipated. Trailing edge tip erosion occurred just as the tip was leaving the recess. It was caused by impingement of momentary vortex cavitation which dissipated once the tip cleared the recess.

Back erosion occurred in two locations. Leading edge tip erosion appeared to occur just as the blade was leaving the recess and entering unblocked flow. Erosion along the trailing edge was complete and well defined. It occurred from $\theta \approx 0°$ to $\theta \approx 80°$. At that point, the blade exited the recess and all remaining back cavitation quickly dissipated.

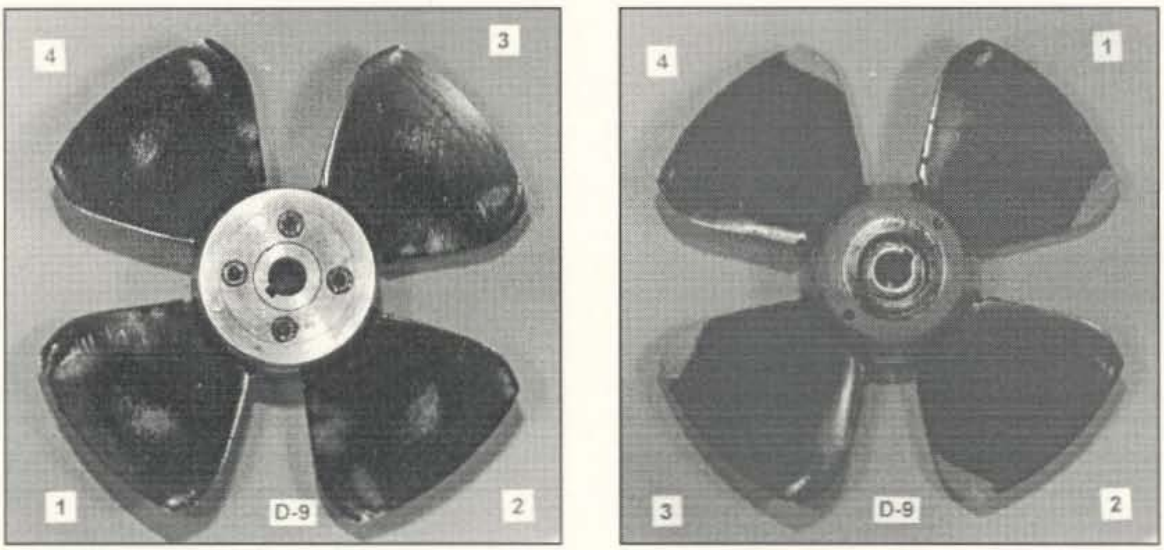

Figure 62: Erosion Results for D-9 (Face and Back: J = 0.41, σ = 4.73)

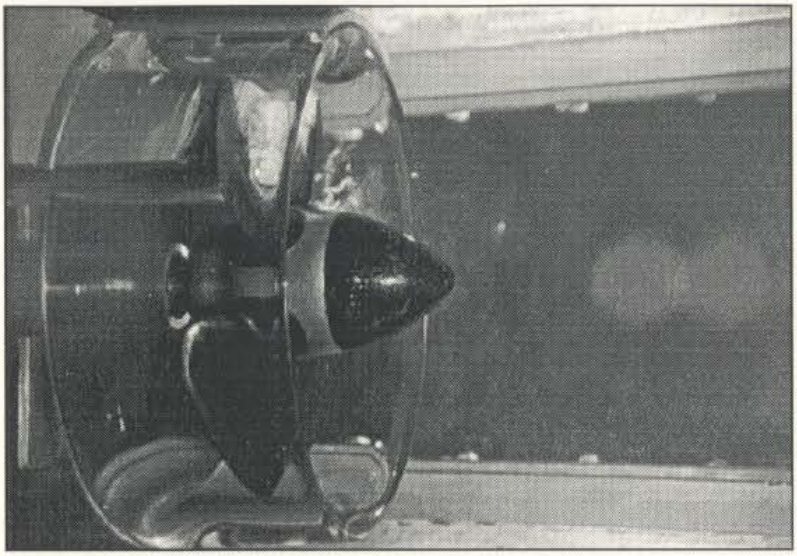

Figure 63: Cavitation During Test No. D-9

4.2.2 Erosion Results

Following the paint problems which were experienced during the open propeller test program, a new ink was selected for the ducted propeller tests. This new ink was ideal and paint peel was not a problem, as indicated by the test results.

Of particular interest, following the first test with this propeller, pitting was actually noted on the blade surfaces of the face. These pits were located in the same regions that were identified during the D-1 paint test.

As with the open propeller, a 30 minute test was performed as a check to determine if a 15 minute duration would be suitable for the ducted tests. The 30 minute test did show more erosion than the shorter test (see Figure 64), but this must be qualified. For both tests, the same regions were affected by erosion. More erosion was measured for the 30 minute tests since film removal over the regions was more complete

than it was for the 15 minute test. The 15 minute test was deemed acceptable for the remaining tests.

Experimental results indicated that the amount of face erosion increased with increasing advance coefficient (see Figure 65, face). As stated for the open propeller tests, the reverse of this trend might have been expected. Back erosion was minimally affected by changes in advance coefficient (see Figure 65, back). Slightly more erosion was noted at J = 0.4, but this increase was small compared to the overall blade area.

Blade/block clearances of 1, 5 and 20 millimetres were used (J = 0.4) to study proximity effects for the ducted propeller. More erosion occurred at the 5 mm gap than occurred with the smaller gap (for both face and back). The amount of erosion then decreased as the gap was increased further (see Figure 66). The trend indicates that erosion reaches a peak some distance away from the block, and then decreases as the clearance is increased further. To accurately define the trend, more experiments would be required at various gaps. Back erosion was minimally affected over the range of gaps that were tested, although the increase at 5 mm was noted.

When comparing erosion with the cavitation number (see Figure 67), less erosion was present at the higher cavitation number. This was as expected.

Since the ducted propeller model was variable pitch, the pitch angle was changed for one experiment. As expected, more erosion occurred at the higher pitch angle of 25° (see Figure 68). Due to the higher geometric pitch angle, the blades were more heavily loaded for the same wake conditions than they were for ϕ = 10°. A higher pitch angle on

the blades will result in lower pressures over the blade surfaces. Therefore, cavitation is more likely and hence, erosion is also more likely.

As with the open propeller, percent erosion was plotted for each blade to determine if any noticeable trends existed. The results for Test No. D-1 have been presented here (see Figure 69). For all other ducted tests, the plots may be found in Appendix E. The plots for D-1 show that blades 1 and 2 experienced more face erosion than blades 3 and 4. This was common for all tests (except for D-3, which was performed at atmospheric pressure and showed approximately equal erosion between all blades). Compared to face erosion, there was less variation between blades for back erosion. No noticeable trends were noted for back erosion.

Two possible conclusions may be drawn concerning the blade erosion trends. First, since the propeller was variable pitch, the pitch may not have been set exactly the same for each blade. Second, geometric variations may exist on one or more of the blades. The erosion trend may have been caused by a combination of both factors, however, it is likely that the first factor was dominant.

For the reasons given above, one may expect that the same erosion trend would appear on the back. However, this is not necessarily the case. If the pitch of a particular blade was higher than the others, that blade would experience more cavitation. Since back cavities were relatively large during these tests (compared to the blades), this cavitation increase would not dramatically affect the back. Since the back cavities shed cloud cavitation onto the face of the following blades, an increase in back cavitation

meant that the face would experience higher levels of cavitation, hence the reason for varied erosion if the blade pitch varied compared to other blades.

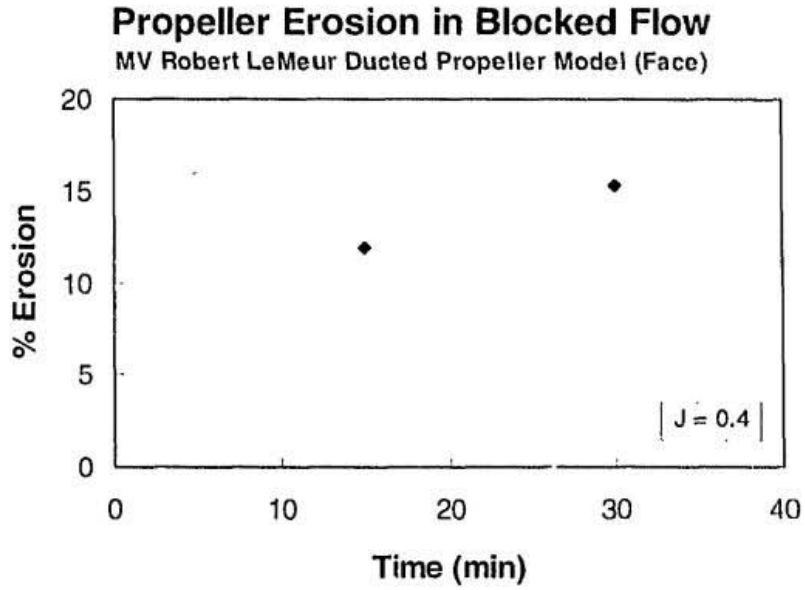

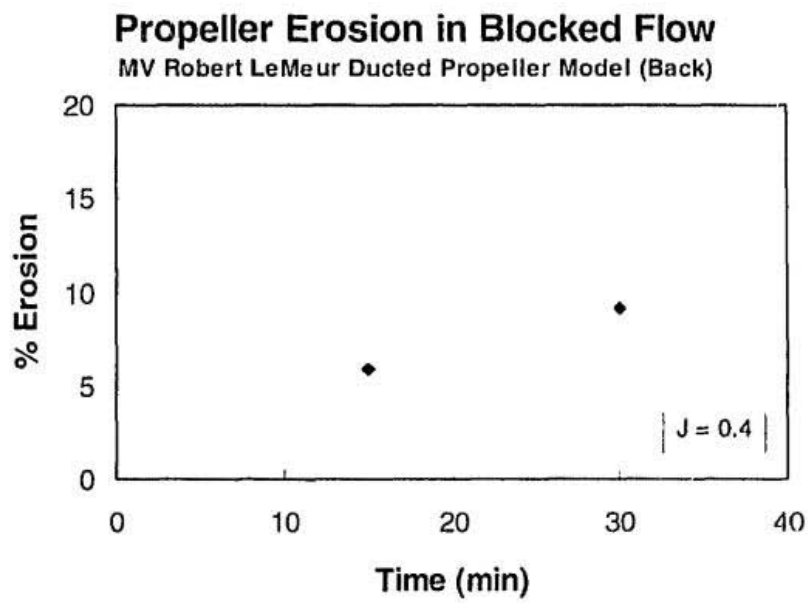

Figure 64: Ducted Propeller Erosion Results (Face and Back: % Erosion vs. Time)

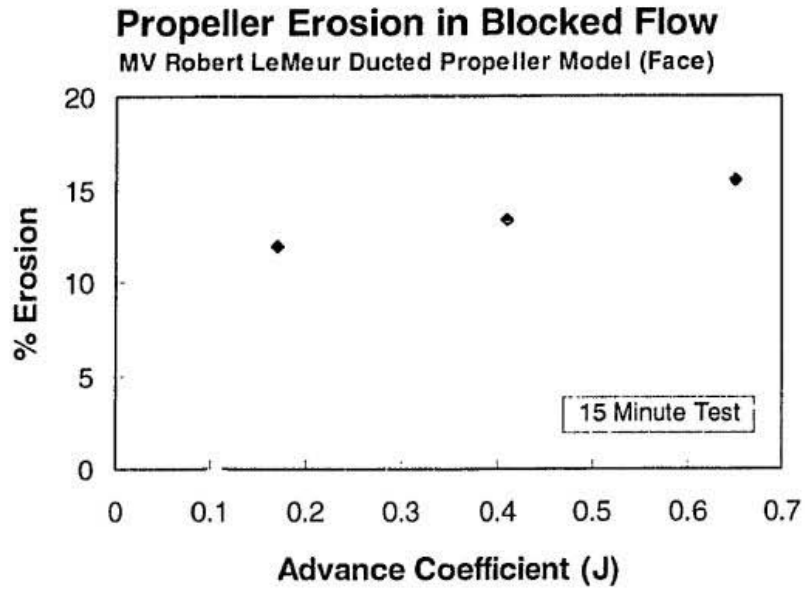

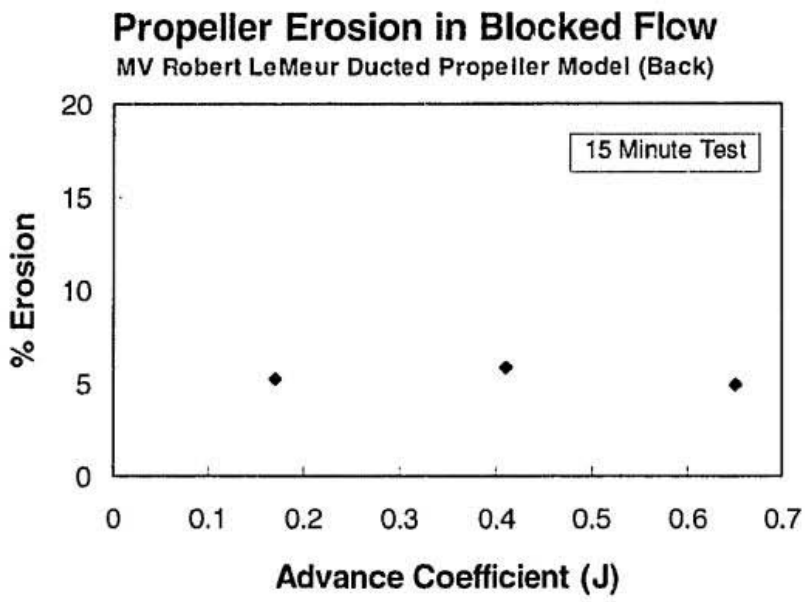

Figure 65: Ducted Propeller Erosion Results (Face and Back: % Erosion vs. Advance Coefficient)

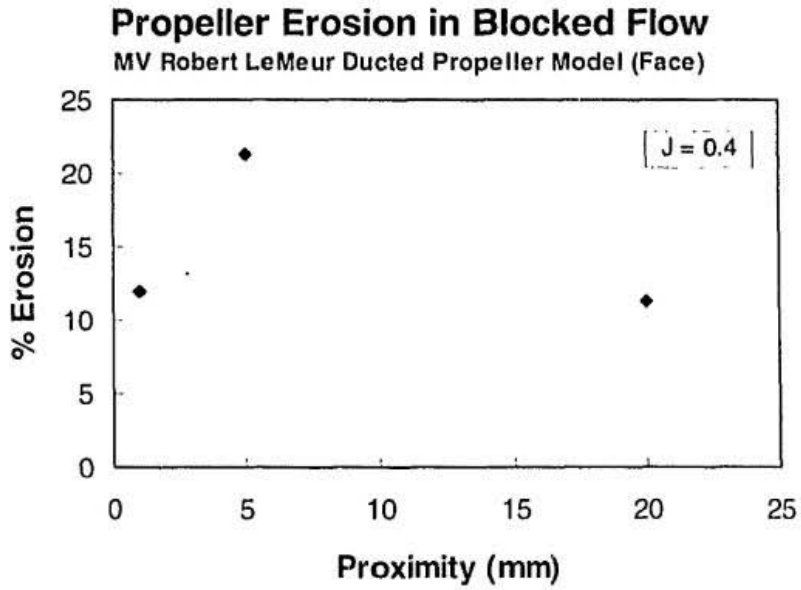

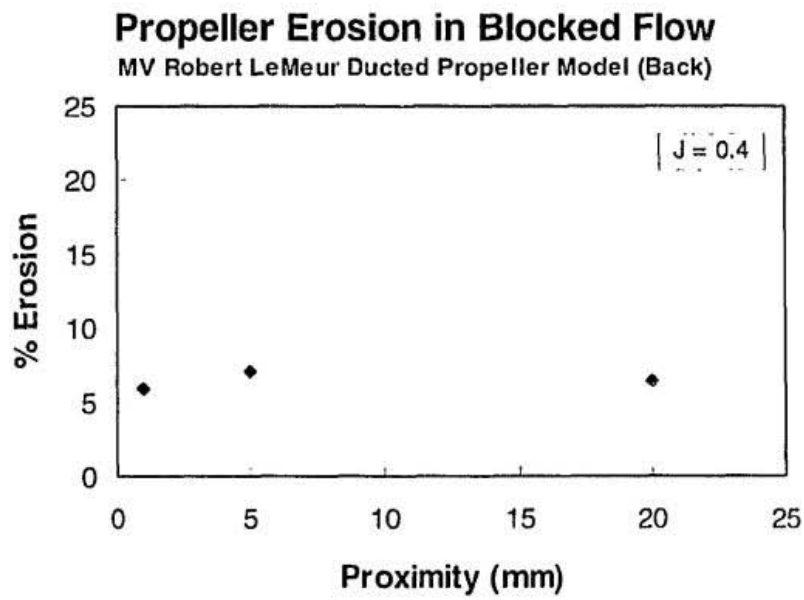

Figure 66: Ducted Propeller Erosion Results (Face and Back: % Erosion vs. Proximity)

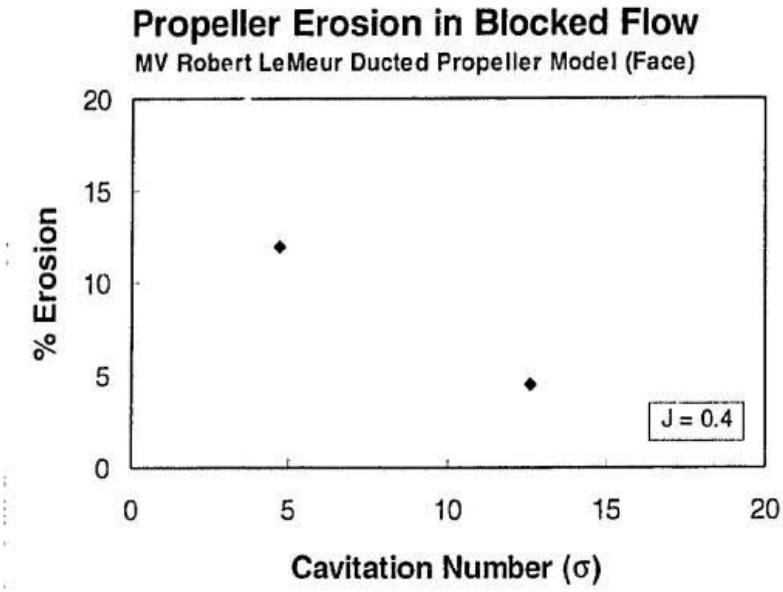

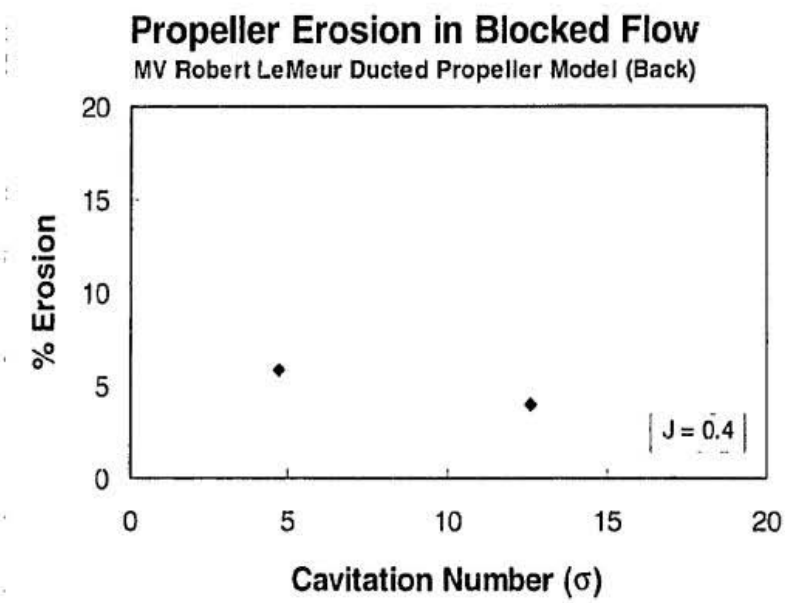

Figure 67: Ducted Propeller Erosion Results (Face and Back: % Erosion vs. Cavitation Number)

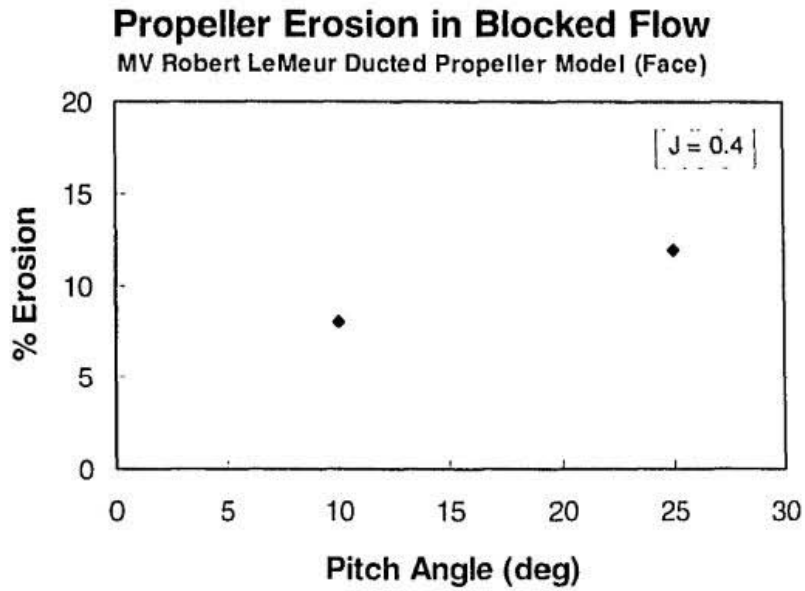

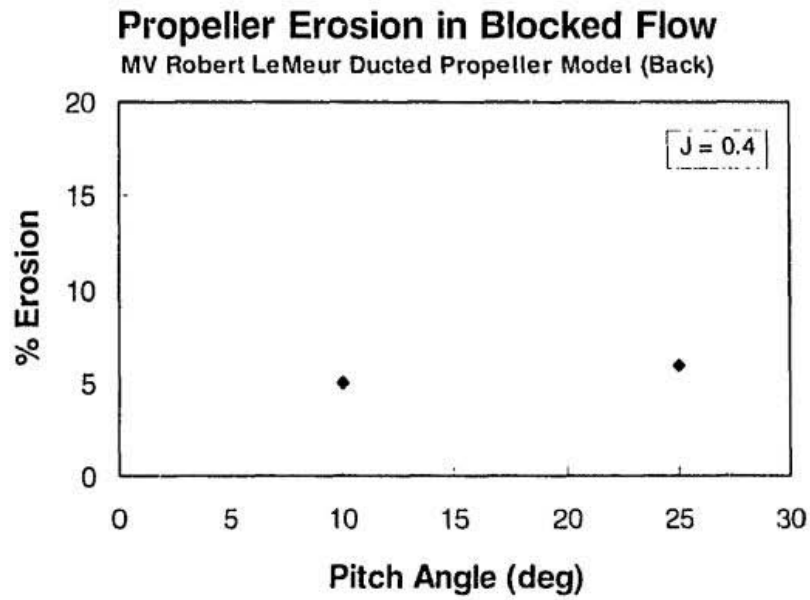

Figure 68: Ducted Propeller Erosion Results (Face and Back: % Erosion vs. Pitch Angle)

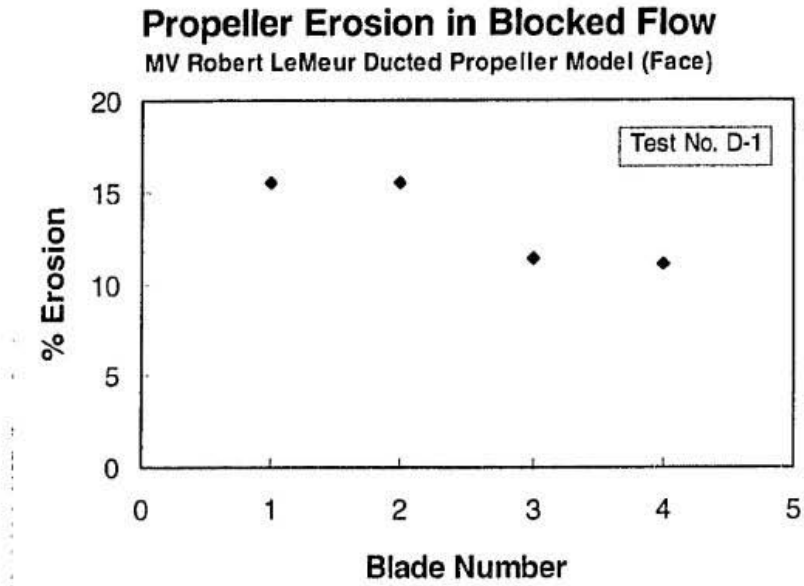

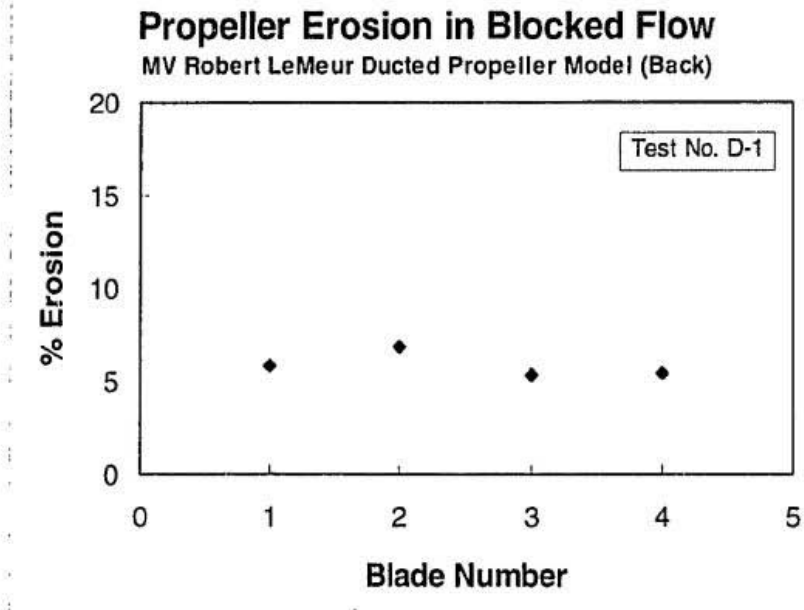

Figure 69: Ducted Propeller Erosion Results for Test No. D-1 (Face and Back: % Erosion vs. Blade Number)

4.3 Comparison of Erosion Results

One of the major concerns which arises when comparing erosion results from different tests is related to the ink used as the soft surface. When different inks are used, one ink may be more robust than another. In other words, given the same test conditions, the amount of erosion which occurs may be different for each of the inks.

The *Crown* ink used with the open propeller model was subject to paint peel. Evidence of this was obvious from the photographs of the test results. For the ducted propeller tests, the *Avery* ink showed no signs of paint peel: the erosion patterns between blades were similar in location and extent. The erosion occurred as the removal of speckles of the painted surface, which indicated that the coating was thin. (This was as required for a proper paint test.) As a result, any area measurements that were made for the open propeller may be exaggerated due to paint peel. For the comparisons made below, paint effects are highlighted as necessary to explain and clarify the test results

An important point to note regarding these tests is that the comparisons which have been made are relative. The intent was not to quote actual amounts of erosion for one test versus another. Of greater significance, differences or similarities between an open propeller and a ducted propeller, operating in blocked flow, have been identified. Therefore, despite the fact that paint peel occurred during the open test program, trends were still identified from the test results.

For both propellers, a standard test duration of 15 minutes was chosen. A 30 minute test was also performed in each case as a check. Both propellers showed more

erosion during the 30 minute test. At the end of a 15 minute test, the extent and location of erosion was already defined. More erosion was measured during the 30 minute test since the film removal over the eroded regions was more complete than it was for the 15 minute test. In both cases, the 15 minute test duration was deemed suitable since the location and extent of erosion were well defined during that time.

Over a range of advance coefficients, both propellers showed more face erosion at higher J values. The trend appeared to increase more steeply for the open propeller than it did for the ducted propeller. However, since paint peel did occur during some of the open tests, the steepness of the curve may be exaggerated. Nevertheless, the open propeller results predicted the same general trend for face erosion that was predicted from the ducted propeller test results. For both propellers, back erosion was minimally affected by changes in advance coefficient, although slightly more back erosion was noted at J=0.4 (about 1% of the blade area) than at the other J values.

Upon examining the proximity effects on both propellers, the test results predicte l another trend. As the blade/block clearance was increased, erosion also increased until it reached a peak. After this point was reached, the amount of erosion decreased with further increases in clearance. For these tests, the highest erosion was measured at a gap of 5 mm. While the trend was applicable for both face and back erosion, more erosion occurred on the face. Due to the limited number of data points, the actual curves that the trends follow for each propeller cannot be predicted accurately from the results given here. More tests would be required to accurately define the curves.

For the open propeller proximity tests, paint peel was noted to occur. The face erosion which was measured for the 5 mm gap test appeared to be excessive. A second test was performed at the same conditions with almost identical results. Paint peel was apparent for both of these tests. Therefore, the initial trend identified for the open propeller may be skewed upward. However, the general form of the trend was identified: erosion increased with increasing blade/block clearance until a peak was reached, after which point erosion decreased with further increases in clearance.

When considering the effect of the cavitation number, less erosion should occur as the cavitation number is increased. At higher cavitation numbers, less cavitation occurs, therefore, there is less opportunity for erosion to take place. For both propellers, face erosion followed this trend: there was less erosion at higher cavitation numbers. For the ducted propeller, this was also applicable for back erosion. However, for the open propeller, more back erosion was measured for the higher cavitation number. Examination of the photographed erosion results indicated that paint peel was a factor in this test. Even though the regions of erosion during this test were relatively common between blades, the edges of the eroded boundaries showed signs of tearing, which is typical of paint peel.

The variability of erosion between blades for each test was also studied for both propellers. For the ducted propeller, blades 1 and 2 tended to show more face erosion than blades 3 and 4. This was attributed to slight variations in the pitch of each blade since the blades were positioned manually before testing began. Geometric variations in the blades may have also been a factor. For the open propeller, no trends were identified

and the amount of erosion was variable between blades. This, in part, was probably the result of paint peel. Had the *Avery* ink been used for the open propeller tests, less variability in the erosion results would have been likely. If a trend had been identified for the open propeller, it would have led to the conclusion that there may have been geometric differences between blades.

Generally, given the same test conditions, the ducted propeller experienced a higher percentage of erosion than the open propeller. For an open propeller operating in blocked flow, the cloud cavitation usually dissipated once the blade reached an angle of $\theta \approx 100°$. For the ducted propeller, the influence of the nozzle caused the cavitation to persist longer than it would for an open propeller operating in similar conditions, sometimes to $\theta \approx 180°$. Therefore, cavitation on the ducted propeller had a greater opportunity to cause erosion.

4.4 Pressure Sensitive Film Trials

Upon completion of Test No. D-8, two tests with *PRESCALE* were attempted using the ducted propeller. These tests were attempted before test D-9. Since the blade angles had not been changed for tests D-1 to D-8, this allowed the pitch angle to remain set at 25° for the pressure sensitive film tests. Following the procedure outlined in Chapter 3, surface preparation and film application were completed (see Figure 70). The first test, P-1, was to have been completed with $J = 0.4$ and $\sigma = 4.5$. The full blockage was used with a blade/block clearance of 20 mm.

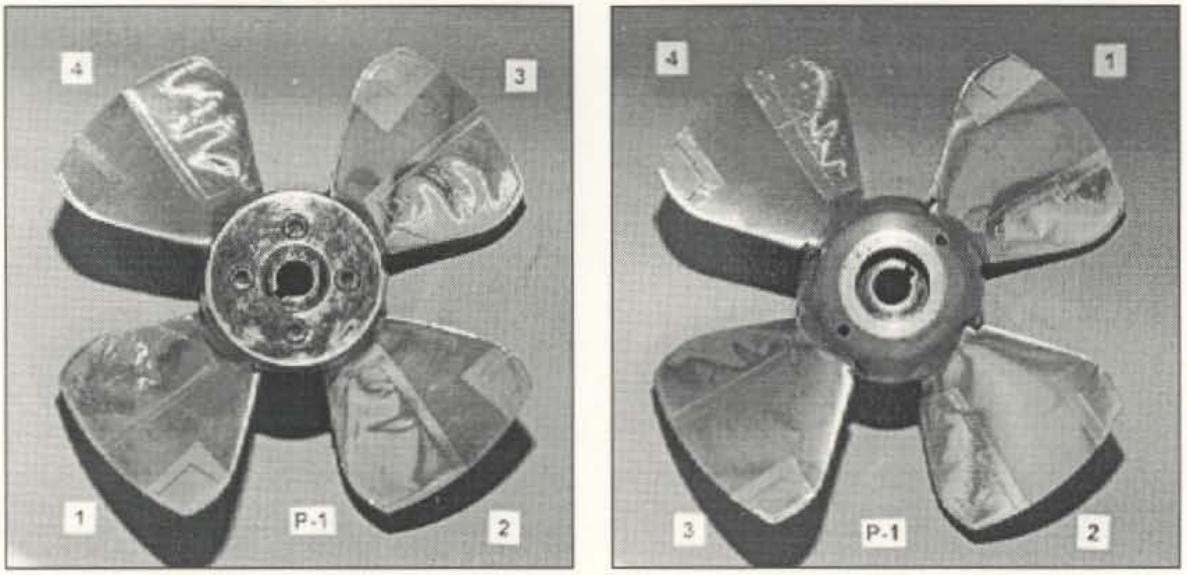

Figure 70: Ducted Propeller (Face and Back) Before Test No. P-1

Following the test procedures that were previously outlined, tunnel pressure and water speed were set before propeller rotation was initiated. Propeller rotational speed was then steadily increased to the required setting over a span of approximately 10 seconds. Cavitation began approximately half way through the ramp-up period. Within 5 to 15 seconds of cavitation initiation, tape and pressure sensitive film were torn from the model as a result of the violent cloud (see Figure 71). The test was terminated at this point. No measurements could be made.

Taking particular care to ensure that the anchoring tape was smoothly applied without any air bubbles present below the surface, the propeller was prepared for another test. The same test was repeated as Test No. P-2. As for P-1, tape and film were torn away from the model upon the initiation of cavitation. No measurements could be made. Time constraints on the work led to a decision to terminate this component of the test program.

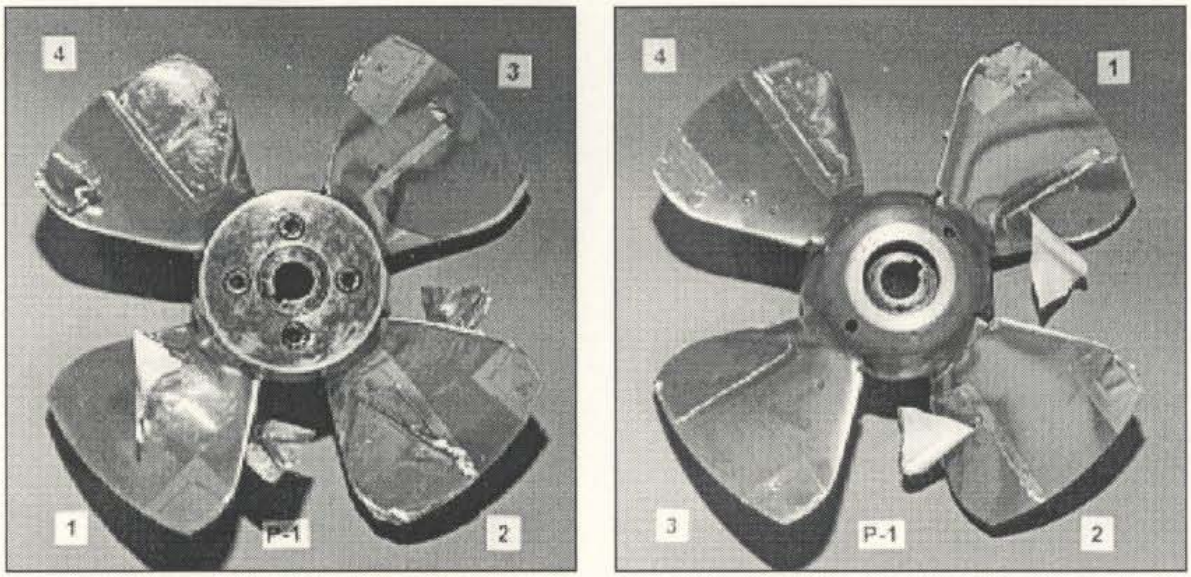

Figure 71: Ducted Propeller (Face and Back) Following Test Attempt

Chapter 5
Full Scale Examinations

5.1 General

When erosion experiments are performed, it is always desirable to compare the test results to the full scale propellers. Visual examinations provide the best opportunity to study the propellers. However, this is not always possible as it requires that the ships in question be dry-docked. If this is the case, examination of propeller damage reports is the next best option.

Concerning the *R-Class* propellers, visual examinations were not possible as the *R-Class* ships were on active duty during the time that this work was completed. Since the *MV Robert LeMeur* was afloat, it was not possible to examine her ducted propellers.

To illustrate the varied types of damage that ice-class ships may experience, damage reports for three ships have been discussed. These ships include two CCG ice-breakers with open fixed pitch propellers, for which damage reports were available and visual examinations were completed. While their propellers are different from those of the *R-Class* vessels, the damage which is shown is typical of that which may be found on open fixed pitch ice-class propellers. The third ship was the *MV Robert LeMeur*, whose

ducted controllable pitch propeller was modelled for these erosion experiments. Blade erosion damage was reported by CANMAR for the *LeMeur*, but this was not caused by cavitation in ice-blocked flow. Rather, the damage resulted after gravel was ingested through the propellers (Brydon, 1995).

In most cases, the damage that is observed can be attributed to impacts with ice. However, since ice-class propellers are generally optimized for strength, and not for hydrodynamic performance (the blade sections are usually thickened), the possibility of propeller cavitation is heightened. Whether in blocked or open flow, cavitation is undesirable as it can lead to blade damage and reduced efficiency.

It should be noted that the total amount of time that propellers spend operating in ice conditions is low. This implies that the amount of time spent in blocked flow is also low. Therefore, although blockage conditions can be severe, there is little time for erosion to occur.

5.2 *CCGS Sir Humphrey Gilbert*

Hofmann et al. (1991) reported on propeller damage for this vessel. At that time, no blade distortions (cracks, tears, deformations, etc.) were observed, but severe pitting over the entire surface was noted. This pitting was attributed to cavitation erosion. The propeller, which was made from vanadium steel, was susceptible to cavitation due to its inherently poor hydrodynamical shape. Blade sections had been thickened for increased strength and the leading and trailing edges were rounded to allow maximum thickness as far as possible along the span towards the edges. Due to the thick rounded edges, early

flow separation occurred, resulting in a heightened possibility of cavitation. The poor surface condition of the blades also led to a reduction in efficiency.

In contrast, propellers from the same ship were examined in 1994 and again in 1995 (Doucet, 1994 and Doucet, 1995b). At the time, evidence of pitting damage was minimal (see Figure 72). Blade damage was predominantly the result of impacts with ice (see Figure 73). These propellers (see Figure 74) were made from an alloy of manganese, aluminium and bronze (*Superston 70*: a trade name of Stone Marine Canada Ltée., PQ, and Stone Manganese Marine Ltd., UK). The propellers were still exposed to the same cavitation phenomenon that was described previously, however, the new propeller material was much more resistant to erosion damage, as illustrated in the photographs.

Canadian Coast Guard (Newfoundland Region) experience indicated that erosion of ice-class propellers was a problem for those made from vanadium steel. Those made from *Superston 70* have not experienced erosion problems (Conway, 1994). This illustrates the importance of proper selection of propeller materials for resistance to cavitation erosion.

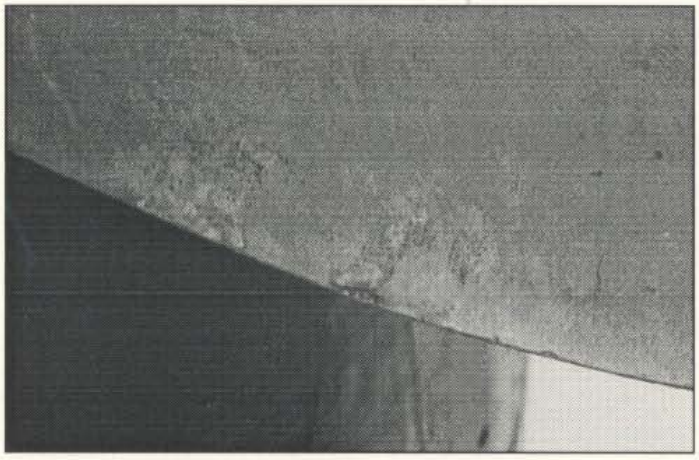

Figure 72: Pitting Damage on Repaired Region (leading edge, face, starboard side)

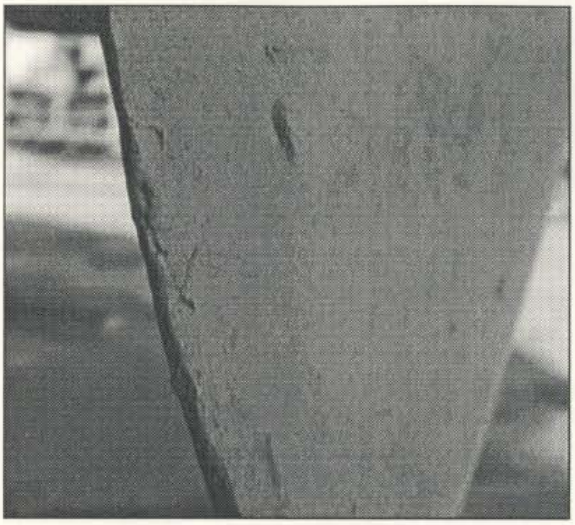

Figure 73: Impact Damage (leading edge, face, starboard side)

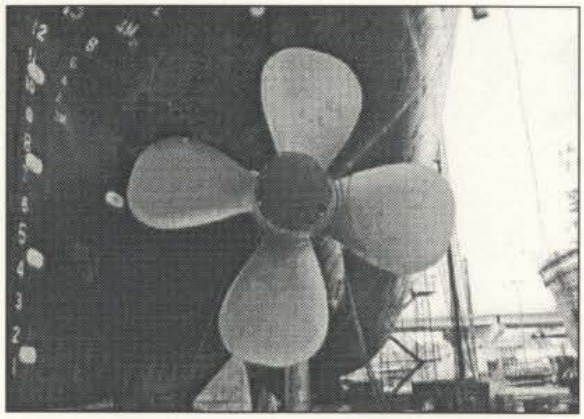

Figure 74: Starboard Propeller from the *CCGS Sir Humphrey Gilbert*

5.3 CCGS Ann Harvey

Hofmann et al. (1991) also performed a propeller examination for this vessel. At the time, extensive edge damage was noted, primarily along the trailing edge. Since the propellers were fixed pitch, this damage probably occurred when the vessel was backing as the trailing edge becomes the leading edge when reversing. Observed damage was in the form of tears, deformations due to impacts, and edge cracks. Erosion was not noted. The propeller material was *Superston 70.* (It should be noted that the *CCGS Ann Harvey*, an 1100-Series ice-breaker, has a propeller design that is very similar to that used on the *R-Class* (1200-Series) ice-breakers, whose propeller type was tested in the experiments reported in this document.)

The propellers of this vessel (see Figure 75 to Figure 77) were also examined in 1994 (Doucet, 1994). They were removed from the ship as one had suffered a broken

blade, necessitating propeller replacement. These propellers, also made from *Superston 70*, showed no signs, whatsoever, of erosion damage. The damage that was present was typical of that which results from impacts with ice. A subsequent examination in 1995, when the ship was again dry-docked, also showed no evidence of erosion. These propellers had been in service for one year (Doucet, 1995b).

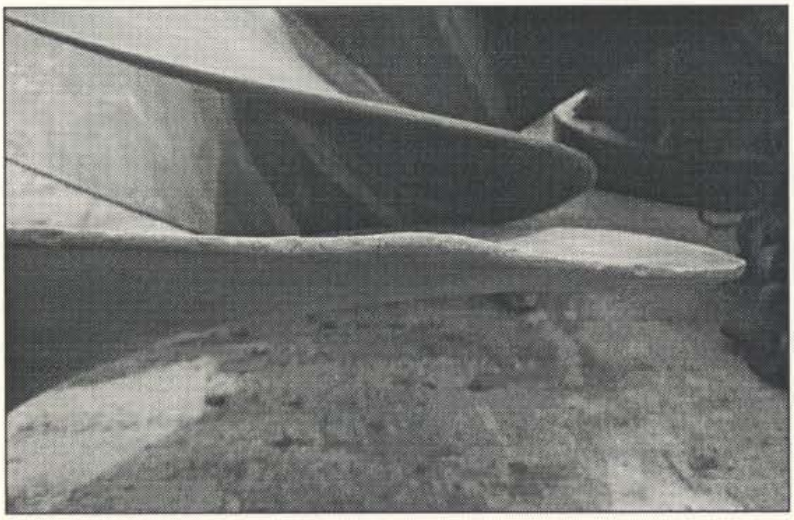

Figure 75: Impact Damage (trailing edge, face, blade 2, port propeller)

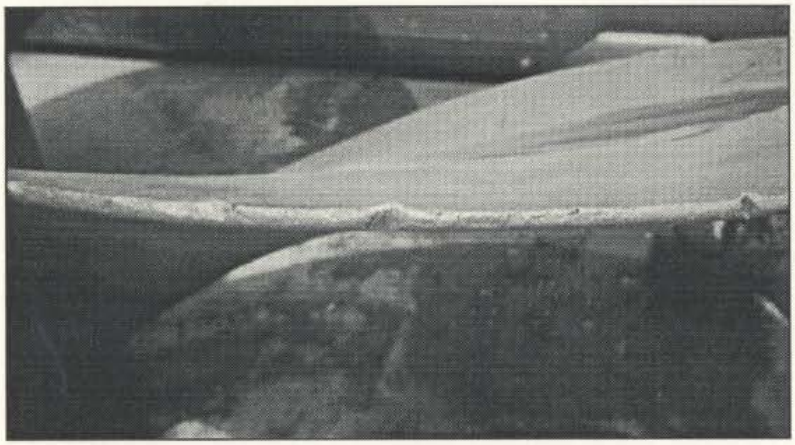

Figure 76: Impact Damage (trailing edge, face, blade 4, port propeller)

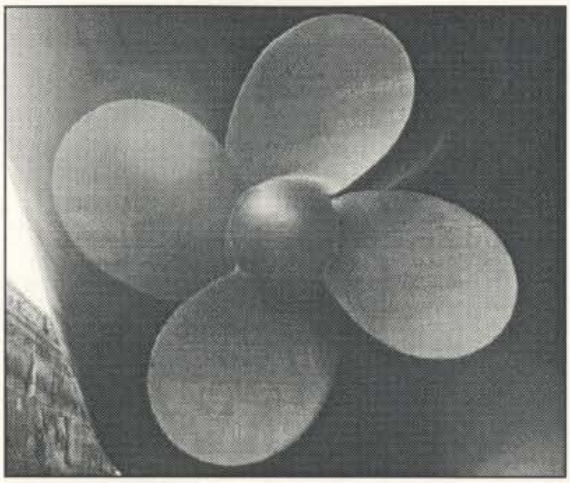

Figure 77: Port Propeller from the *CCGS Ann Harvey*

5.4 *MV Robert LeMeur*

In 1995, CANMAR was solicited for information pertaining to cavitation erosion damage for the *MV Robert LeMeur* propellers (see Figure 78). Their response did not include any reference to cavitation erosion. The damage records and photographs which were sent documented erosion damage that was caused by ingestion of gravel through the propellers (see Figure 79 and Figure 80). Of particular interest, Figure 81 shows the instrumented blade that was used during the propeller/ice interaction project which was reported by Laskow et. al. (1986).

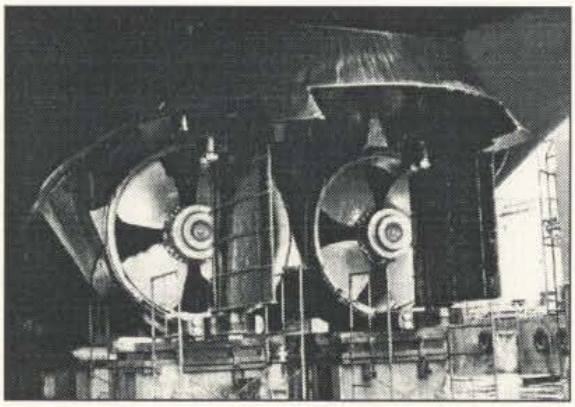

Figure 78: Ducted Propellers from the *MV Robert LeMeur*

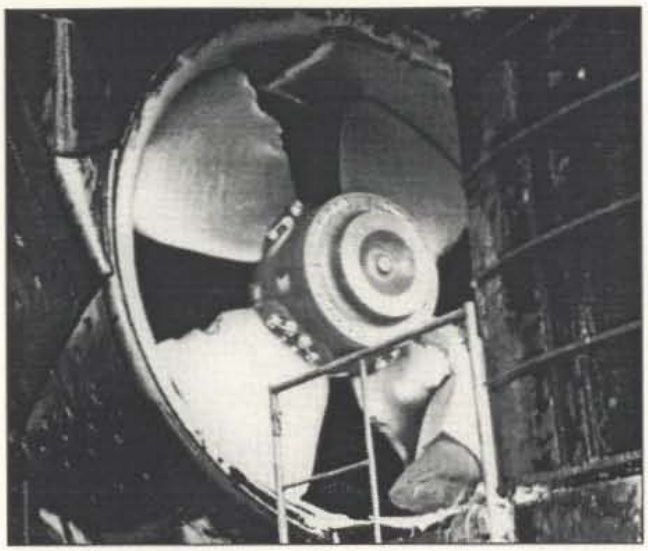

Figure 79: Blade Damage on Port Propeller

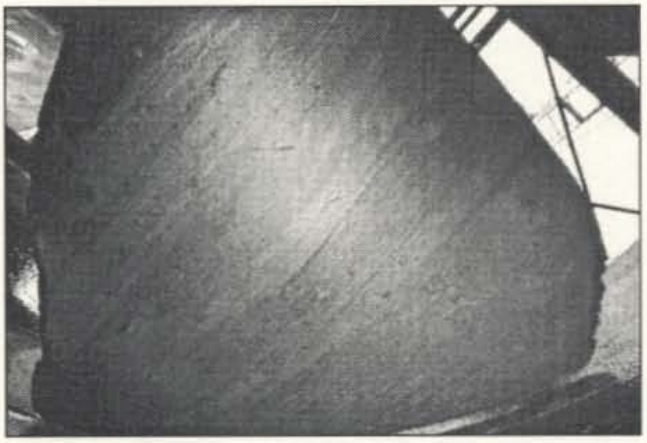

Figure 80: Blade Damage on Starboard Propeller

Figure 81: Damage to Starboard Blade (note instrumentation locations)

Chapter 6
Conclusions

An erosion study, using paint films, was conducted in the cavitation tunnel at the Institute for Marine Dynamics, NRC, to investigate the possibility of cavitation erosion of ice-class propellers in blocked flow. The purpose of these experiments was to determine the extent and location of erosion which a propeller may experience in blocked flow.

Two model propellers were used for this study: the first was an open, fixed pitch propeller while the second was a ducted, variable pitch propeller. During testing, a simulated ice blockage was installed ahead of the propeller model to block the flow into the propeller. Tests were carried out over a range of advance coefficients for various test conditions. The resulting types of cavitation were documented, the erosion patterns were photographed, the eroded areas were measured and comparisons were made between tests.

Dimensional analysis was initially applied to the problem. For this analysis, relevant variables were chosen and a partial solution was formulated. The resulting dimensionless parameters were discussed with regards to their relevance in designing cavitation erosion experiments. Since the study only focused on the hydrodynamic effects of blocked flow, metallurgical variables were not included in the analysis.

Operation of these propeller models in the wake of the simulated ice-blockage resulted in severe cavitation and erosion. Both vortex and cloud cavitation were observed. Even at atmospheric pressure, cavitation and erosion resulted.

During the open propeller test program, problems with paint peel were experienced. Evidence of this was obvious: tear marks, typical of paint peel, were evident along the boundaries of some eroded regions. As a result, the area measurements made for the open propeller may be exaggerated. The occurrence of this phenomenon was accounted for in the discussions pertaining to the open propeller. The trends which were predicted from the open propeller data, discussed below, were still deemed to be valid as they agreed in principle with the trends predicted from the ducted propeller data.

Before the ducted propeller test program was started, an extensive study was undertaken to find a new ink suitable for erosion tests. The following inks were tested: *Crown Blue Toolmakers Ink*, *Starrett Kleenscribe Blue Layout Dye*, *Dykem Layout Blue*, *Precision Red Layout Fluid*, *AOTAK*, *SSPA Stencil Ink* and *Avery* marker ink. While the other inks were difficult to apply or exhibited some form of paint peel, the *Avery* ink was easily applied and did not peel. Based on the experience gained from these ink trials, the *Avery* marker ink is recommended for future erosion tests in the IMD cavitation tunnel.

For the ducted propeller test program, paint peel did not occur. For any given test, the erosion patterns between blades were consistent in both location and extent. Differences between blades could be attributed to the fact that the pitch of each blade was set separately, and hence, the pitch may have been slightly different from blade to blade.

Erosion occurred on both sides of the propeller models during these experiments. For both propellers, back erosion was predominant along the trailing edge. For the open propeller, face erosion occurred, near $r/R \approx 0.70$, along the leading edge, at mid-span and along the trailing edge. Face erosion on the ducted propeller occurred predominantly in the mid-span region, also near $r/R \approx 0.70$. For all experiments, the observed cavitation patterns were scrutinized to identify when, during a blade revolution, erosion of a given region occurred.

Generally, given the same test conditions, the ducted propeller experienced a higher percentage of erosion than the open propeller. Cavitation persisted longer for the ducted propeller than it did for the open propeller due to the influence of the nozzle. Therefore, cavitation on the ducted propeller had a greater opportunity to cause erosion.

Test duration was set at 15 minutes for both propellers. A 30 minute test was also performed for each model as a check. The location and extent of the eroded regions were the same regardless of which duration was chosen. At the end of the 30 minute tests, more erosion was measured since the film removal within the affected regions was more complete than it was for similar 15 minute tests. A 15 minute test duration was deemed acceptable for these experiments since the location and extent of erosion were well defined within this time.

For both propellers, the amount of face erosion increased with increasing advance coefficient. The trend was steeper for the open propeller, but, since paint peel occurred during some of these tests, the steepness of the curve may be exaggerated. Nevertheless,

the same trend was predicted for both the open propeller and the ducted propeller. Normally, one would expect more cavitation, and hence more erosion, as the advance coefficient was reduced since the propeller loading is normally increased at the lower J values. However, this reversal was likely caused by the non-uniform wake behind the block. As each blade operated within and outside the wake, the differences in flow conditions, between the blocked flow and the unblocked flow regions, would be greater at higher advance coefficients than they would be at lower J values. The manner in which cavitation clouds passed from the back of a blade to the face of a following blade was affected by changes in the advance coefficient.

Changes in the advance coefficient had a minimal effect on back erosion. At J = 0.4, slightly more erosion occurred than at the other J values, but this was only about 1% of the blade area. Since the cavities which affected the back of the propeller models were relatively large, additional increases in the amount of cavitation, as occurred when J was increased, took place away from the blade surfaces. Therefore, the additional cavitation only minimally affected the blade surface.

Pertaining to proximity, as the blade/block clearance was increased, erosion also increased until it reached a peak. Further increases in clearance resulted in reduced erosion. This trend was applicable to both the face and back of both propellers, but higher erosion occurred on the face. For these experiments, the peak occurred at a gap of 5 mm. However, due to the limited number of points, the true trend of the curve could not be determined. More experiments would be required to further define the curves.

Paint peel did occur during the open propeller proximity tests, in particular, during the tests with a 5 mm gap. As a result, the face erosion trend for the open propeller may be skewed upwards. However, the general form of the trend agrees well with that predicted from the ducted propeller test results.

The effects of changes in the cavitation number were also investigated. Since less cavitation occurs as the cavitation number is increased, there is less opportunity for erosion to occur. This was applicable for face erosion on both propellers and for back erosion on the ducted propeller. However, for the open propeller, more erosion occurred on the back at the higher cavitation number. Subsequent examination of the erosion results attributed this to paint peel.

Additionally, since the pitch could be varied on the ducted propeller, this variable was also examined. As expected, more erosion occurred at the higher pitch angle of 25°. At this pitch angle, the blades were more heavily loaded for the same wake conditions than they were for $\phi = 10°$, resulting in more cavitation.

Finally, variability of erosion between blades for each test was examined for both models. For the ducted propeller, blades 1 and 2 consistently showed more erosion than blades 3 and 4. This was attributed to slight variations in the pitch of each blade since the blades were positioned manually before testing began. No noticeable trends were identified for the open propeller as the blade erosion was variable between blades and between tests. Since paint peel was a problem for the open tests, this may have masked trends that would have otherwise appeared if a more suitable ink had been used.

Additionally, two tests were attempted using pressure sensitive films to allow for estimation of the impact pressures on the blade surfaces. Both of these tests were unsuccessful since the films were torn from the blades. The adhesive tape used for securing the films was unable to withstand the cavitation loads which resulted in blocked flow and the films were damaged within 5 to 15 seconds of cavitation initiation. If future tests are to be completed using this type of film, a method for successfully securing the same to the blades must be devised. An alternative to using pressure sensitive films would be to use pressure transducers, however, the results would be localized. Use of pressure transducers would require modifications to the blades so that the sensors could be fitted into and flush with the blade surfaces.

Extreme momentary cavitation at full scale occurs during propeller/ice interaction, as has already been demonstrated from video records of full scale tests on the *USCGS Polar Star* (Transport Development Centre, 1995). Vibration in these conditions can be severe. Such intense cavitation leads to the possibility of erosion damage at full scale.

However, examination of full scale open, fixed pitch propellers showed minimal cavitation erosion damage. This is probably because most ice pieces either pass through the propeller or are deflected to the side. Full scale cavitation has been observed during these types of events. In the event that large ice pieces are encountered, blockage and ice milling events will generally persist for no more than a few seconds. Cavitation damage on these propellers is more prevalent in the vicinity of blade edges which have been damaged from impacts with ice. The resulting deformations usually provide locations for

cavitation inception, with the resulting cavitation being present even when the propeller is operating in subsequent free-running conditions.

Visual examinations of the open, fixed pitch propellers from two Canadian Coast Guard ice-breakers were completed. The propellers examined were unaffected by cavitation erosion. Damage which was observed was typical of that which results from impacts with ice (tears, gouges, bent edges, etc.). However, the importance of material selection was also highlighted. Made from a different material, an older propeller from one of the ships exhibited severe pitting.

Since blocked flow conditions are more prevalent for ducted propellers, erosion damage may be a more severe problem than it is for open propellers operating in similar conditions. In particular, on multi-screw vessels with ducted propellers, operation may continue even if one of the propellers is blocked. Clearing of the blockage will not be done until vibration becomes excessive or forward thrust is severely impaired. As a result, propeller blockages could be of a few minutes duration.

No evidence of full scale cavitation erosion was obtained pertaining to the ducted propeller that was tested. However, reliance was placed on service records taken for these propellers after they sustained damage caused by gravel ingestion. Visual examinations of full scale ducted propellers which continually operate in heavy ice conditions should be conducted to determine if there is any correlation between model results and actual conditions.

References

Al-Hashem, A., Caceres, P.G., Riad, W.T., and Shalaby, H.M., (1995), "Cavitation Corrosion Behaviour of Cast Nickel-Aluminum Bronze in Seawater", *Corrosion: The Journal of Science and Engineering*, Vol. 51, No. 5, pp. 331-342.

Auret, J.G., Damm, O.F.R.A., Wright, G.J., and Robinson, F.P.A., (1993a), "Cavitation Erosion of Copper and Aluminium in Water at Elevated Temperature", *Tribology International*, Vol. 26, No. 6, pp. 421-429.

Auret, J.G., Damm, O.F.R.A., Wright, G.J., and Robinson, F.P.A., (1993b), "The Influence of Water Air Content on Cavitation Erosion in Distilled Water", *Tribology International*, Vol. 26, No. 6, pp. 430-432.

Avner, S.H., (1974), *Introduction to Physical Metallurgy*, 2nd ed., McGraw-Hill Book Company, Toronto, p. 332.

Bjärne, E., (1983), "Further Studies of Propeller Cavitation Erosion", *Proceedings of the 2nd International Conference on Cavitation*, Edinburgh, pp. 141-149.

Bjärne, E., (1995),"'Queen Elizabeth 2', Cure of Blade Root Cavitation Erosion", *Proceedings: PROPCAV'95*, University of Newcastle-Upon-Tyne, Newcastle-Upon-Tyne, United Kingdom, pp. 141-150.

Bose, N. and Jones, S.J., (1993), *Application to NSERC for a Strategic Grant*, Memorial University of Newfoundland, St. John's, Newfoundland, Canada, (internal document).

Brydon, W.A., (1995), Personal Communication: *Damage Report for MV Robert LeMeur Propellers*, Canadian Marine Drilling Limited (CANMAR), Calgary, Alberta, Canada.

Burton, R.A., and Burton, R.G., (1992), "Surface Stresses from Pinpoint Cavitation in a Viscous Film", *Tribology Transactions*, Vol. 35, No. 4, pp. 756-760.

Carlton, J.S., (1994), *Marine Propellers and Propulsion*, Butterworth-Heinemann Ltd., Oxford.

Chen, Y.L., and Israelachvili, J., (1991), "New Mechanism of Cavitation Damage", *Science*, Vol. 252, pp. 1157-1160.

Conway, W.G., (1994), Personal Communication: *Discussion Pertaining to Propellers of CCG Ice-Breakers that Operate in the Newfoundland Region*, Regional Fleet Engineering Superintendent, Newfoundland Region, Canadian Coast Guard, St. John's, Newfoundland.

Daugherty, R.L, Franzini, J.B., and Finnemore, E.J., (1985), *Fluid Mechanics with Engineering Applications*, 8th ed., McGraw-Hill Publishing Company, Toronto.

Deeprose, W.M., King, N.W., McNulty, P.J., and Pearsall, I.S., (1976), "Cavitation Noise, Flow Noise and Erosion", *Cavitation: A Conference Arranged by the Fluid*

Machinery Group of the IMechE, The Institution of Mechanical Engineers, Edinburgh, pp. 373-381.

Doucet, J.M., (1992a), "Cavitation Tunnel Manometer Calibration", Ocean Engineering Research Centre, Report No. OERC92-TR-HYD-92004, Memorial University of Newfoundland, St. John's, Newfoundland, Canada.

Doucet, J.M., (1992b), "Cavitation Tunnel Instruction Manual", Ocean Engineering Research Centre, Report No. OERC92-TR-HYD-92005, Memorial University of Newfoundland, St. John's, Newfoundland, Canada.

Doucet, J.M. (1994), *Notes: Full Scale Propeller Examinations (1994) for CCGS Ann Harvey and CCGS Sir Humphrey Gilbert*, (unpublished).

Doucet, J.M., Bose, N., Walker, D., and Jones, S.J., (1995a), "Cavitation Erosion on a Model Ice Class Propeller In Blocked Flow", *Proceedings: PROPCAV'95*, University of Newcastle-Upon-Tyne, Newcastle-Upon-Tyne, United Kingdom, pp. 229-238.

Doucet, J.M., (1995b), *Notes: Full Scale Propeller Examinations (1995) for CCGS Ann Harvey and CCGS Sir Humphrey Gilbert*, (unpublished).

Doucet, J.M., Bose, N., Walker, D., and Jones, S.J., (1996), "Cavitation Erosion in Blocked Flow with a Ducted Ice-Class Propeller", *Proceedings of the 15th International Conference on Offshore Mechanics and Arctic Engineering*, American Society of Mechanical Engineers, pp. 121-128.

Emerson, A., and Patience, G., (1976), "The Prediction and Prevention of Cavitation Erosion of Marine Propellers", *Cavitation: A Conference Arranged by the Fluid Machinery Group of the IMechE*, The Institution of Mechanical Engineers, Edinburgh, pp. 233-240.

Franc, J.P., Michel, J.M., and Trong, H., (1992), "An Experimental Investigation of Scale Effects in Cavitation Erosion", *Proceedings of the Institution of Mechanical Engineers: Cavitation - International Conference (1992)*, Mechanical Engineering Publications Limited, Suffolk, England, pp. 111-119.

Hammitt, F.G., (1980), *Cavitation and Multiphase Flow Phenomena*, McGraw-Hill International Book Company, Montreal.

Harvald, Sv. Aa., (1983), *Resistance and Propulsion of Ships*, John Wiley & Sons, Toronto, pp. 186-198.

Hobbs, J.M., (1976), "Vibratory Cavitation Erosion Testing at Nel", *Cavitation: A Conference Arranged by the Fluid Machinery Group of the IMechE*, The Institution of Mechanical Engineers, Edinburgh, pp. 269-274.

Hofmann, T., McPherson, C.J., and Bose, N., (1991), "Propeller Blade Damage Attributable to Vessel Operation in Ice", *Proceedings of the 11th International Conference on Port and Ocean Engineering Under Arctic Conditions (POAC'91)*, pp. 773-784.

Huang, T.T. (Chairman), Kuiper, G. (Secretary), and 7 others, (1990), "Report of the Cavitation Committee", *Proceedings of the 19th International Towing Tank Conference (ITTC)*, pp. 161-233.

Janakiram, K.S., and Rao, C.S., (1976), "Effects of Velocity and Frequency of Impacts on Erosion Due to Liquid Jets", *Cavitation: A Conference Arranged by the Fluid Machinery Group of the IMechE*, The Institution of Mechanical Engineers, Edinburgh, pp. 261-268.

Jandal Scientific, (1993a), *MOCHA Image Analysis Software: User's Manual*, San Rafael, California, USA.

Jandal Scientific, (1993b), *MOCHA Image Analysis Software: Reference Manual*, San Rafael, California, USA.

Jandal Scientific, (1994), *MOCHA Automated Image Analysis Software: Addendum for Version 1.2*, San Rafael, California, USA.

Kadoi, H., and Sasajima, T., (1978), "Cavitation Erosion Prediction Using a 'Soft Surface'", *International Shipbuilding Progress*, Vol. 25, No. 286, pp. 141-150.

Kato, H., (1975a), "A Consideration on Scaling Laws of Cavitation Erosion", *International Shipbuilding Progress*, Vol. 22, No. 253, pp. 305-327.

Kato, H., (1975b), "A New Cavitation Erosion Test Method and its Application to a Ducted Propeller", *International Shipbuilding Progress*, Vol. 22, No. 253, pp. 291-304.

Kato, H., (1992), "Recent Advances and Future Proposal on Cavitation Erosion Research", *Proceedings of the International Symposium on Propulsors and Cavitation*, Hamburg, STG. Nr 3007, pp. 224-233.

Kato, H., Maeda, M., and Nakashima, Y., (1981), "A Comparison and Evaluation of Various Cavitation Erosion Test Methods", *Trans. ASME Symp. on Cavitation Erosion in Fluid Systems*, pp. 83-94.

Kato, H., Maeda, T., and Magaino, A., (1979), "Mechanism and Scaling of Cavitation Erosion", *Proceedings of the Twelfth Symposium on Naval Hydrodynamics (1978)*, National Academy of Sciences, Washington, D.C., pp. 452-469.

Kenkeremath, D., and Thiruvengadam A.P., (1976), "Analysis and Characterization of Particles Produced by Cavitation Erosion", *Cavitation: A Conference Arranged by the Fluid Machinery Group of the IMechE*, The Institution of Mechanical Engineers, Edinburgh, pp. 285-295.

Knapp, R.T., (1955), "Recent Investigations of the Mechanism of Cavitation and Cavitation Damage", *Transactions of the American Society of Mechanical Engineers*, Vol. 77, No. 7, pp. 1045-1054.

Knapp, R.T., Daily, J.W., and Hammitt, F.G., (1970), *Cavitation*, McGraw-Hill Book Company, Toronto.

Kuiper, G., (1978), "Cavitation Scale Effects", *International Shipbuilding Progress*, Vol. 25, No. 284, pp. 81-90.

Laskow, V., Spencer, P., and Bayly, I., (1986), "The MV Robert LeMeur Ice/Propeller Interaction Project: Full Scale Data," *Marine Technology*, Vol. 23, No. 4, pp. 301-319.

Lindgren, H., and Bjärne, E., (1976), "Studies of Propeller Cavitation Erosion", *Cavitation: A Conference Arranged by the Fluid Machinery Group of the IMechE*, The Institution of Mechanical Engineers, Edinburgh, pp. 241-251.

Lindroos, H., and Björkestam, H., (1986), "Hydrodynamic Loads Developed During Ice-Clogging of a Propeller Nozzle and Means to Prevent the Clogging", *Proceedings of Polartech'86, The International Offshore and Navigation Conference and Exhibition*, Helsinki, Finland, pp. 1061-1092.

Morgan, W.B. (Chairman) and 7 others, (1975), "Report of the Cavitation Committee", *Proceedings of the 14th International Towing Tank Conference (ITTC)*, pp. 15-331.

Nainar, J., and Pola, E., (1976), "Resistance of Various Materials to Cavitation-Erosion Damage", *Cavitation: A Conference Arranged by the Fluid Machinery Group of the IMechE*, The Institution of Mechanical Engineers, Edinburgh, pp. 261-268.

O'Brien, T.P., (1962), *The Design of Marine Screw Propellers*, Hutchinson Scientific & Technical, London.

Plesset, M.S., and Ellis, A.T., (1955), "On the Mechanism of Cavitation Damage", *Transactions of the American Society of Mechanical Engineers*, Vol. 77, No. 7, pp. 1055-1064.

Rawson, K.J., and Tupper, E.C., (1984), *Basic Ship Theory: Volume 2*, 3rd ed., Longman Scientific & Technical, Essex, England, pp. 389-401.

Shalaby, H.M., Al-Hashem, A., Al-Mazeedi, H., and Abdullah, A., (1995), "Field and Laboratory Study of Cavitation Corrosion of Nickel Aluminium Bronze in Sea Water", *British Corrosion Journal*, Vol. 30, No. 1, pp. 63-70.

Shalnev, K.K., Shalobasov, I.A., Kozirev, S.P., Bologa, M.K., and Paukov, Y.N., (1976), "Experimental Investigation of Effect of External Magnetic and Electric Fields on Cavitation and Erosion", *Cavitation: A Conference Arranged by the Fluid Machinery Group of the IMechE*, The Institution of Mechanical Engineers, Edinburgh, pp. 275-283.

Sharp, J.J., Deb, A. and Deb, M.K., (1992), "Applications of Matrix Manipulation in Dimensional Analysis Involving Large Numbers of Variables", *Marine Structures*, Vol. 5, pp. 333-348.

Shima, A., Ihara, A., Miura, N., and Tomaru, H., (1992), "Cavitation Damage Study with a Rotating Disk at the High Peripheral Velocities", *Journal of Hydraulic Research*, Vol. 30, No. 4, pp. 521-538.

Stinebring, D.E., Arndt, R.E.A., and Holl, J.W., (1977), "Scaling of Cavitation Damage", *Journal of Hydronautics*, Vol. 11, No. 3, pp. 67-73.

Suhrbier, K.R. (Chairman), Parkin, B.R. (Secretary) and 7 others, (1987), "Report of the Cavitation Committee", *Proceedings of the 18th International Towing Tank Conference (ITTC)*, pp. 159-219.

Tanibayashi, H., and Nakanishi, M., (1973), "On the Method of Cavitation Tests for Prediction of Tip Erosion of Propeller", *JSNAJ*, Vol. 133, pp. 57-64.

Transport Development Centre, (1995), *Video Record of Cavitation Affecting a Propeller of the USCGS Polar Star*, Government of Canada, Montreal, PQ.

van Manen, J.D., and van Oossanen, P., (1988), *Chapter 6: Propulsion* in *Principles of Naval Architecture*, (Lewis, E., ed.), Vol. II., The Society of Naval Architects and Marine Engineers, Jersey City, New Jersey, United States, pp. 127-254.

Walker, D., and Bose, N., (1994a), "Hydrodynamic Loads and Dynamic Effects of Cavitation on Ice Class Propellers in Simulated Ice Blocked Flow", *Proceedings of the Propellers/Shafting '94 Symposium*, The Society of Naval Architects and Marine Engineers, Virginia Beach, Virginia, United States, pp. 20-1 to 20-19.

Walker, D., Bose, N., and Yamaguchi, H., (1994b), "Hydrodynamic Performance and Cavitation of an Open Propeller in a Simulated Ice-Blocked Flow", *Journal of Offshore Mechanics and Arctic Engineering*, Vol. 116, pp. 185-189.

Weast, R.C., ed., (1975), *Handbook of Chemistry and Physics*, 56th edition, CRC Press, Cleveland, Ohio, USA, p. D-180.

Williams, F.M., Spencer, D., Mathews, S.T., and Bayly, I., (1992), "Full Scale Trials in Level Ice with Canadian R-Class Ice-Breaker", *Transactions of the Society of Naval Architects and Marine Engineers*, Vol. 100, pp. 293-313.

Yamaguchi, H., (1993), "Paint for Cavitation Erosion Paint Test", University of Tokyo, personal communication with Dr. Neil Bose.

YSI Incorporated, (1995a), *YSI Model 50B Dissolved Oxygen Meter Instructions*, Yellow Springs, Ohio, USA.

YSI Incorporated, (1995b), *Operating Instructions: YSI Dissolved Oxygen Probes*, Yellow Springs, Ohio, USA.

Appendix A

PRESCALE Pressure Detecting Sheet: Product Information

FUJIFILM PRESCALE - Pressure Detecting Sheet

FUJIFILM Prescale is a unique sheet designed to convert the pressure into a color of corresponding density, a novel means of pressure measurement responding to the requirements of various industries.

Prescale allows immediate and direct observation of the pressure distribution between the pressurized mechanical parts which could not be measured by the conventional methods. Also the absolute pressure can be determined from the color density measured by the densitometer specifically designed for Prescale or by the standard color chart.

STRUCTURE

Prescale is composed of "A-sheet" having a layer of microencapsulated color forming material and "C-sheet" having a layer of a color developing material. The thin and uniform coated layers, which are essential to the Prescale, are realized by highly sophisticated coating technologies derived from photographic film manufacture.

A-sheet consists of :

Substrate, a hardly breakable polyester film of low compressibility;
Intermediate layer for binding the substrate and the microcapsule layer; and
Microcapsule layer containing a color forming material which generates a vivid color when reacted with the color developing material.

C-sheet consists of :

Substrate, a hardly breakable polyester film of low compressibility;
Intermediate layer for binding the substrate and the color developer layer; and
Color developer layer composed of a highly active color developing material which generates a vivid color when reacted with the color forming material.

WORKING PRINCIPLE

In the pressure measurement, the A-sheet and C-sheet are superposed, with the coated sides face to face.

Upon application of a pressure, the microcapsules are broken and the released color forming material reacts with the color developing material to generate a color on the C-sheet.

The microcapsule layer consists of microcapsules of various sizes. The larger microcapsules are broken by a weaker pressure while smaller ones require a stronger pressure for breakage.
An exact relationship between the pressure and the developed color density is realized by the precise control of capsule size, size distribution and capsule wall thickness. Thus the developed color not only provides a graphic presentation of pressure distribution but also serves for the determination of pressure either by the measurement with densitometer or by comparison with standard color samples.

ADVANTAGES

1. No preparation required for the measurement :

   You can immediately stard measurement by simply cutting the Prescale sheets into the required shape.

2. Pressure measurements in the places where the conventional methods are not applicable :

   Prescale enables the measurement for example of pressure between the tightly pressed parts, or contact pressure between rolls.

3. Directly observable pressure distribution :

   The pressure distribution over the entire surface is displayed in a directly observable pattern.

4. Simple determination of pressure :

The pressure can be simply determined by measuring the color density with the densitometer FPD101 designed for this purpose or with the standard color samples.

PRODUCT GRADES AND SPECIFICATIONS

Prescale A-sheet is availabe in three grades : for Low Pressure (10 - 100 kg/cm^2), Medium Pressure (70 – 250 kg/cm^2), and High Pressure (200 -700 kg/cm^2), which should be selected according to the pressure to be measured.

Prescale C-sheet can be used in combination with either grade of A-sheet.

Grade

Sheet	Grade	Applicable Pressure range	Package
A-sheet	Low Pressure	10 – 100 kg/cm^2	Roll; 270 mm (width) x 10 m (length)
	Medium Pressure	70 – 250 kg/cm^2	
	High Pressure	200– 700 kg/cm^2	Roll; 270 mm (width) x 10 m (length)
C-sheet	Common	10 - 700 kg/cm^2	

Specifications

Thickness	A-sheet	105 μ
	C-sheet	95 μ
Accuracy	± 10%	
Usable temperature range	5°C - 35°C	
Usable humidity range	20% RH - 90% RH	

EASY METHOD OF USE

1. Cut the Prescale sheets into the necessary shape from each roll.

2. Superpose the A-sheet and C-sheet with the coated sides (inside surface of each roll) face to face.

3. Insert the superposed sheets into the place to be measured, and apply the pressure.

4. Extract the sheets. The pressure distribution is readily observable by the color density pattern formed on the C-sheet.

5. The pressure at each point can be determined by measuring the color density with the densitometer FPD101 designed exclusively for this purpose and converting the density into the pressure from the attached standard conversion chart.

* Quick determination of pressure : Approximate pressure can be determined by visual comparison of color density with the standard color samples attached to the standard conversion chart.

EXAMPLES OF APPLICATIONS

PRESCALE is useful for measuring :

Pressure between pressed surfaces in engines, gear boxes, turbines, valves, pumps, hydraulic cylinders, compressors etc. :

for determining the tightening pressure of bolts and nuts,

for confirming the uniform tightening between mechanical parts,

for locating the leaking places,

for designing gaskets and packings,

for training of correct machine assembly,

for effective determining the position of strain-gauge.

Engagement between gear teeth :

for determining the pressure and pressure distribution on the teeth,

for confirming uniform power transmission,

for identifying the presence of excessive force leading to teeth breakage.

Pressure under heavy equipment :

for determining the pressure on the supports for receiving heavy machinery,

for designing tread pattern of automobile tires.

Contact pressure and pressure pattern in brakes and clutches :

Roll contact pressure in coating machines, paper mills, press printers, etc. :

for determining the pressure and its distribution between rolls,

for adjusting the roll nip pressure,

for checking the grinding of rolls,

for determining the proper amount of crowning.

Pressure between press molds :

for identifying excessive pressure or abrasion in the molds.

Impact pressure :

for determining the pressure and its distribution in the package drop test,

for selecting suitable packaging material standing the prolonged shipment.

Pressure in flat presses for plywood making :

Winding pressure :

for measuring the pressure distribution on the film or paper winding,

for determining the pressure on the coil bobbins.

Others :

for determining the place and the pressure of cavitation on the wings,

for determining the foot pressure in orthopedic diagnosis.

Structure

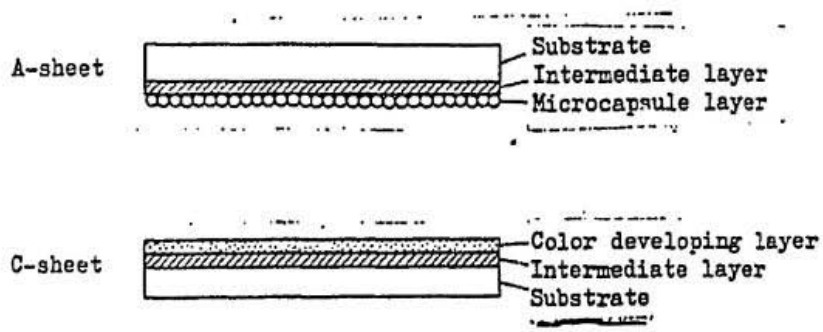

Fuji Photo Film Co., Ltd.
Paper Products Sales Dept.
2-26-30, Nishi-Azabu,
Minato-ku, Tokyo, JAPAN

Appendix B

Open Propeller Model Tests: Data Sheets

SUMMARY OF OPEN PROPELLER TESTS

Propeller Model:	R-Class
Diameter (m):	0.2

Test No.	Manometer Readings (mm Hg) Tunnel Pressure Left	Tunnel Pressure Right	Water Velocity Left	Water Velocity Right	Water Temp (°C)	P_V (kPa)	n (RPM)	n (RPS)	P_O (kPa)	V_A (m/s)	J	σ
O-1	204.0	702.0	462.5	478.5	20.0	2.3	1506	25.1	40.0	2.01	0.40	2.99
O-2	487.0	438.0	469.0	473.0	20.0	2.3	1504	25.1	107.4	1.01	0.20	8.36
O-3	211.0	695.5	452.0	489.0	20.0	2.3	1515	25.3	41.7	3.06	0.61	3.09
O-4	210.5	695.5	469.0	473.0	20.0	2.3	1504	25.1	41.6	1.01	0.20	3.13
O-5	211.0	696.0	462.5	478.5	20.0	2.3	1520	25.3	41.6	2.01	0.40	3.06
O-6	212.0	695.0	469.0	473.0	20.0	2.3	1511	25.2	41.9	1.01	0.20	3.12
O-7	211.5	695.0	462.5	479.0	20.0	2.3	1520	25.3	41.8	2.05	0.40	3.08
O-8	211.0	695.0	452.0	489.0	20.0	2.3	1514	25.2	41.7	3.06	0.61	3.10
O-9	211.0	695.0	462.5	478.5	20.0	2.3	1520	25.33	41.7	2.01	0.40	3.07
O-10	216.5	690.0	462.5	478.5	20.0	2.3	1530	25.5	43.0	2.01	0.39	3.13
O-11	211.0	695.0	462.5	478.5	20.0	2.3	1516	25.3	41.7	2.01	0.40	3.09
O-12	211.5	695.0	462.5	478.5	20.0	2.3	1500	25.0	41.8	2.01	0.40	3.16
O-13	211.0	695.0	462.0	479.0	20.0	2.3	1530	25.5	41.7	2.08	0.41	3.03
O-14	211.0	695.0	462.5	478.5	20.0	2.3	1539	25.7	41.7	2.01	0.39	3.00
O-15	205.5	700.0	459.0	481.5	20.0	2.3	1518	25.3	40.4	2.39	0.47	2.98
O-16	206.0	700.0	461.0	480.0	20.0	2.3	1520	25.3	40.5	2.19	0.43	2.98

NOTES: Propeller model was fixed pitch.
Test duration set at 15 minutes, except for experiment O-5, which was 30 minutes.

CAVITATION TUNNEL PROPELLER TESTS

Experimenter: M. Doucet Date: Sept. 1/95 Page: 1 of 1
Propeller Model: R-Class Diameter: 0.2m
Test No.: 0-1
Test Description: Erosion Test - Paint

REQUIRED TEST CONDITIONS & ASSUMED VALUES

J	0.4	
V_A	2.0 m/s	16 mm Hg
n	1500 RPM	
P_o	40000 Pa	498 mm Hg
P_v	2300 Pa	
σ	3.0	

Gas Content	40	%
Degree of Blockage:	3	
Proximity to Blockage:	1	mm
Test Duration:	15	min
Water Temp. (asum'd):	20	°C

MEASURED TEST PARAMETERS & ACTUAL TEST CONDITIONS

J	0.4
V_A	2.01 m/s
n	1506 RPM
P_o	40000 Pa
P_v	2300 Pa
σ	2.99

Manometer Readings

	Manometer (mm Hg)		
	Left	Right	Δh
Vel.	442.5	458.5	16
Pres.	204	702	498

Gas Content	(Initial):	33.0	%
	(Final):	36.0	%
Degree of Blockage:		3	
Proximity to Blockage:		≈1	mm
Test Duration:		15	min
Water Temp.:	(Initial):		°C
	(Final):	18.5	°C

ADDITIONAL NOTES AND INFORMATION

Test Set-up: Paint: Carwin Blue Technicians Ink

Experiment:

Photographs & Video:

CAVITATION TUNNEL PROPELLER TESTS

Experimenter: M. Drucet Date: Sept. 5/95 Page: 1 of ___
Propeller Model: R-Class Diameter: 0.2m
Test No.: C-2
Test Description: Erosion Test - Paint

REQUIRED TEST CONDITIONS & ASSUMED VALUES

J	0.2		
V_A	1.0 m/s	4	mm Hg
n	1500 RPM		
P_o	101325 Pa	0	mm Hg
P_v	2300 Pa		
σ	7.9		

Gas Content	100	%
Degree of Blockage:	3	
Proximity to Blockage:	≈ 1	mm
Test Duration:	15	min
Water Temp. (asum'd):	20	°C

MEASURED TEST PARAMETERS & ACTUAL TEST CONDITIONS

J	0.2	
V_A	1.01	m/s
n	1504	RPM
P_o	102400	Pa
P_v	2300	Pa
σ	8.36	

Manometer Readings

	Manometer (mm Hg)		
	Left	Right	Δh
Vel.	469	473	4
Pres.	487	438	-49

Gas Content	(Initial):	49.8	%
	(Final):	45.0	%
Degree of Blockage:		3	
Proximity to Blockage:		≈ 1	mm
Test Duration:		15	min
Water Temp.:	(Initial):		°C
	(Final):	19.4	°C

ADDITIONAL NOTES AND INFORMATION

Test Set-up: Paint: Crown Blue Tadwaker's Ink

Experiment:

Photographs & Video:

CAVITATION TUNNEL PROPELLER TESTS

Experimenter: M. Doucet Date: Sept. 6/95 Page: 1 of
Propeller Model: R-Class Diameter: 0.12m
Test No.: 0-3
Test Description: Erosion Test - Paint

REQUIRED TEST CONDITIONS & ASSUMED VALUES

J	0.6		
V_A	3.0	m/s	35.5 mm Hg
n	1500	RPM	
P_o	40000	Pa	498 mm Hg
P_v	2300	Pa	
σ	3.0		

Gas Content	40	%
Degree of Blockage:	3	
Proximity to Blockage:	1	mm
Test Duration:	15	min
Water Temp. (asum'd):	20	°C

MEASURED TEST PARAMETERS & ACTUAL TEST CONDITIONS

J	0.61	
V_A	3.06	m/s
n	1515	RPM
P_o	41700	Pa
P_v	2300	Pa
σ	3.09	

Manometer Readings

	Manometer (mm Hg)		
	Left	Right	Δh
Vel.	452	489	37
Pres.	211	695.5	484.5

Gas Content	(Initial):	33.6	%
	(Final):	44.1	%
Degree of Blockage:		3	
Proximity to Blockage:		≈1	mm
Test Duration:		15	min
Water Temp.:	(Initial):	19.6	°C
	(Final):	19.8	°C

ADDITIONAL NOTES AND INFORMATION

Test Set-up: Paint: Crown Blue Toolmakers Ink

Experiment:

Photographs & Video:

CAVITATION TUNNEL PROPELLER TESTS

Experimenter: M. Doucet Date: Sept. 7/95 Page: 1 of ___
Propeller Model: R-Class Diameter: 0.2m
Test No.: C-4
Test Description: Erosion Test - Paint

REQUIRED TEST CONDITIONS & ASSUMED VALUES

J	0.2		
V_A	1.0 m/s	4	mm Hg
n	1500 RPM		
P_o	40000 Pa	498	mm Hg
P_v	2300 Pa		
σ	3.0		

Gas Content	40	%
Degree of Blockage:	3	
Proximity to Blockage:	1	mm
Test Duration:	15	min
Water Temp. (asum'd):	20	°C

MEASURED TEST PARAMETERS & ACTUAL TEST CONDITIONS

J	0.2	
V_A	1.01	m/s
n	1504	RPM
P_o	41600	Pa
P_v	2300	Pa
σ	3.13	

Manometer Readings

	Manometer (mm Hg)		
	Left	Right	Δh
Vel.	469	473	4
Pres.	210.5	695.5	485

Gas Content	(Initial):	30.1	%
	(Final):	34.6	%
Degree of Blockage:		3	
Proximity to Blockage:		≈1	mm
Test Duration:		15	min
Water Temp.:	(Initial):		°C
	(Final):	19.7	°C

ADDITIONAL NOTES AND INFORMATION

Test Set-up: Paint: Crown Blue Tradmakers Ink

Experiment:

Photographs & Video:

CAVITATION TUNNEL PROPELLER TESTS

Experimenter: M. Doucet Date: Sept. 12/95 Page: 1 of ____
Propeller Model: R-Class Diameter: 0.2 m
Test No.: 0-5
Test Description: Erosion Test- Paint

REQUIRED TEST CONDITIONS & ASSUMED VALUES

J	0.4	
V_A	2.0 m/s	16 mm Hg
n	1500 RPM	
P_o	40000 Pa	498 mm Hg
P_v	2300 Pa	
σ	3.0	

Gas Content	40	%
Degree of Blockage:	3	
Proximity to Blockage:	1	mm
Test Duration:	30	min
Water Temp. (asum'd):	20	°C

MEASURED TEST PARAMETERS & ACTUAL TEST CONDITIONS

J	0.4
V_A	2.01 m/s
n	1520 RPM
P_o	41600 Pa
P_v	2300 Pa
σ	3.06

Manometer Readings

	Manometer (mm Hg)		
	Left	Right	Δh
Vel.	462.5	478.5	16
Pres.	211	696	485

Gas Content	(Initial):	37.0	%
	(Final):	37.6	%
Degree of Blockage:		3	
Proximity to Blockage:		~1	mm
Test Duration:		30	min
Water Temp.:	(Initial):	19.2	°C
	(Final):	19.3	°C

ADDITIONAL NOTES AND INFORMATION

Test Set-up: Paint: Crown Blue Toolmaker's Ink

Experiment:

Photographs & Video:

CAVITATION TUNNEL PROPELLER TESTS

Experimenter: M. Doucet Date: Sept. 13/95 Page: 1 of ___
Propeller Model: R-Class Diameter: 0.2m
Test No.: 0-6
Test Description: Erosion Test - Paint

REQUIRED TEST CONDITIONS & ASSUMED VALUES

J	0.2	
V_A	1.0 m/s	4 mm Hg
n	1500 RPM	
P_o	40000 Pa	498 mm Hg
P_v	2300 Pa	
σ	3.0	

Gas Content	40	%
Degree of Blockage:	2	
Proximity to Blockage:	1	mm
Test Duration:	15	min
Water Temp. (asum'd):	20	°C

MEASURED TEST PARAMETERS & ACTUAL TEST CONDITIONS

J	0.2	
V_A	1.01 m/s	
n	1511 RPM	
P_o	41900 Pa	
P_v	2300 Pa	
σ	3.12	

Manometer Readings

	Manometer (mm Hg)		
	Left	Right	Δh
Vel.	469	473	4
Pres.	212	695	483

Gas Content	(Initial):	40.8	%
	(Final):	44.2	%
Degree of Blockage:		2	
Proximity to Blockage:		≈ 1	mm
Test Duration:		15	min
Water Temp.:	(Initial):		°C
	(Final):	19.4	°C

ADDITIONAL NOTES AND INFORMATION

Test Set-up: Paint: Crown Blue Taelmakers Ink

Experiment:

Photographs & Video:

CAVITATION TUNNEL PROPELLER TESTS

Experimenter: M. Doucet Date: Sept. 14/95 Page: 1 of ___
Propeller Model: K-Class Diameter: 0.2m
Test No.: C-7
Test Description: Erosion Test – Paint

REQUIRED TEST CONDITIONS & ASSUMED VALUES

J	0.4		
V_A	2.0 m/s	11	mm Hg
n	1500 RPM		
P_o	40000 Pa	498	mm Hg
P_v	2300 Pa		
σ	3.0		

Gas Content	40	%
Degree of Blockage:	2	
Proximity to Blockage:	1	mm
Test Duration:	15	min
Water Temp. (asum'd):	20	°C

MEASURED TEST PARAMETERS & ACTUAL TEST CONDITIONS

J	0.4	
V_A	2.05	m/s
n	1520	RPM
P_o	41800	Pa
P_v	2300	Pa
σ	3.08	

Manometer Readings

	Manometer (mm Hg)		
	Left	Right	Δh
Vel.	462.5	479	16.5
Pres.	211.5	695	483.5

Gas Content	(Initial):	34.7	%
	(Final):	38.7	%
Degree of Blockage:		2	
Proximity to Blockage:		≈ 1	mm
Test Duration:		15	min
Water Temp.:	(Initial):	19.4	°C
	(Final):	19.7	°C

ADDITIONAL NOTES AND INFORMATION

Test Set-up: Paint: Crown Blue Teelmakers Ink

Experiment:

Photographs & Video:

CAVITATION TUNNEL PROPELLER TESTS

Experimenter: M. Doucet Date: Sept. 15/95 Page: 1 of
Propeller Model: R-Class Diameter: 0.2m
Test No.: C-8
Test Description: Erosion Test - Paint

REQUIRED TEST CONDITIONS & ASSUMED VALUES

J	0.6		
V_A	3.0	m/s	355 mm Hg
n	1500	RPM	
P_o	40000	Pa	498 mm Hg
P_v	2300	Pa	
σ	3.0		

Gas Content	40	%
Degree of Blockage:	2	
Proximity to Blockage:	1	mm
Test Duration:	15	min
Water Temp. (asum'd):	20	°C

MEASURED TEST PARAMETERS & ACTUAL TEST CONDITIONS

J	0.61	
V_A	3.06	m/s
n	1514	RPM
P_o	41200	Pa
P_v	2300	Pa
σ	3.10	

Manometer Readings

	Manometer (mm Hg)		
	Left	Right	Δh
Vel.	452	489	37
Pres.	211	695	484

Gas Content	(Initial):	32.8	%
	(Final):	39.8	%
Degree of Blockage:		2	
Proximity to Blockage:		≈1	mm
Test Duration:		15	min
Water Temp.:	(Initial):		°C
	(Final):	20.1	°C

ADDITIONAL NOTES AND INFORMATION

Test Set-up: Paint. Crown Blue Toolmakers Ink

Experiment:

Photographs & Video:

CAVITATION TUNNEL PROPELLER TESTS

Experimenter: M. Doucet Date: Sept. 18/95 Page: 1 of ___
Propeller Model: R-Class Diameter: 0.2m
Test No.: 0-9
Test Description: Erosion Test - Paint

REQUIRED TEST CONDITIONS & ASSUMED VALUES

J	0.4	
V_A	2.2 m/s	16 mm Hg
n	1500 RPM	
P_o	40,000 Pa	498 mm Hg
P_v	2300 Pa	
σ	3.0	

Gas Content	40	%
Degree of Blockage:	3	
Proximity to Blockage:	5	mm
Test Duration:	15	min
Water Temp. (asum'd):	20	°C

MEASURED TEST PARAMETERS & ACTUAL TEST CONDITIONS

J	0.40	
V_A	2.01	m/s
n	1520	RPM
P_o	41700	Pa
P_v	2300	Pa
σ	3.05	

Manometer Readings

	Manometer (mm Hg)		
	Left	Right	Δh
Vel.	462.5	478.5	16
Pres.	211	1.95	484

Gas Content	(Initial):	32.8	%
	(Final):	36.9	%
Degree of Blockage:		3	
Proximity to Blockage:		5	mm
Test Duration:		15.5	min
Water Temp.:	(Initial):		°C
	(Final):	17.4	°C

ADDITIONAL NOTES AND INFORMATION

Test Set-up: Paint: Crown Blue Toolmaker's Ink

Experiment: Erosion seems excessive; paint was from end of cavl.

Photographs & Video:

CAVITATION TUNNEL PROPELLER TESTS

Experimenter: M. Doucet Date: Sept. 19/95 Page: 1 of
Propeller Model: R-Class Diameter: 0.2m
Test No.: C-10
Test Description: Erosion Test - Paint

REQUIRED TEST CONDITIONS & ASSUMED VALUES

J	0.4		
V_A	2.0 m/s	16	mm Hg
n	1500 RPM		
P_o	40000 Pa	498	mm Hg
P_v	2300 Pa		
σ	3.0		

Gas Content	40	%
Degree of Blockage:	3	
Proximity to Blockage:	10	mm
Test Duration:	15	min
Water Temp. (asum'd):	20	°C

MEASURED TEST PARAMETERS & ACTUAL TEST CONDITIONS

J	0.39	
V_A	2.01	m/s
n	1530	RPM
P_o	43000	Pa
P_v	2300	Pa
σ	3.13	

Manometer Readings

	Manometer (mm Hg)		
	Left	Right	Δh
Vel.	462.5	478.5	16
Pres.	216.5	690	473.5

Gas Content	(Initial):	42.8	%
	(Final):	42.6	%
Degree of Blockage:		3	
Proximity to Blockage:		10	mm
Test Duration:		14 3/3	min
Water Temp.:	(Initial):		°C
	(Final):	17.3	°C

ADDITIONAL NOTES AND INFORMATION

Test Set-up: Paint - Crown Blue Toolmakers Ink

Experiment: Control problems with propeller speed; speed varied between 1525 and 1558 RPM

Test terminated with ≈ 20 seconds remaining due to loss of steady control (speed jumped abruptly to 2100 RPM before shutdown).

Photographs & Video:

CAVITATION TUNNEL PROPELLER TESTS

Experimenter: M. Doucet Date: Sept. 20/95 Page: 1 of ____
Propeller Model: R-Class Diameter: 0.2m
Test No.: 0-11
Test Description: Erosion Test - Paint

REQUIRED TEST CONDITIONS & ASSUMED VALUES

J	0.4		
V_A	2.0 m/s	16	mm Hg
n	1500 RPM		
P_o	40000 Pa	498	mm Hg
P_v	2300 Pa		
σ	3.0		

Gas Content	40	%
Degree of Blockage:	3	
Proximity to Blockage:	20	mm
Test Duration:	15	min
Water Temp. (asum'd):	20	°C

MEASURED TEST PARAMETERS & ACTUAL TEST CONDITIONS

J	0.40	
V_A	2.01	m/s
n	1516	RPM
P_o	41700	Pa
P_v	2300	Pa
σ	3.09	

Manometer Readings

	Manometer (mm Hg)		
	Left	Right	Δh
Vel.	462.5	478.5	16
Pres.	211	695	484

Gas Content	(Initial):	35.1	%
	(Final):	39.8	%
Degree of Blockage:		3	
Proximity to Blockage:		20	mm
Test Duration:		15	min
Water Temp.:	(Initial):		°C
	(Final):	17.4	°C

ADDITIONAL NOTES AND INFORMATION

Test Set-up: Paint: Crown Blue Toolmakers Ink

Experiment:

Photographs & Video:

CAVITATION TUNNEL PROPELLER TESTS

Experimenter: M. Doucet Date: Sept. 22/95 Page: 1 of ___
Propeller Model: R-Class Diameter: 0.2m
Test No.: 0-12
Test Description: Erosion Test - Paint
(Repeat of 0-9)

REQUIRED TEST CONDITIONS & ASSUMED VALUES

J	0.4		
V_A	2.0 m/s	16	mm Hg
n	1500 RPM		
P_o	40600 Pa		mm Hg
P_v	2300 Pa		
σ	3.0		

Gas Content	40	%
Degree of Blockage:	3	
Proximity to Blockage:	5	mm
Test Duration:	15	min
Water Temp. (asum'd):	20	°C

MEASURED TEST PARAMETERS & ACTUAL TEST CONDITIONS

J	0.40	
V_A	2.01	m/s
n	1500	RPM
P_o	41800	Pa
P_v	2300	Pa
σ	3.16	

Manometer Readings

	Manometer (mm Hg)		
	Left	Right	Δh
Vel.	462.5	478.5	16
Pres.	211.5	695	483.5

Gas Content	(Initial):	34.8	%
	(Final):	39.3	%
Degree of Blockage:		3	
Proximity to Blockage:		5	mm
Test Duration:		15	min
Water Temp.:	(Initial):	17.5	°C
	(Final):	17.6	°C

ADDITIONAL NOTES AND INFORMATION

Test Set-up: Paint: Crown Blue Toolmakers Ink

Experiment:

Photographs & Video:

CAVITATION TUNNEL PROPELLER TESTS

Experimenter: M. Doucet Date: Oct. 5/95 Page: 1 of ____
Propeller Model: B-Class Diameter: C-2in
Test No.: O-13
Test Description: Erosion Test - Paint
(Repeat of C-1 → test new ink)

REQUIRED TEST CONDITIONS & ASSUMED VALUES

J	0.4		
V_A	2.0 m/s	16 mm Hg	
n	1500 RPM		
P_o	40000 Pa	498 mm Hg	
P_v	2300 Pa		
σ	3.0		

Gas Content	40	%
Degree of Blockage:	3	
Proximity to Blockage:	1	mm
Test Duration:	15	min
Water Temp. (asum'd):	20	°C

MEASURED TEST PARAMETERS & ACTUAL TEST CONDITIONS

J	0.41	
V_A	2.08	m/s
n	1530	RPM
P_o	41700	Pa
P_v	2300	Pa
σ	3.03	

Manometer Readings

	Manometer (mm Hg)		
	Left	Right	Δh
Vel.	462	479	17
Pres.	211	695	484

Gas Content	(Initial):	26.8	%
	(Final):	30.6	%
Degree of Blockage:		3	
Proximity to Blockage:		≈1	mm
Test Duration:		15	min
Water Temp.:	(Initial):	17.4	°C
	(Final):	17.3	°C

ADDITIONAL NOTES AND INFORMATION

Test Set-up: Paint: Starrett Klemscribe Blue Layout Dye

Experiment:

Photographs & Video:

CAVITATION TUNNEL PROPELLER TESTS

Experimenter: M. Doucet Date: Oct. 6/95 Page: 1 of ___
Propeller Model: R-Class Diameter: 0.2m
Test No.: 0-14
Test Description: Erosion Test- Paint

REQUIRED TEST CONDITIONS & ASSUMED VALUES

J	0.4	
V_A	2.0 m/s	16 mm Hg
n	1500 RPM	
P_o	40000 Pa	498 mm Hg
P_v	2300 Pa	
σ	3.0	

Gas Content	40	%
Degree of Blockage:	—	
Proximity to Blockage:	—	mm
Test Duration:	15	min
Water Temp. (asum'd):	20	°C

MEASURED TEST PARAMETERS & ACTUAL TEST CONDITIONS

J	0.39	
V_A	2.01 m/s	
n	1539 RPM	
P_o	41700 Pa	
P_v	2300 Pa	
σ	3.0	

Manometer Readings

	Manometer (mm Hg)		
	Left	Right	Δh
Vel.	462.5	478.5	16
Pres.	211	695	484

Gas Content	(Initial):	35.0	%
	(Final):	38.7	%
Degree of Blockage:		—	
Proximity to Blockage:		—	mm
Test Duration:		15	min
Water Temp.:	(Initial):	17.1	°C
	(Final):	17.1	°C

ADDITIONAL NOTES AND INFORMATION

Test Set-up: Open Flow

Paint: Crown Blue Toolmakers Dye (new stock)

Experiment:

Photographs & Video:

CAVITATION TUNNEL PROPELLER TESTS

Experimenter: M. Doucet Date: Oct. 10/95 Page: 1 of
Propeller Model: R-Class Diameter: 0.2m
Test No.: O-15
Test Description: Existing Test - Paint
(Repeat of O-14)

REQUIRED TEST CONDITIONS & ASSUMED VALUES

J	0.4		
V_A	2.6 m/s	16 mm Hg	
n	1500 RPM		
P_o	40000 Pa	498 mm Hg	
P_v	2300 Pa		
σ	3.0		

Gas Content	40	%
Degree of Blockage:	–	
Proximity to Blockage:	–	mm
Test Duration:	15	min
Water Temp. (asum'd):	20	°C

MEASURED TEST PARAMETERS & ACTUAL TEST CONDITIONS

J	0.47	
V_A	2.34	m/s
n	1518	RPM
P_o	40400	Pa
P_v	2320	Pa
σ	2.98	

Manometer Readings

	Manometer (mm Hg)		
	Left	Right	Δh
Vel.	459	481.5	22.5
Pres.	205.5	700	494.5

Gas Content	(Initial):	27.5	%
	(Final):	31.0	%
Degree of Blockage:		–	
Proximity to Blockage:		–	mm
Test Duration:		15	min
Water Temp.:	(Initial):		°C
	(Final):	15.9	°C

ADDITIONAL NOTES AND INFORMATION

Test Set-up: Open Flow

Paint: Crown Blue Toolmaker's Dye (new stock)

Experiment:

Photographs & Video:

CAVITATION TUNNEL PROPELLER TESTS

Experimenter: M. Doucet Date: Oct. 11/95 Page: 1 of ___
Propeller Model: R-Class Diameter: 0.2m
Test No.: C-16
Test Description: Erosion Paint Test (Repeat of C-14)

REQUIRED TEST CONDITIONS & ASSUMED VALUES

J	0.4		
V_A	2.0 m/s	16	mm Hg
n	1500 RPM		
P_o	40000 Pa	448	mm Hg
P_v	2300 Pa		
σ	3.0		

Gas Content	40	%
Degree of Blockage:	—	
Proximity to Blockage:	—	mm
Test Duration:	15	min
Water Temp. (asum'd):	20	°C

MEASURED TEST PARAMETERS & ACTUAL TEST CONDITIONS

J	0.43	
V_A	2.19	m/s
n	1520	RPM
P_o	40500	Pa
P_v	2300	Pa
σ	2.98	

Manometer Readings

	Manometer (mm Hg)		
	Left	Right	Δh
Vel.	461	480	19
Pres.	206	700	494

Gas Content	(Initial):	34.8	%
	(Final):	39.0	%
Degree of Blockage:		—	
Proximity to Blockage:		—	mm
Test Duration:		15	min
Water Temp.:	(Initial):	15.0	°C
	(Final):	15.9	°C

ADDITIONAL NOTES AND INFORMATION

Test Set-up: Open Flow

Paint: Starrett Kleenscribe Blue Layout Dye

Experiment:

Photographs & Video:

Appendix C

Ducted Propeller Model Tests: Data Sheets

SUMMARY OF DUCTED PROPELLER TESTS

Propeller Model:	Robert LeMeur
Diameter (m):	0.2

Test No.	Manometer Readings (mm Hg) Tunnel Pressure Left	Tunnel Pressure Right	Water Velocity Left	Water Velocity Right	Water Temp (°C)	P_V (kPa)	n (RPM)	n (RPS)	P_O (kPa)	V_A (m/s)	J	σ
D-1	211.0	695.0	465.0	476.0	20.0	2.3	1225	20.4	41.7	1.67	0.41	4.73
D-2	214.0	692.0	465.0	476.5	20.0	2.3	1226	20.4	42.5	1.71	0.42	4.81
D-3	485.0	439.0	466.0	475.5	20.0	2.3	1225	20.4	107.0	1.55	0.38	12.56
D-4	213.5	693.0	469.5	471.5	20.0	2.3	1231	20.5	42.3	0.71	0.17	4.75
D-5	208.0	697.5	456.0	484.0	20.0	2.3	1223	20.4	41.1	2.66	0.65	4.66
D-6	211.0	695.0	465.0	476.5	20.0	2.3	1225	20.4	41.7	1.71	0.42	4.73
D-7	208.0	698.0	462.0	478.0	20.0	2.3	1225	20.4	41.0	2.01	0.49	4.64
D-8	209.0	696.0	464.0	476.5	20.0	2.3	1220	20.3	41.4	1.78	0.44	4.72
D-9	211.0	695.0	465.0	476.0	20.0	2.3	1225	20.4	41.7	1.67	0.41	4.73

NOTES: Propeller model was variable pitch. All tests were completed at a nominal pitch angle of 25°, except for test D-9, which was performed at a pitch angle of 10°.
Test duration set at 15 minutes, except for experiment D-9, which was 30 minutes.

CAVITATION TUNNEL PROPELLER TESTS

Experimenter: M. Doucet Date: Dec. 4/95 Page: 1 of 1
Propeller Model: Robert LeMeur Diameter: 0.2m
Test No.: D-1
Test Description: Erosion Test
Paint

REQUIRED TEST CONDITIONS & ASSUMED VALUES

J	0.4	
V_A	1.6 m/s	10 mm Hg
n	1225 RPM	
P_o	40020 Pa	498 mm Hg
P_v	2300 Pa	
σ	4.5	

Gas Content	40	%
Degree of Blockage:	3	
Proximity to Blockage:	1	mm
Test Duration:	15	min
Water Temp. (asum'd):	20	°C

MEASURED TEST PARAMETERS & ACTUAL TEST CONDITIONS

J	0.41	
V_A	1.67 m/s	
n	1225 RPM	
P_o	41700 Pa	
P_v	2300 Pa	
σ	4.73	

Manometer Readings

	Manometer (mm Hg)		
	Left	Right	Δh
Vel.	465	476	11
Pres.	211	695	484

Gas Content	(Initial):	36.7	%
	(Final):	38.9	%
Degree of Blockage:		3	
Proximity to Blockage:		1	mm
Test Duration:		15	min
Water Temp.:	(Initial):	14.0	°C
	(Final):	13.9	°C

ADDITIONAL NOTES AND INFORMATION

Test Set-up: Paint Type: Avery Marker

Experiment:

Photographs & Video:

CAVITATION TUNNEL PROPELLER TESTS

Experimenter: M. Doucet
Propeller Model: Robert Lemieux
Test No.: D-2
Test Description: Erosion Test Paint

Date: Dec. 5/95
Page: 1 of 1
Diameter: 0.2m

REQUIRED TEST CONDITIONS & ASSUMED VALUES

J	0.4		
V_A	1.1 m/s	10	mm Hg
n	1225 RPM		
P_o	40000 Pa	498	mm Hg
P_v	2300 Pa		
σ	4.5		

Gas Content	40	%
Degree of Blockage:	3	
Proximity to Blockage:	1	mm
Test Duration:	30	min
Water Temp. (asum'd):	20	°C

MEASURED TEST PARAMETERS & ACTUAL TEST CONDITIONS

J	0.42	
V_A	1.21	m/s
n	1226	RPM
P_o	41500	Pa
P_v	2306	Pa
σ	4.31	

Manometer Readings

	Manometer (mm Hg)		
	Left	Right	Δh
Vel.	465	476.5	11.5
Pres.	214	692	478

Gas Content	(Initial):	41.1	%
	(Final):	42.8	%
Degree of Blockage:		3	
Proximity to Blockage:		1	mm
Test Duration:		30	min
Water Temp.:	(Initial):	14.0	°C
	(Final):	13.7	°C

ADDITIONAL NOTES AND INFORMATION

Test Set-up: Paint Type: Avery Marker

Experiment: Fluctuations in RPM req'd small adjustments during test. (between 1210 - 1245 RPM)

Photographs & Video:

CAVITATION TUNNEL PROPELLER TESTS

Experimenter: M. Drouet Date: Dec. 6/95 Page: 1 of ____
Propeller Model: Robert LeMieux Diameter: 0.2 in
Test No.: D-3
Test Description: Erosion Test
Paint

REQUIRED TEST CONDITIONS & ASSUMED VALUES

J	0.4		
V_A	1.6 m/s	10	mm Hg
n	1225 RPM		
P_o	101325 Pa	0	mm Hg
P_v	2300 Pa		
σ	11.9		

Gas Content	100	%
Degree of Blockage:	3	
Proximity to Blockage:	1	mm
Test Duration:	15	min
Water Temp. (asum'd):	20	°C

MEASURED TEST PARAMETERS & ACTUAL TEST CONDITIONS

J	0.38	
V_A	1.55	m/s
n	1225	RPM
P_o	102200	Pa
P_v	2300	Pa
σ	12.56	

Manometer Readings

	Manometer (mm Hg)		
	Left	Right	Δh
Vel.	466	475.5	9.5
Pres.	485	439	-46

Gas Content	(Initial):	44.8	%
	(Final):	45.6	%
Degree of Blockage:		3	
Proximity to Blockage:		1	mm
Test Duration:		15	min
Water Temp.:	(Initial):	13.8	°C
	(Final):	13.5	°C

ADDITIONAL NOTES AND INFORMATION

Test Set-up: Paint Type: Avery Marker

Experiment: P_o (Actual) is higher because of the head of water in the tunnel.

Photographs & Video:

CAVITATION TUNNEL PROPELLER TESTS

Experimenter: M. Doucet Date: Dec. 7/95 Page: 1 of
Propeller Model: Robert LeMeur Diameter: 0.2m
Test No.: D-4
Test Description: Erosion Test
Paint

REQUIRED TEST CONDITIONS & ASSUMED VALUES

J	0.2	
V_A	0.8 m/s	2.5 mm Hg
n	1225 RPM	
P_o	40000 Pa	498 mm Hg
P_v	2300 Pa	
σ	4.5	

Gas Content	40	%
Degree of Blockage:	3	
Proximity to Blockage:	1	mm
Test Duration:	15	min
Water Temp. (asum'd):	20	°C

MEASURED TEST PARAMETERS & ACTUAL TEST CONDITIONS

J	0.17	
V_A	0.71 m/s	
n	1231 RPM	
P_o	42300 Pa	
P_v	2300 Pa	
σ	4.75	

Manometer Readings

	Manometer (mm Hg)		
	Left	Right	Δh
Vel.	469.5	471.5	2
Pres.	213.5	693	479.5

Gas Content	(Initial):	35.2	%
	(Final):	35.3	%
Degree of Blockage:		3	
Proximity to Blockage:		1	mm
Test Duration:		15	min
Water Temp.:	(Initial):	13.7	°C
	(Final):	13.8	°C

ADDITIONAL NOTES AND INFORMATION

Test Set-up: Paint: Avery Marker ; Drying Time: 1 hr.

Experiment:

Photographs & Video:

CAVITATION TUNNEL PROPELLER TESTS

Experimenter: M. Doucet Date: Dec. 11/95 Page: 1 of ____
Propeller Model: Robert LeMeur Diameter: 0.2 m
Test No.: D-5
Test Description: Erosion Test
Paint

REQUIRED TEST CONDITIONS & ASSUMED VALUES

J	0.6	
V_A	2.5 m/s	24.5 mm Hg
n	1285 RPM	
P_o	40000 Pa	498 mm Hg
P_v	2300 Pa	
σ	4.5	

Gas Content	40	%
Degree of Blockage:	3	
Proximity to Blockage:	1	mm
Test Duration:	15	min
Water Temp. (asum'd):	20	°C

MEASURED TEST PARAMETERS & ACTUAL TEST CONDITIONS

J	0.65	
V_A	2.66 m/s	
n	1223 RPM	
P_o	41100 Pa	
P_v	2300 Pa	
σ	4.66	

Manometer Readings

	Manometer (mm Hg)		
	Left	Right	Δh
Vel.	456	484	28
Pres.	208	697.5	489.5

Gas Content	(Initial):	34.8	%
	(Final):	38.0	%
Degree of Blockage:		3	
Proximity to Blockage:		1	mm
Test Duration:		15	min
Water Temp.:	(Initial):	13.0	°C
	(Final):	13.1	°C

ADDITIONAL NOTES AND INFORMATION

Test Set-up: Paint: Avery Marker ; Drying Time: 3/4 hr.

Experiment:

Photographs & Video:

CAVITATION TUNNEL PROPELLER TESTS

Experimenter: M. Daucet Date: Dec. 12/95 Page: 1 of ___
Propeller Model: Robert LeMeur Diameter: 0.2m
Test No.: D-6
Test Description: Erosion Test
Paint

REQUIRED TEST CONDITIONS & ASSUMED VALUES

J	0.4	
V_A	1.6 m/s	10 mm Hg
n	1225 RPM	
P_o	41000 Pa	498 mm Hg
P_v	2300 Pa	
σ	4.5	

Gas Content	40	%
Degree of Blockage:	3	
Proximity to Blockage:	5	mm
Test Duration:	15	min
Water Temp. (asum'd):	20	°C

MEASURED TEST PARAMETERS & ACTUAL TEST CONDITIONS

J	[redacted]0.42
V_A	1.71 m/s
n	1225 RPM
P_o	41200 Pa
P_v	2300 Pa
σ	4.73

Manometer Readings

	Manometer (mm Hg)		
	Left	Right	Δh
Vel.	465	476.5	11.5
Pres.	211	695	484

Gas Content	(Initial):	33.3	%
	(Final):	38.6	%
Degree of Blockage:		3	
Proximity to Blockage:		5	mm
Test Duration:		15	min
Water Temp.:	(Initial):	13.2	°C
	(Final):	13.5	°C

ADDITIONAL NOTES AND INFORMATION

Test Set-up: Paint: Avery Marker; Drying Time: ≈½ hr.

Experiment:

Photographs & Video:

CAVITATION TUNNEL PROPELLER TESTS

Experimenter: M. Doucet Date: Dec. 12/95 Page: 1 of ____
Propeller Model: Robert LeMieux Diameter: 0.2m
Test No.: D-7
Test Description: Erosion Test
Paint

REQUIRED TEST CONDITIONS & ASSUMED VALUES

J	0.4	
V_A	1.6 m/s	10 mm Hg
n	1225 RPM	
P_o	40000 Pa	498 mm Hg
P_v	2300 Pa	
σ	4.5	

Gas Content	40	%
Degree of Blockage:	—	
Proximity to Blockage:	—	mm
Test Duration:	15	min
Water Temp. (asum'd):	20	°C

MEASURED TEST PARAMETERS & ACTUAL TEST CONDITIONS

J	0.49	
V_A	2.01 m/s	
n	1225 RPM	
P_o	41000 Pa	
P_v	2300 Pa	
σ	4.64	

Manometer Readings

	Manometer (mm Hg)		
	Left	Right	Δh
Vel.	462	478	16
Pres.	208	698	490

Gas Content	(Initial):	40.0	%
	(Final):	41.0	%
Degree of Blockage:		—	
Proximity to Blockage:		—	mm
Test Duration:		15	min
Water Temp.:	(Initial):	13.5	°C
	(Final):	13.3	°C

ADDITIONAL NOTES AND INFORMATION

Test Set-up: Open Flow Test - No Blockage
Paint: Avery Marker

Experiment:

Photographs & Video:

CAVITATION TUNNEL PROPELLER TESTS

Experimenter: M. Doucet Date: Dec. 13/95 Page: 1 of
Propeller Model: Robert LeMeur Diameter: 0.2m
Test No.: D-8
Test Description: Erosion Test
Paint

REQUIRED TEST CONDITIONS & ASSUMED VALUES

J	0.4	
V_A	1.6 m/s	10 mm Hg
n	1225 RPM	
P_o	40000 Pa	498 mm Hg
P_v	2300 Pa	
σ	4.5	

Gas Content	40	%
Degree of Blockage:	3	
Proximity to Blockage:	20	mm
Test Duration:	15	min
Water Temp. (asum'd):	20	°C

MEASURED TEST PARAMETERS & ACTUAL TEST CONDITIONS

J	0.44	
V_A	1.78 m/s	
n	1220 RPM	
P_o	41400 Pa	
P_v	2300 Pa	
σ	4.72	

Manometer Readings

	Manometer (mm Hg)		
	Left	Right	Δh
Vel.	464	476.5	12.5
Pres.	209	196	487

Gas Content	(Initial):	35.1	%
	(Final):	35.8	%
Degree of Blockage:		3	
Proximity to Blockage:		20	mm
Test Duration:		15	min
Water Temp.:	(Initial):	14.0	°C
	(Final):	13.6	°C

ADDITIONAL NOTES AND INFORMATION

Test Set-up: Paint: Avery Marker

Experiment:

Photographs & Video:

CAVITATION TUNNEL PROPELLER TESTS

Experimenter: M. Doucet Date: Dec. 15/95 Page: 1 of ____
Propeller Model: Robert LeMeur Diameter: 0.2m
Test No.: D-9
Test Description: Erosion Test
Paint

REQUIRED TEST CONDITIONS & ASSUMED VALUES

J	0.4		
V_A	1.6 m/s	10 mm Hg	
n	1225 RPM		
P_o	40000 Pa	498 mm Hg	
P_v	2300 Pa		
σ	4.5		

Gas Content	40	%
Degree of Blockage:	3	
Proximity to Blockage:	5	mm
Test Duration:	15	min
Water Temp. (asum'd):	20	°C

Pitch Angle = 10°

MEASURED TEST PARAMETERS & ACTUAL TEST CONDITIONS

J	0.41	
V_A	1.67	m/s
n	1225	RPM
P_o	41700	Pa
P_v	2300	Pa
σ	4.73	

Manometer Readings

	Manometer (mm Hg)		
	Left	Right	Δh
Vel.	465	476	11
Pres.	211	695	484

Gas Content	(Initial):	46.3	%
	(Final):	42.1	%
Degree of Blockage:		3	
Proximity to Blockage:		5	mm
Test Duration:		15	min
Water Temp.:	(Initial):	14.7	°C
	(Final):	13.9	°C

Pitch Angle = 10°

ADDITIONAL NOTES AND INFORMATION

Test Set-up: Paint: Avery Marker

Experiment:

Photographs & Video:

Appendix D

Open Propeller Model Tests:
% Erosion vs. Blade Number

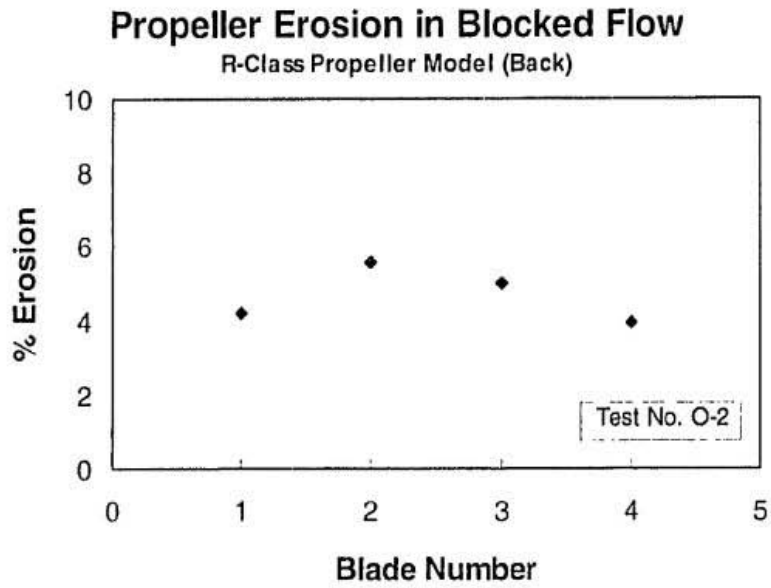
Propeller Erosion in Blocked Flow
R-Class Propeller Model (Back)
% Erosion
10
8
6
4
2
0
0
1
2
3
4
5
Blade Number
Test No. O-2

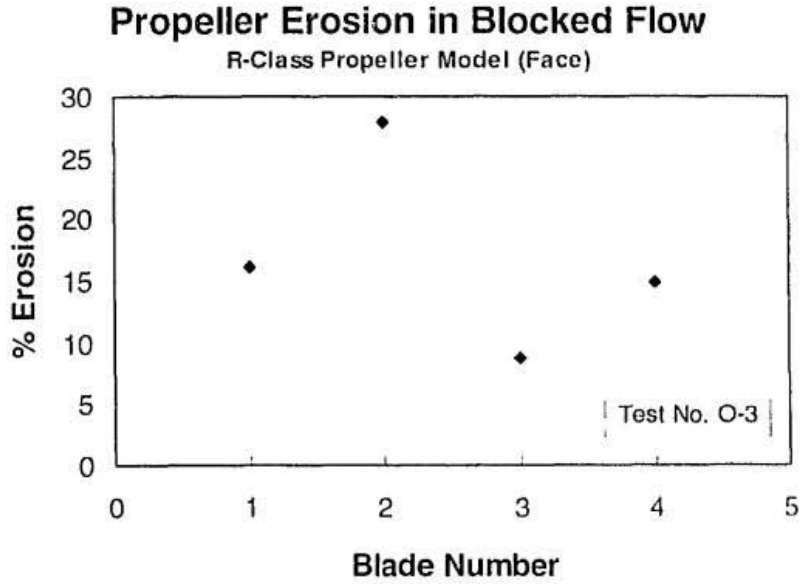
Propeller Erosion in Blocked Flow
R-Class Propeller Model (Face)
% Erosion
30
25
20
15
10
5
0
0
1
2
3
4
5
Blade Number
Test No. O-3

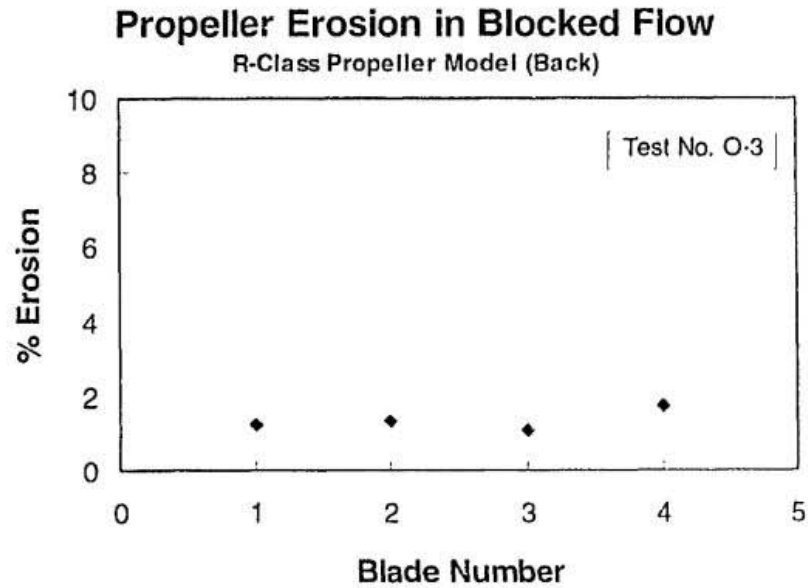
Propeller Erosion in Blocked Flow
R-Class Propeller Model (Back)
% Erosion
10
8
6
4
2
0
0
1
2
3
4
5
Blade Number
Test No. O-3

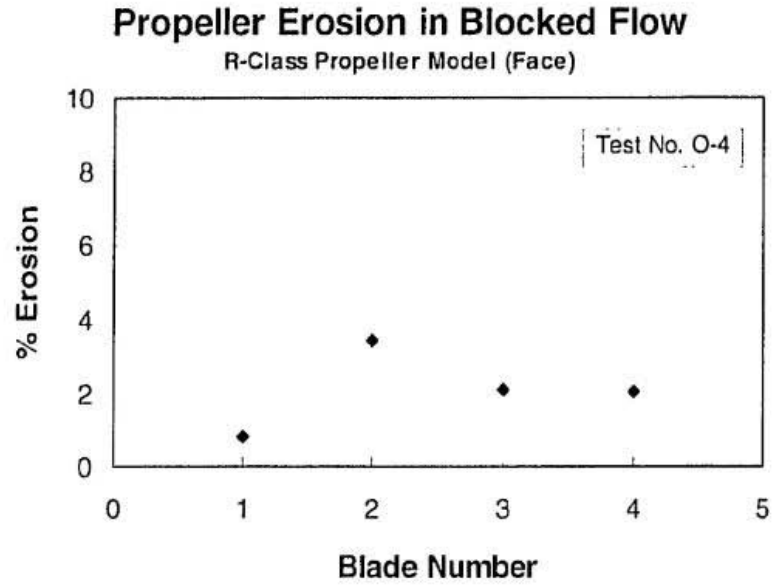
Propeller Erosion in Blocked Flow
R-Class Propeller Model (Face)
Test No. O-4
% Erosion
Blade Number
0
2
4
6
8
10
0
1
2
3
4
5

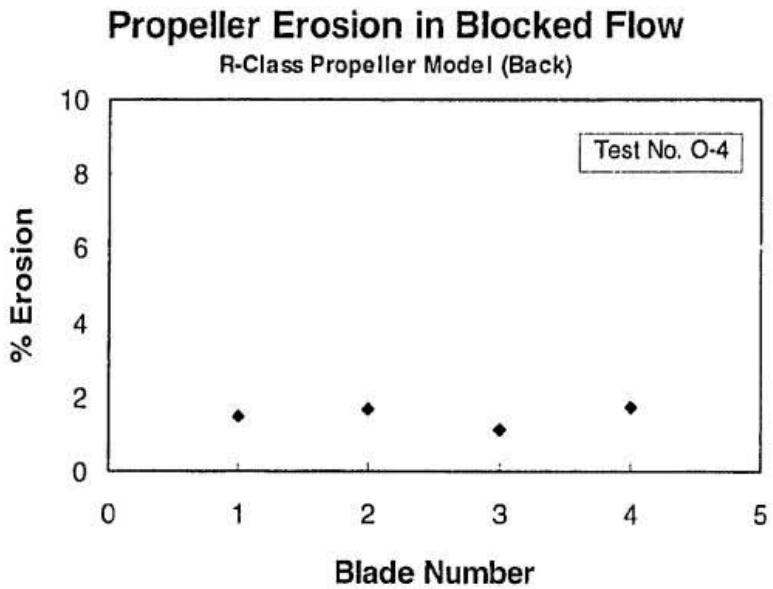
Propeller Erosion in Blocked Flow
R-Class Propeller Model (Back)
Test No. O-4
% Erosion
Blade Number
0
2
4
6
8
10
0
1
2
3
4
5

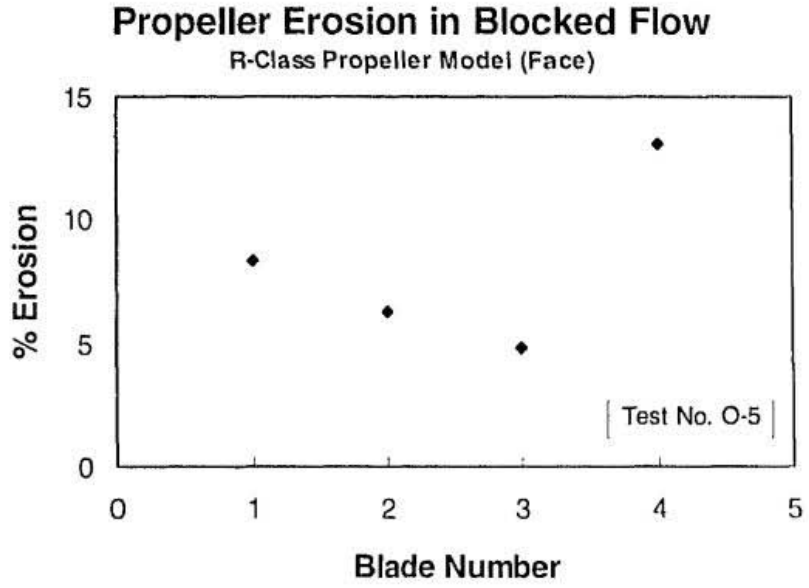
Propeller Erosion in Blocked Flow
R-Class Propeller Model (Face)
% Erosion
15
10
5
0
0
1
2
3
4
5
Blade Number
Test No. O-5

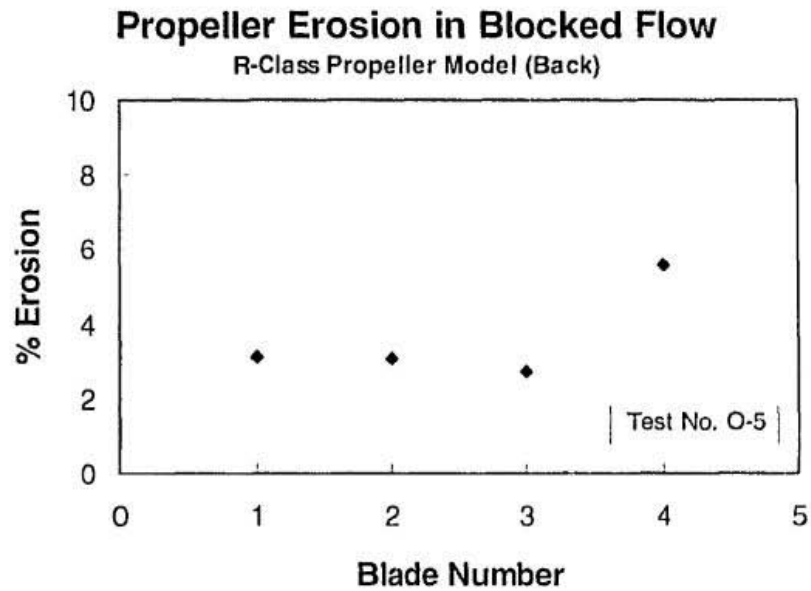
Propeller Erosion in Blocked Flow
R-Class Propeller Model (Back)
% Erosion
10
8
6
4
2
0
0
1
2
3
4
5
Blade Number
Test No. O-5

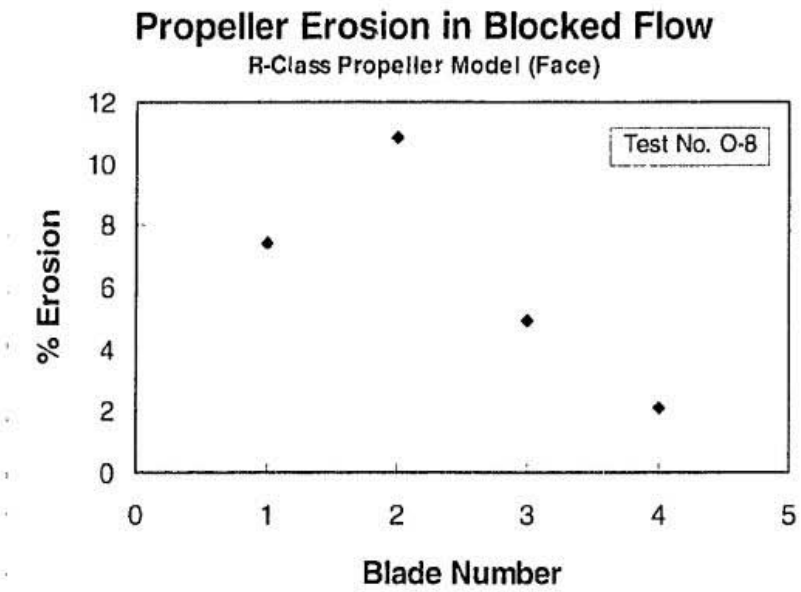
Propeller Erosion in Blocked Flow
R-Class Propeller Model (Face)
Test No. O-8
% Erosion
Blade Number
0
2
4
6
8
10
12
0
1
2
3
4
5

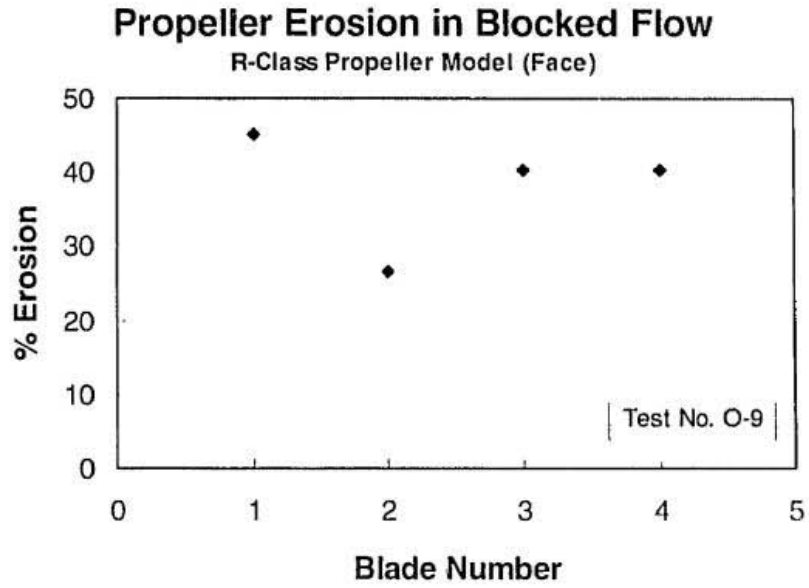
Propeller Erosion in Blocked Flow
R-Class Propeller Model (Face)
% Erosion
50
40
30
20
10
0
0
1
2
3
4
5
Blade Number
Test No. O-9

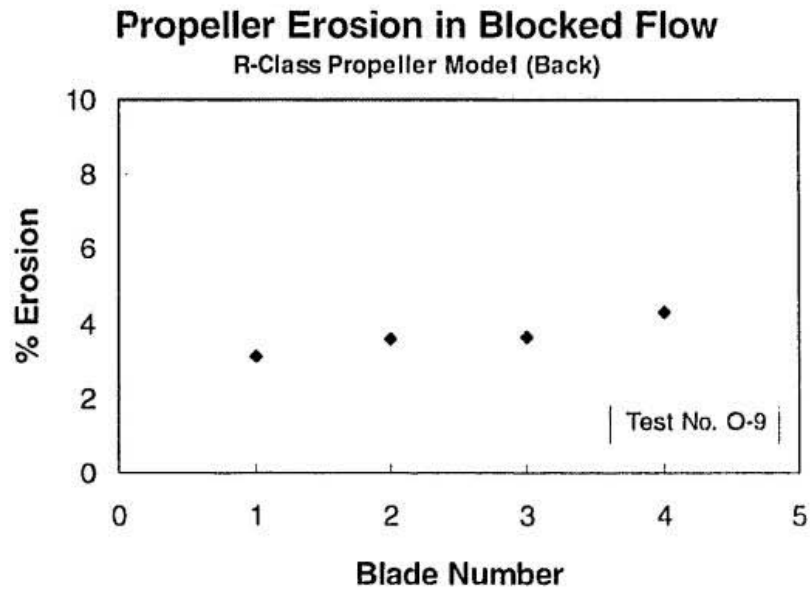
Propeller Erosion in Blocked Flow
R-Class Propeller Model (Back)
% Erosion
10
8
6
4
2
0
0
1
2
3
4
5
Blade Number
Test No. O-9

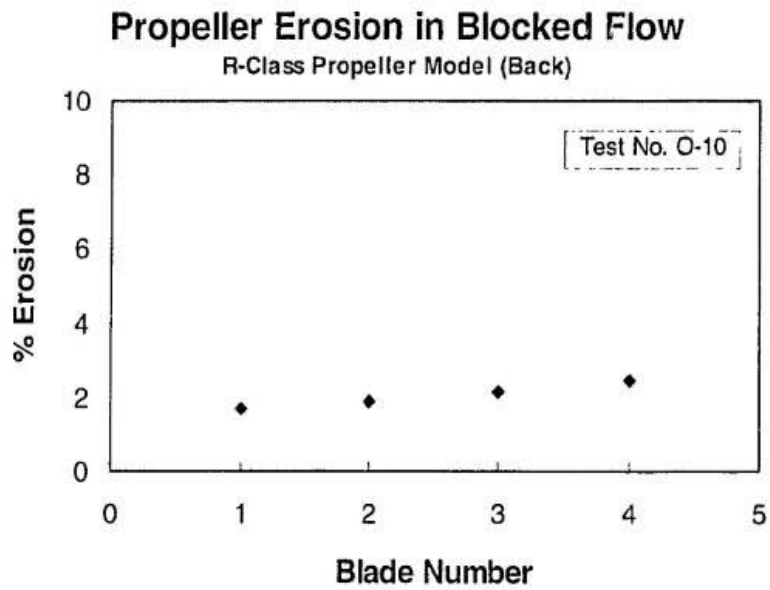
Propeller Erosion in Blocked Flow
R-Class Propeller Model (Back)
Test No. O-10
% Erosion
Blade Number
0
2
4
6
8
10
0
1
2
3
4
5

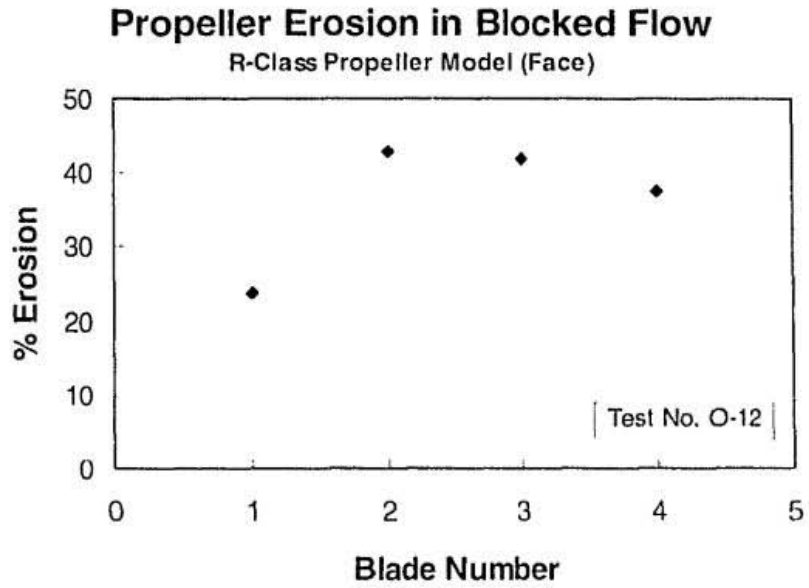
Propeller Erosion in Blocked Flow
R-Class Propeller Model (Face)
% Erosion
50
40
30
20
10
0
0
1
2
3
4
5
Blade Number
Test No. O-12

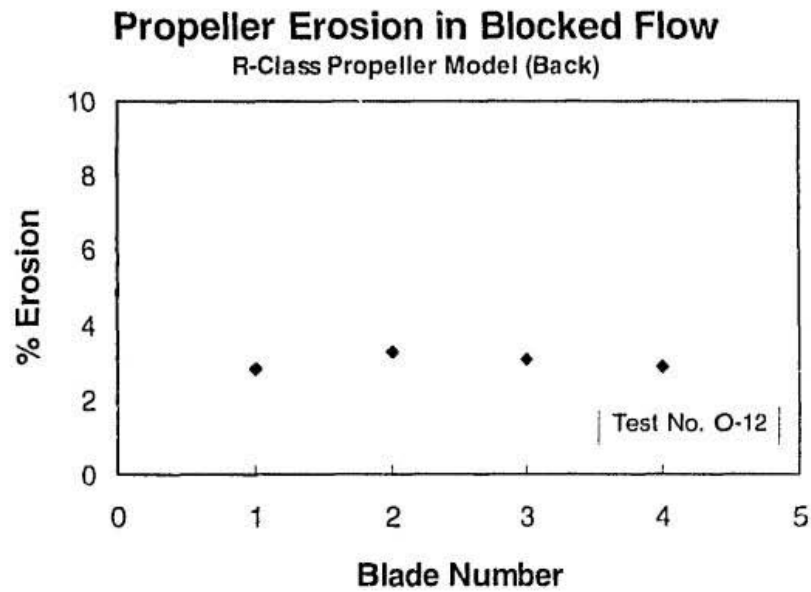
Propeller Erosion in Blocked Flow
R-Class Propeller Model (Back)
% Erosion
10
8
6
4
2
0
0
1
2
3
4
5
Blade Number
Test No. O-12

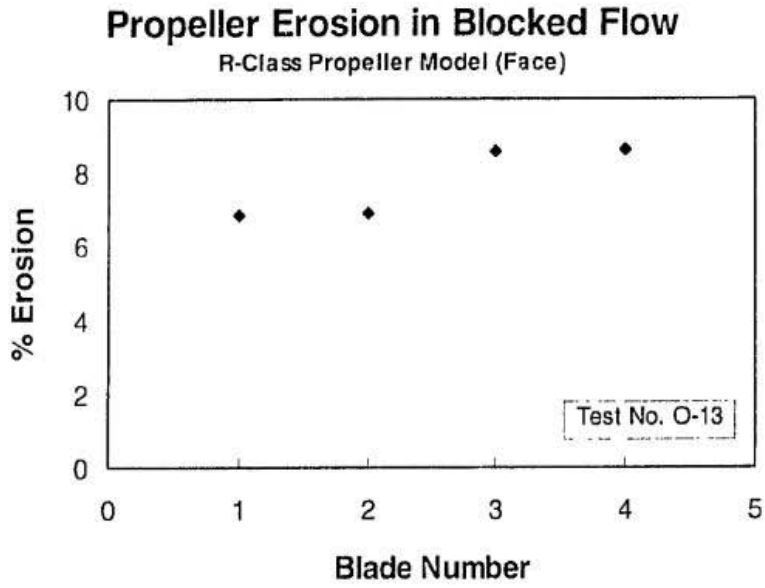
Propeller Erosion in Blocked Flow
R-Class Propeller Model (Face)
% Erosion
10
8
6
4
2
0
0
1
2
3
4
5
Blade Number
Test No. O-13

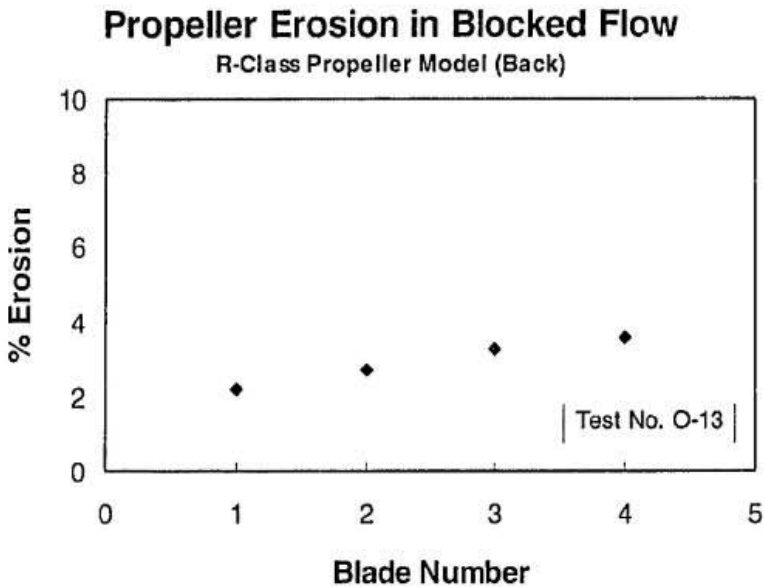
Propeller Erosion in Blocked Flow
R-Class Propeller Model (Back)
% Erosion
10
8
6
4
2
0
0
1
2
3
4
5
Blade Number
Test No. O-13

Appendix E

Ducted Propeller Model Tests: % Erosion vs. Blade Number

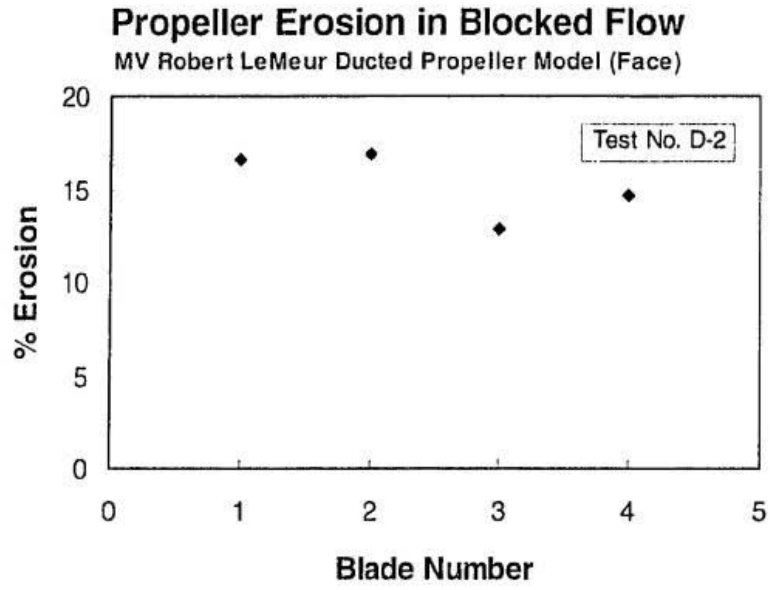
Propeller Erosion in Blocked Flow
MV Robert LeMeur Ducted Propeller Model (Face)
Test No. D-2
% Erosion
Blade Number
0
5
10
15
20
0
1
2
3
4
5

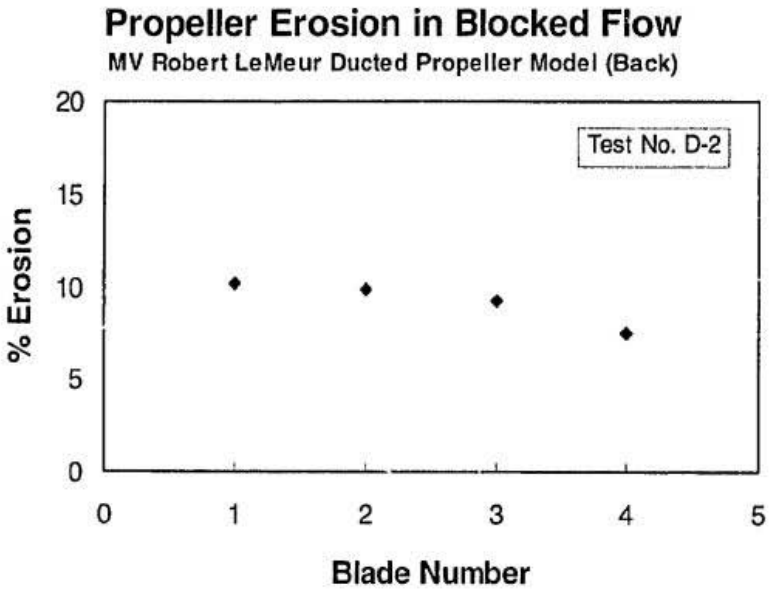
Propeller Erosion in Blocked Flow
MV Robert LeMeur Ducted Propeller Model (Back)
Test No. D-2
% Erosion
Blade Number
0
5
10
15
20
0
1
2
3
4
5

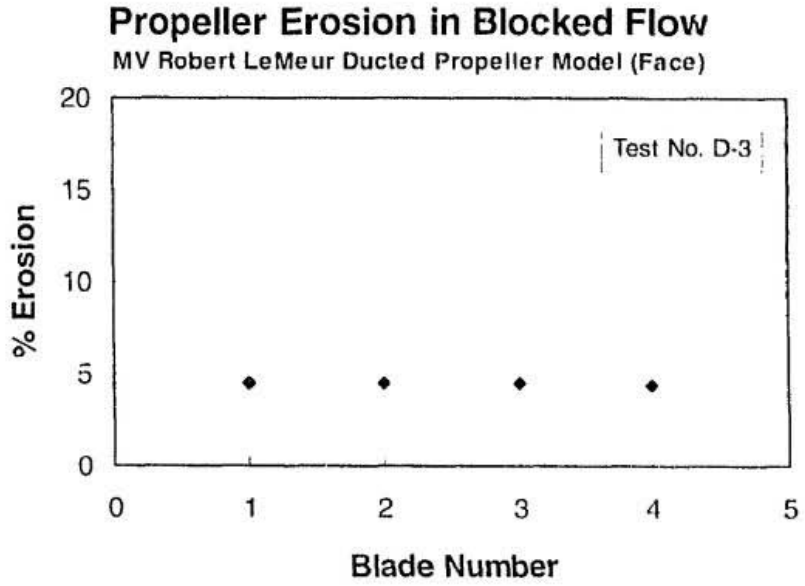
Propeller Erosion in Blocked Flow
MV Robert LeMeur Ducted Propeller Model (Face)
Test No. D-3
% Erosion
Blade Number
0
5
10
15
20
0
1
2
3
4
5

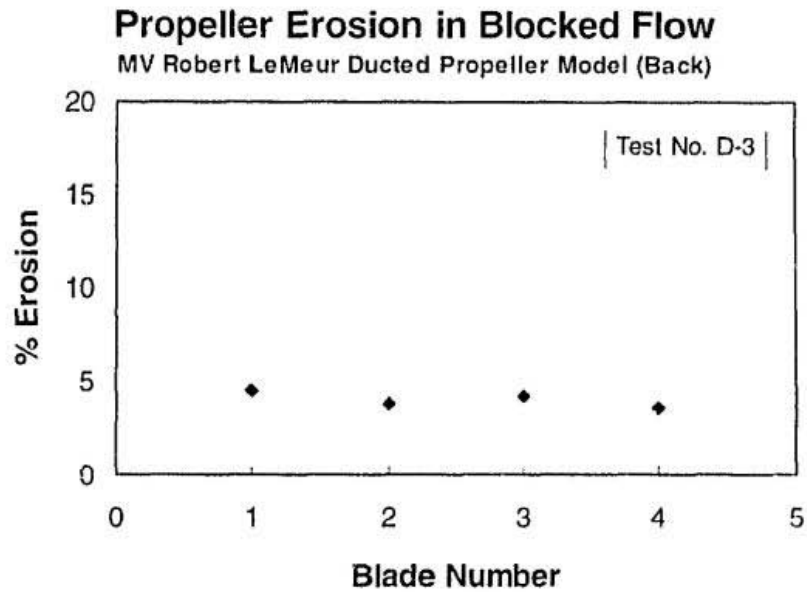
Propeller Erosion in Blocked Flow
MV Robert LeMeur Ducted Propeller Model (Back)
Test No. D-3
% Erosion
Blade Number
0
5
10
15
20
0
1
2
3
4
5

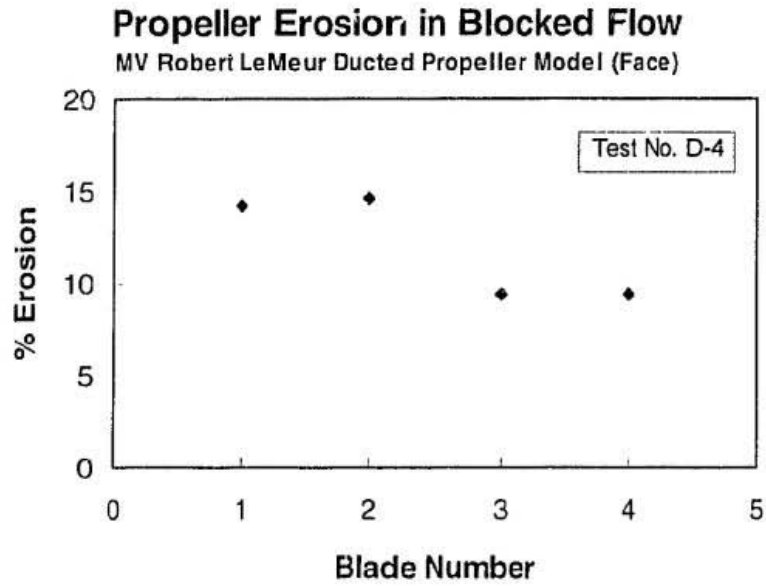
Propeller Erosion in Blocked Flow
MV Robert LeMeur Ducted Propeller Model (Face)
Test No. D-4
% Erosion
Blade Number
0
5
10
15
20
0
1
2
3
4
5

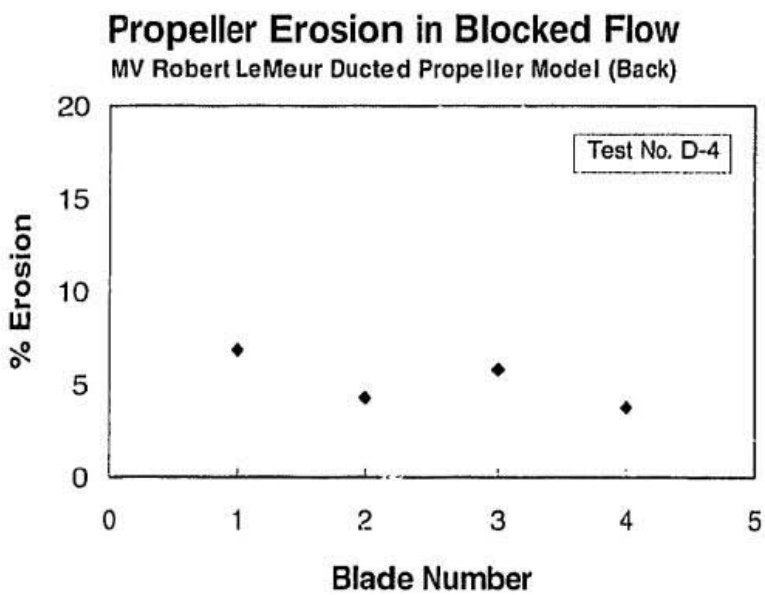
Propeller Erosion in Blocked Flow
MV Robert LeMeur Ducted Propeller Model (Back)
Test No. D-4
% Erosion
Blade Number
0
5
10
15
20
0
1
2
3
4
5

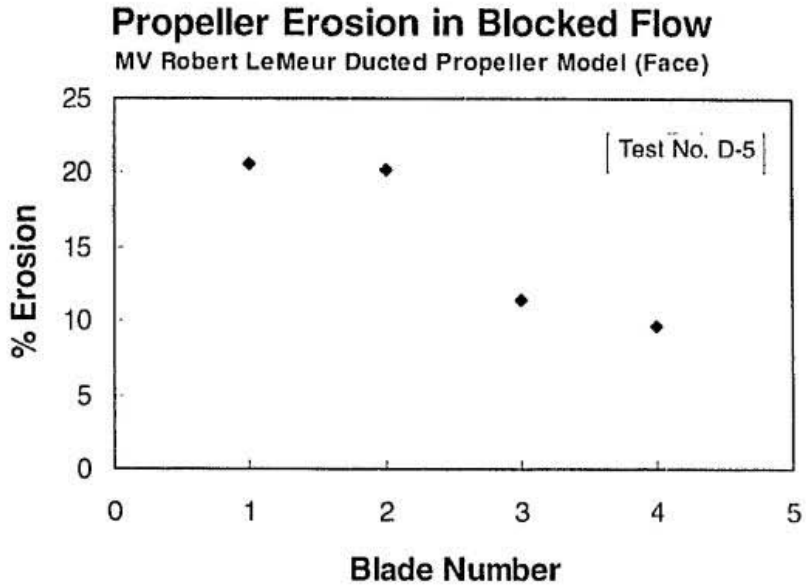
Propeller Erosion in Blocked Flow
MV Robert LeMeur Ducted Propeller Model (Face)
Test No. D-5
% Erosion
Blade Number
0
5
10
15
20
25
0
1
2
3
4
5

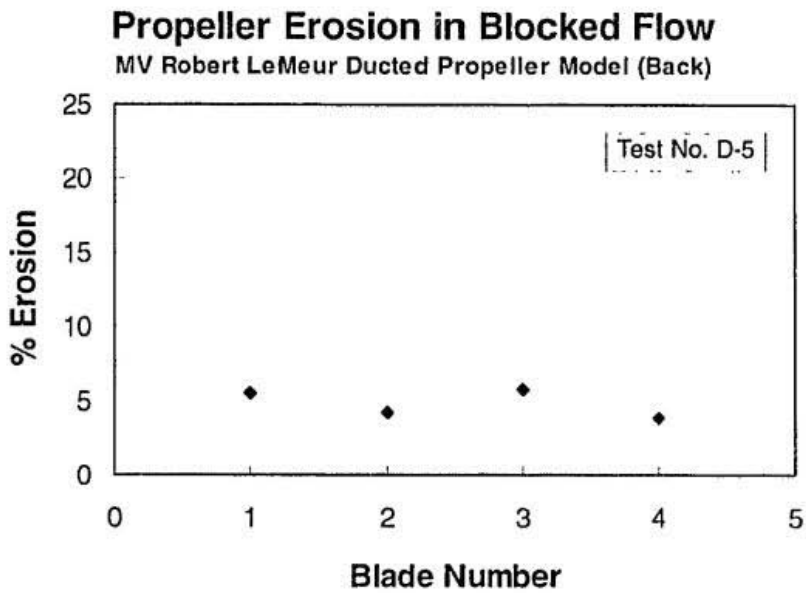
Propeller Erosion in Blocked Flow
MV Robert LeMeur Ducted Propeller Model (Back)
Test No. D-5
% Erosion
Blade Number
0
5
10
15
20
25
0
1
2
3
4
5

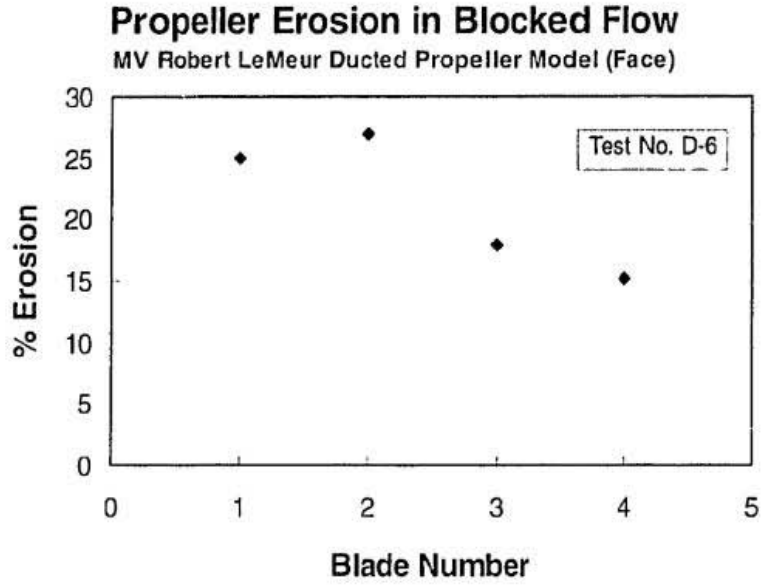
Propeller Erosion in Blocked Flow
MV Robert LeMeur Ducted Propeller Model (Face)
Test No. D-6
% Erosion
Blade Number
0
5
10
15
20
25
30
0
1
2
3
4
5

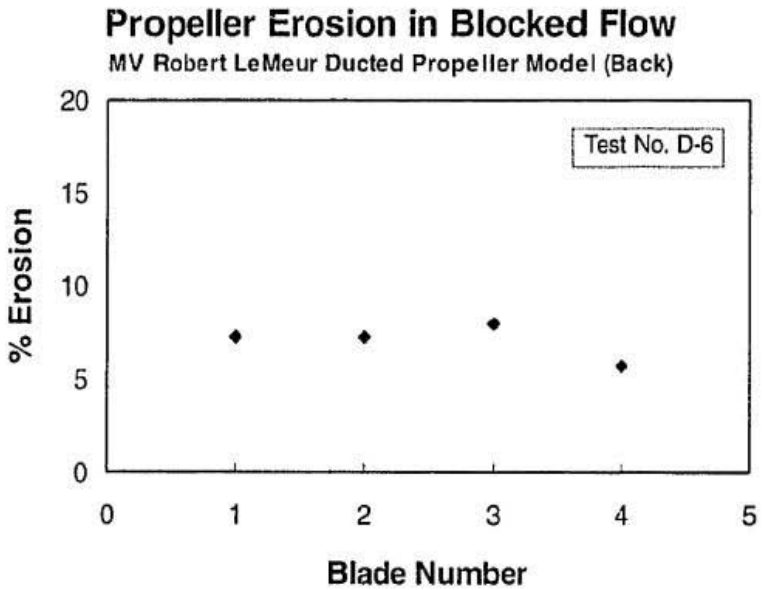
Propeller Erosion in Blocked Flow
MV Robert LeMeur Ducted Propeller Model (Back)
Test No. D-6
% Erosion
Blade Number
0
5
10
15
20
0
1
2
3
4
5

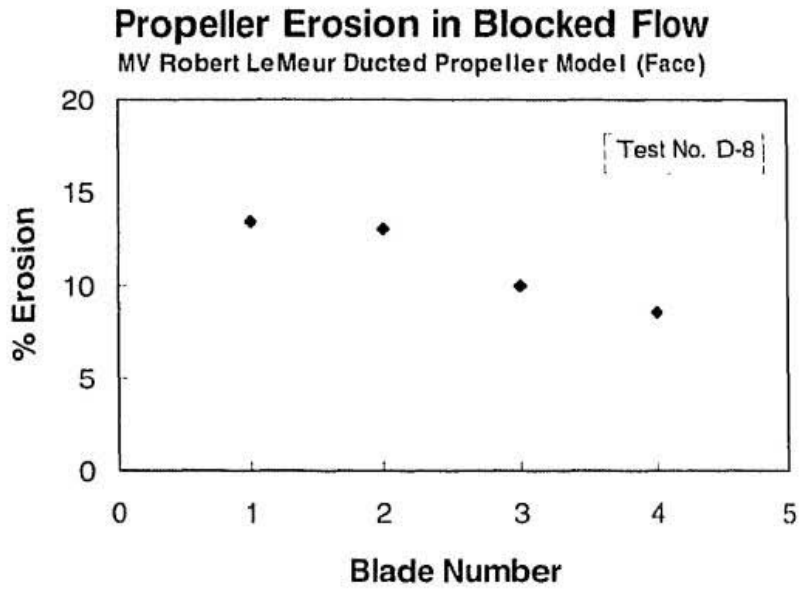
Propeller Erosion in Blocked Flow
MV Robert LeMeur Ducted Propeller Model (Face)
Test No. D-8
% Erosion
Blade Number
0
5
10
15
20
0
1
2
3
4
5

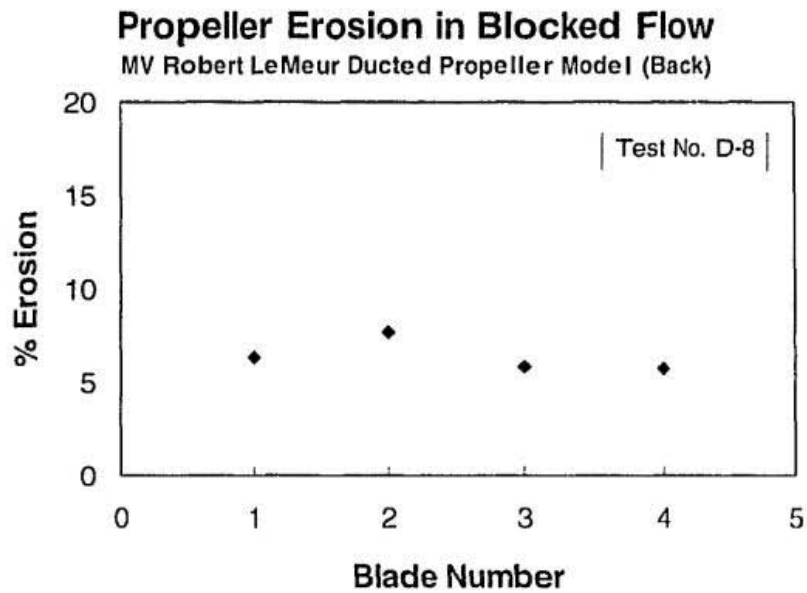
Propeller Erosion in Blocked Flow
MV Robert LeMeur Ducted Propeller Model (Back)
Test No. D-8
% Erosion
Blade Number
0
5
10
15
20
0
1
2
3
4
5

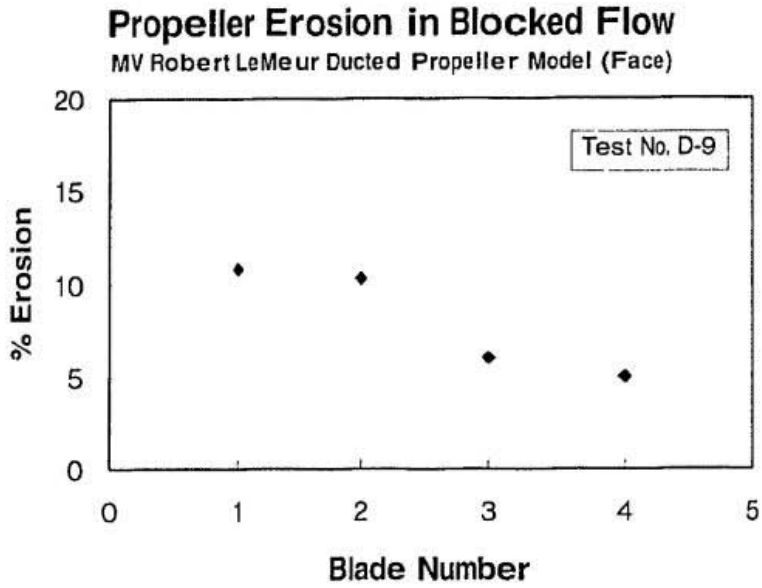
Propeller Erosion in Blocked Flow
MV Robert LeMeur Ducted Propeller Model (Face)
Test No. D-9
% Erosion
Blade Number
0
5
10
15
20
0
1
2
3
4
5

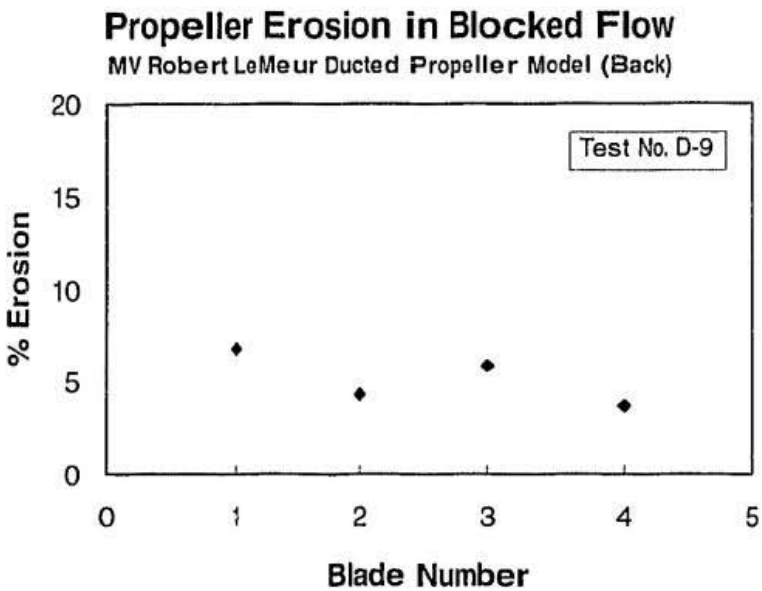
Propeller Erosion in Blocked Flow
MV Robert LeMeur Ducted Propeller Model (Back)
Test No. D-9
% Erosion
Blade Number
0
5
10
15
20
0
1
2
3
4
5